Pathogenesis of SHH medulloblastoma in mice

Dissertation der Fakultät für Biologie

der Ludwig-Maximilians-Universität München

Jasmin Ohli

born in Altötting

Munich, 1st December 2016

Diese Dissertation wurde unter Leitung von Prof. Dr. Ulrich Schüller am Zentrum für Neuropathologie und Prionforschung der Ludwig-Maximilians-Universität angefertigt und von Prof. Dr. Wolfgang Enard vertreten.

Erstgutachter: Herr Prof. Dr. Wolfgang Enard

Zweitgutachter: Frau Prof. Dr. Angelika Böttger

Sondergutachter: Herr Prof Dr.med. Ulrich Schüller

Tag der Abgabe: 01.12.2016

Tag der mündlichen Prüfung: 17.05.2017

ERKLÄRUNG

Ich versichere hiermit an Eides statt, dass meine Dissertation selbstständig und ohne unerlaubte Hilfsmittel angefertigt worden ist.

Die vorliegende Dissertation wurde weder ganz, noch teilweise bei einer anderen Prüfungskommission vorgelegt.

Ich habe noch zu keinem früheren Zeitpunkt versucht, eine Disseration einzureichen oder an einer Doktorprüfung teilzunehmen.

München, Dezember 2016

Jasmin Ohli

Parts of this work have been published as:

Wnt/β-catenin signaling inhibits the Shh pathway and impairs tumor growth in Shh-dependent medulloblastoma.

Pöschl J, Bartels M, Ohli J, Bianchi E, Kuteykin-Teplyakov K, Grammel D, Ahlfeld J, Schüller U.

Acta Neuropathol. 2014;127(4):605-7. doi: 10.1007/s00401-014-1258-2.

and

Localization of SHH medulloblastoma in mice depends on the age at its initiation.

Ohli J, Neumann JE, Grammel D, Schüller U.

Acta Neuropathol. 2015 Aug;130(2):307-9. doi: 10.1007/s00401-015-1453-9. Epub 2015 Jun 20.

Table of Contents

Summary

Medulloblastoma (MB) is the most common malignant brain tumor of childhood that comprises at least four molecularly distinct subgroups. One subgroup is characterized by aberrant Sonic hedgehog (SHH) signalling. Despite the ubiquitous activation of the SHH pathway within this subgroup, there is clear evidence that tumors with a SHH profile may vary in certain molecular and clinical aspects. Targeted therapies as a novel treatment modality for MB patients are especially intriguing for primary and relapsed SHH-MB. As more drugs targeting the Hh pathway become available and enter clinical trials, it is important to know how to stratify the patients for different drugs in order to maximize response rates and to prevent unnecessary treatment failures.

In a first project, we aimed to characterize tumor localization in murine Shh-associated models. Using well established mouse models we show here that oncogenic transformation of cerebellar granule cell precursors at early developmental time points may result in the formation of midline and hemispheric medulloblastoma. On the other side, oncogenic transformation at later developmental time points exclusively results in the formation of hemispheric medulloblastoma. These data, which perfectly match to the recently published observations in human patients, indicate that granule neuron precursors are biologically distinct in different cerebellar compartments and that localization of SHH medulloblastoma is dependent on the time rather than the kind of genetic alteration.

In a second project, we aimed to investigate the effect of the Wnt pathway on Shh-associated medulloblastoma. Previous studies were able to show that Wnt/ß-Catenin activation might be able to inhibit Shh-associated medulloblastoma growth through downregulation of the Shh pathway. Considering a possible therapeutic approach, *in vitro* treatments with lithium chloride, a well-known Wnt/ß-Catenin agonist, were carried out. Lithium chloride treatment *in vitro* resulted in a decrease of granule neuron precursor and tumor cell viability.

In the third project, we aimed to better understand the mechanisms in MB of primary and secondary resistance to drugs targeting the Hh pathway. To this end, we generated new

mouse models, characterized and used these and already existing genetically engineered mouse models (GEMMs). We aimed to further expand our pre-existing repertoire of murine SHH-activated MB models in order to have a spectrum of tumors that are driven by mutations at different levels of the Hh pathway, such as *PTCH1, SMO*, or *MYCN*, and with different combinations of other mutations in additional pathways that may co-operate with HH signalling (e.g. *TP53* or *PIK3CA*). The mouse strains *Math1-creER^{T2}::lsl-SmoM2$^{Fl/+}$*, *Math1-creER^{T2}::lsl-SmoM2$^{Fl/+}$ lsl-Pik3ca$^{Fl/+}$*, *Math1-creER^{T2}::Ptch1$^{Fl/Fl}$*, *Math1-creER^{T2}::Ptch1$^{Fl/Fl}$ lsl-Pik3ca$^{Fl/+}$, and Math1-creER^{T2}::Ptch1$^{Fl/Fl}$ lsl-Pik3ca$^{Fl/Fl}$* developed Shh-associated medulloblastoma. Our mouse model with a *MYCN* mutation did not develop any tumor, neither as such nor with an additional *TP53* mutation. *Math1-creER^{T2}::lsl-SmoM2$^{Fl/+}$*, *Math1-creER^{T2}::lsl-SmoM2$^{Fl/+}$ lsl-Pik3ca$^{Fl/+}$,* and *Math1-creER^{T2}::Ptch1$^{Fl/Fl}$* mice were then treated with the SMO inhibitor LDE225, that is already used in clinical trials. *Math1-creER^{T2}::lsl-SmoM2$^{Fl/+}$* and *Math1-creER^{T2}::Ptch1$^{Fl/Fl}$* mice first benefit from the treatment, but then also die due to symptoms of the tumor, whereas *Math1-creER^{T2}::lsl-SmoM2$^{Fl/+}$ lsl-Pik3ca$^{Fl/+}$* mice did not show a better prognosis for survival at all. None the less, proliferation was reduced in all tumors treated with LDE225.

Zusammenfassung

Das Medulloblastom (MB) ist ein maligner Hirntumor, welcher vornehmlich im Kindesalter auftritt und in der hinteren Schädelgrube mit starkem Bezug zum Kleinhirn entsteht. Basierend auf variierenden globalen Expressionsprofilen wird das humane Medulloblastom in vier verschiedene molekulare Subgruppen eingeteilt. Während eine dieser Subgruppen durch eine pathologische Aktivierung des Sonic hedgehog (SHH)-Signalwegs charakterisiert ist, weisen trotz dieser Gemeinsamkeit auch die Tumore innerhalb dieser Subgruppe ein beträchtliches Maß an Heterogenität bezüglich molekularer und klinischer Parameter auf. Gezielte Therapien als neuartige Behandlungsmethode für MB-Patienten sind besonders faszinierend für primäre und rezidivierende SHH-MB. Da mehr Medikamente verfügbar sind, die auf den HH-Signalweg abzielen, und in klinischen Studien eingehen, ist es wichtig zu wissen, wie man die Patienten für verschiedene Medikamente stratifiziert, um die Ansprechrate zu maximieren und unnötige Behandlungsfehler zu vermeiden.

In einem ersten Teilprojekt sollte die Tumorlokalisation in murinen Shh-assoziierten Modellen charakterisiert werden. Unter Verwendung gut etablierter Mausmodelle konnten wir hier zeigen, dass die onkogene Transformation von cerebellären Körnerzellvorläufern zu frühen Entwicklungszeitpunkten zur Bildung von Medulloblastomen in der Mittellinie und in den Hemisphären führen kann. Auf der anderen Seite führt die onkogene Transformation zu späteren Entwicklungszeitpunkten ausschließlich zur Bildung von Medulloblastomen in den Hemisphären. Diese Daten, die perfekt zu den kürzlich veröffentlichten Beobachtungen bei menschlichen Patienten passen, deuten darauf hin, dass Körnerzellvorläufer in verschiedenen cerebellären Kompartimenten biologisch verschieden sind und, dass die Lokalisation von SHH-Medulloblastomen von der Zeit abhängt und nicht von der Art der genetischen Veränderung.

In einem zweiten Teilprojekt sollte der Effekt des Wnt-Signalwegs auf Shh-assoziierte Medulloblastome untersucht werden. Frühere Studien konnten zeigen, dass die Wnt/ß-Catenin-Aktivierung in der Lage sein könnte das Wachstum von Shh-assoziierten Medulloblastomen durch die Herunterregulation des Shh-Signalweges zu hemmen. In

Anbetracht eines möglichen therapeutischen Ansatzes wurden *in vitro* Behandlungen mit Lithiumchlorid, einem bekannten Wnt/ß-Catenin-Agonisten durchgeführt. Die Lithiumchloridbehandlung *in vitro* führte zu einer Verringerung der Lebensfähigkeit von Körnerzellvorläufern und Tumorzellen.

Im dritten Teilprojekt zielten wir darauf ab, die Mechanismen von Medulloblastomen mit primären und sekundären Resistenzen gegenüber Substanzen, die gegen den Hh-Signalweg gerichtet sind, besser zu verstehen. Dazu wurden neue Mausmodelle erstellt und charakterisiert, und diese und bereits vorhandene gentechnisch hergestellte Mausmodelle (GEMMs) genutzt. Das bereits vorhandene Repertoire an murinen SHH-aktivierten MB-Modellen sollte weiter ausgebaut werden, um ein Spektrum von Tumoren zu erhalten, mit Mutationen, die auf verschiedenen Ebenen des HH-Signalweges, wie *PTCH1, SMO* oder *MYCN* basieren, und mit verschiedenen Kombinationen anderer Mutationen von zusätzlichen Signalwegen, die mit dem HH-Signalweg kooperieren (z.B. *TP53* oder *PIK3CA*). Die Mauslinien *Math1-creER^{T2}::lsl-SmoM2$^{Fl/+}$*, *Math1-creER^{T2}::lsl-SmoM2$^{Fl/+}$ lsl-Pik3ca$^{Fl/+}$, Math1-creER^{T2}::Ptch1$^{Fl/Fl}$*, *Math1-creER^{T2}::Ptch1$^{Fl/Fl}$ lsl-Pik3ca$^{Fl/+}$, und Math1-creER^{T2}::Ptch1$^{Fl/Fl}$ lsl-Pik3ca$^{Fl/Fl}$* entwickelten Shh-assoziierte Medulloblastome. Unser Mausmodell mit einer MYCN Mutation entwickelte keine Tumoren, auch nicht mit einer zusätzlichen *TP53* Mutation. *Math1-creER^{T2}::lsl-SmoM2$^{Fl/+}$*, *Math1-creER^{T2}::lsl-SmoM2$^{Fl/+}$ lsl-Pik3ca$^{Fl/+}$,* und *Math1-creER^{T2}::Ptch1$^{Fl/Fl}$* Mäuse wurden anschließend mit dem Smo-Inhibitor LDE225 behandelt, der bereits in klinischen Studien genutzt wird. *Math1-creER^{T2}::lsl-SmoM2$^{Fl/+}$* und *Math1-creER^{T2}::Ptch1$^{Fl/Fl}$* Mäuse profitieren zuerst von der Behandlung, sterben aber letztendlich an Symptomen des Tumors, wohingegen *Math1-creER^{T2}::lsl-SmoM2$^{Fl/+}$ lsl-Pik3ca$^{Fl/+}$* Mäuse überhaupt keine bessere Überlebensprognose aufweisen. Trotzdem wurde die Proliferation in allen mit LDE225 behandelten Tumoren reduziert.

1 Introduction

1.1 Function and structure of the cerebellum

The cerebellum is part of the motoric system. It receives sensory information of the brain stem and the spinal cord. The cerebellum on its own is not able to initiate movements, but is responsible for coordination and fine adjustment of course of motions. In this context it is responsible for back-up motor apparatus of posture and movement, the motor activity and eye movement controlled of the cerebrum. In addition, it controls the muscle tone and maintains the balance.

The cerebellum lies in the posterior fossa dorsal to the brain stem (*Mesencephalon, Pons, Medulla oblongata*). Between the cerebellum and the brain stem lies the fourth ventricle filled with cerebrospinal fluid (CSF). The three cerebellar peduncles (*Pedunculus cerebellaris superior*, *medius*, *inferior)* connect the cerebellum with the brain stem and contain afferent as well as efferent fibres. The structuring of the cerebellum in the cerebellar vermis (*Vermis cerebelli*) and both lateral hemispheres (*Hemispheria cerebelli*) are clearly visible. The whole cerebellum contains a fine surface structure which consists of fissures (*Fissurae cerebelli*) and foliage (*Folia cerebelli*). As well as in the cerebrum (*Telencephalon*), the outward lying structure which is rich of neurons is the cortex (*Cortex cerebelli)* and the inner lying white substance with many fibres is the central white matter of the cerebellum (*Corpus medullare cerebelli).*

The adult cerebellar cortex is subdivided into three layers: the molecular layer (ML), the purkinje cell layer (PCL) and the inner granule cell layer (IGL) (Figure 1). Here the ML mainly consists of basket and stellar cells, the PCL consists of purkinje cells and Bergman glia cells and the IGL consist of mature granule cells, golgi cells, and astrocytes. The white matter with nerve cell fibres, astrocytes, and oligodendrocytes and the deep cerebellar nuclei complete the structure of the cerebellum (Altmann 1997).

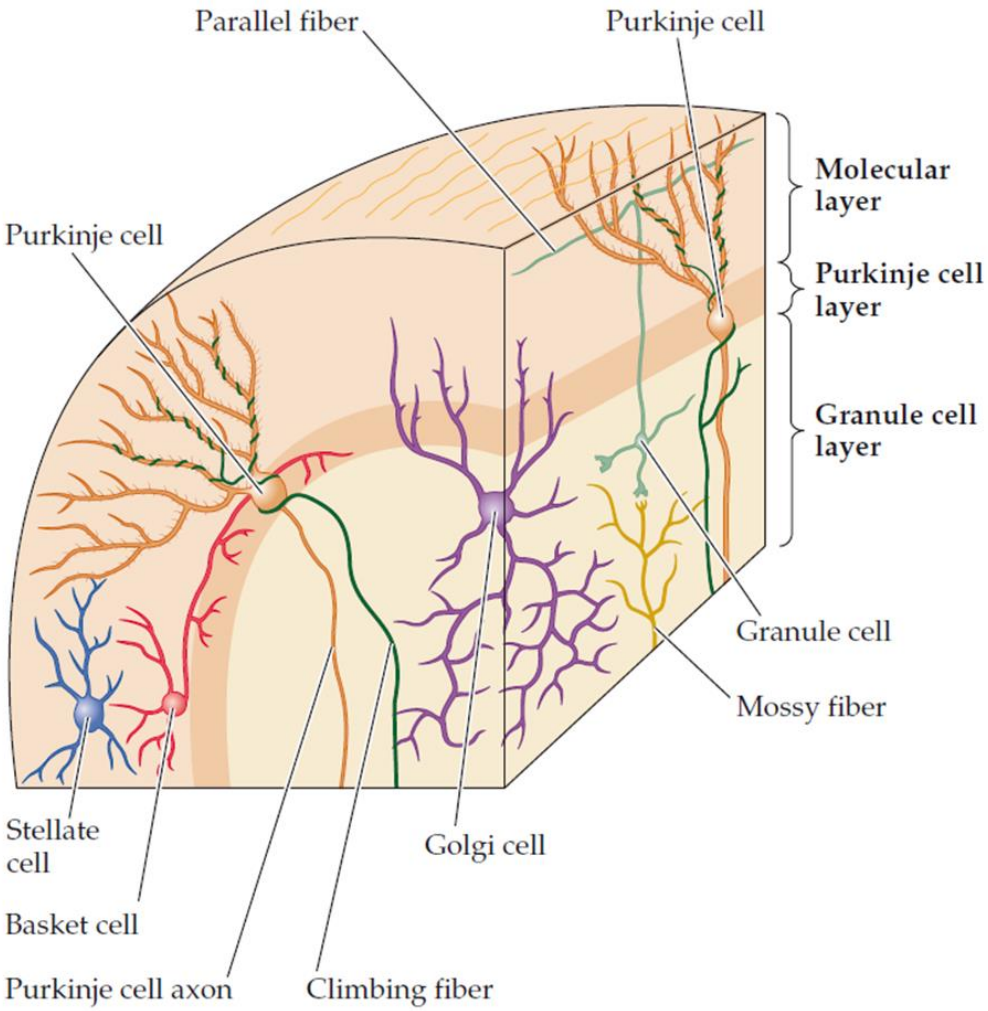

Figure 1 Sketch of the structure and cytoarchitecture of the cerebellar cortex. Sagittal and frontal section of a cerebellar folium with relevant cell types and fibers of the cerebellum ((Purves 2004); Purves et al: *Neuroscience, Third Edition;* with permission of Sinauer Associates).

1.2 Development of the cerebellum

The cells of the central nervous system (CNS) can be broadly divided into glial cells and neuronal cells, both differentiate from multipotential neural progenitor cells (Edlund and Jessell 1999).

The cerebellar granule neuron is by far the most common cell type in the adult cerebellum and forms the innermost granule layer. The following Purkinje cell layer is a monolayer of fan-shaped Purkinje neurons with dendritic arborisation (Palay and Chan-Palay 1974). The cell bodies of the Bergmann glia lie in the region of the cell bodies of Purkinje cells

and their fibres pass the outermost molecular layer to the pial surface (Grosche et al. 2002, Welsch 2006). In addition to the Bergmann glial fibres also the processes of the cerebellar granule neurons, the parallel fibres, and the dendritic arborisation of the Purkinje cells extend into the molecular layer.

The development of the cerebellum in mice starts around embryonic day 9 (E9) with the development of the cerebellar anlage and finishes around postnatal day 20 (P20) (Hatten and Heintz 1995). Here the cerebellum descends from rhombomer r1, the rostral part of the rhombic lip, which is confined by the expression of the transcription factors Otx2 and Hoxa2 and is called the upper rhombic lip (Joyner 1996, Wingate and Hatten 1999, Joyner et al. 2000). The rhombomers r2-r8 form in their entirety the lower rhombic lip (Landsberg et al. 2005). In detail, all cells of the cerebellum stem from two different germinal epithelia. Purkinje cells, cells of the deep cerebellar nuclei and more than 6 different kinds of inhibitory interneurons like e.g. Golgi-, basket- and stellar- cells stem from the dorso-medial ventricular zone along the IV. ventricle (Hallonet and Le Douarin 1993, Dino et al. 2000, Hoshino et al. 2005). The second germinal epithelium, the rhombic lip, is the point of origin of the cerebellar granule cells as well as of a subpopulation of the deep cerebellar nuclei and neurons of different pre-cerebellar nuclei in the brain stem (Wingate and Hatten 1999, Wingate 2001, Machold and Fishell 2005, Wang et al. 2005).

In detail, the development of the cerebellum starts, as in all chordates, with neurulation, the development of the neural tube, as basis for the later central nervous system (CNS). Of the three embryonic germ layers (endoderm, mesoderm and ectoderm) only the central part of the ectoderm contributes to the development of the neural plate and the following folding of the neural tube. The unfolding happens at the neural plate by the development of the neural groove and the dorsal closing to a tubular structure, which represents the early spinal cord. In the inside of the neural tube is the *Liquor cerebrospinalis,* which holds the cavity open for the proper formation of the brain. The neurulation is induced by soluble growth factors of the notochord and the roof plate, which cause a compartmentalization of the embryonic CNS by dorso-ventral gradients of BMP-4 (bone morphogenetic protein 4) and SHH (sonic hedgehog) (Watanabe et al. 1998). The cerebellar primordium develops out of a gap in the dorsal neural tube, which leads to a lateral protrusion on the level of the pontine bend. The dorso-lateral regions of the wing plate bend medially and build up the rhombic lip (RL). Through growth

movement and protrusion of the rhombic lip to dorsal, a transversal placed plate is formed, the neural plate (Duband 2010). The rhombic lip is one of the both germinal zones of the developing cerebellum. Here granule cell precursors originate. Purkinje cells, as an example for cells of the ventricular zone, proliferate in their germinal zone only between embryonic day 11–14 (E11-E14). As these cells migrate radial in the developing cerebellum after they left the cell cycle, granule cell precursors migrate out of the upper rhombic lip, starting at E13–E15, tangential through the surface of the cerebellar anlage and there build up a secondary proliferation zone, the external granule cell layer (EGL) (Hatten and Heintz 1995, Hatten et al. 1997). The mitogen sonic hedgehog (Shh), which is generated by the purkinje cells, leads to a massive expansion of the granule cell population (Wechsler-Reya and Scott 1999). Here the EGL can be subdivided into a superficial zone of proliferating cells and an inner zone of differentiating cells. This subdivision is evident by the expression of different marker genes (RU-49, NeuN, etc.), which are differentially expressed during cerebellar development (Hatten and Heintz 1995, Weyer and Schilling 2003). The localization of these marker genes has shown that the development of cerebellar granule cells can be subdivided into at least 4 phases: neurogenesis, differentiation, migration and generation of synaptic connections. After they have left the cell cycle, granule cells migrate radially along the extensions of the Bergman glia cells into the cerebellum and there form the internal granule cell layer (IGL) (Rakic and Sidman 1973).

1.3 Medulloblastoma

Medulloblastoma (MB) is the most common malignant brain tumor in children. Current treatments for MB include surgical resection followed by irradiation of the entire neuraxis and high-dose chemotherapy. Many patients die despite these treatments, and those who survive often suffer from cognitive deficits and endocrine disorders as a consequence of therapy (Mulhern et al. 2005).

1.3.1 Classification of medulloblastoma

Since 2016 the World Health Organization (WHO) classifies MB based on histology and also molecular features (Louis et al. 2016). For histology several subtypes of the disease are recognized: classic, large cell/anaplastic (LCA), nodular/desmoplastic and MB with extensive nodularity (Louis et al. 2007). Patients with nodular/desmoplastic histology tend to have favourable outcomes, while those with large cell and anaplastic (LCA) histology have the worst prognosis (Eberhart et al. 2002, McManamy et al. 2007). Recent advances in microarray and genomic sequencing technologies have enabled a deeper understanding of MB. Based on such analysis, MBs have now been divided into 4 major molecular subgroups: WNT, Sonic Hedgehog (SHH), Group 3 and Group 4 (Jones et al. 2012, Northcott et al. 2012, Pugh et al. 2012, Robinson et al. 2012, Taylor et al. 2012). The WNT- and the SHH-subgroup are characterized by a constitutive activation of different, highly conserved signalling pathways (WNT- and SHH-signalling) (Figure 2). Since 2016, SHH-activated MB are subclassified into a *TP53*-mutant and a *TP53*-wildtype group (Louis et al. 2016).

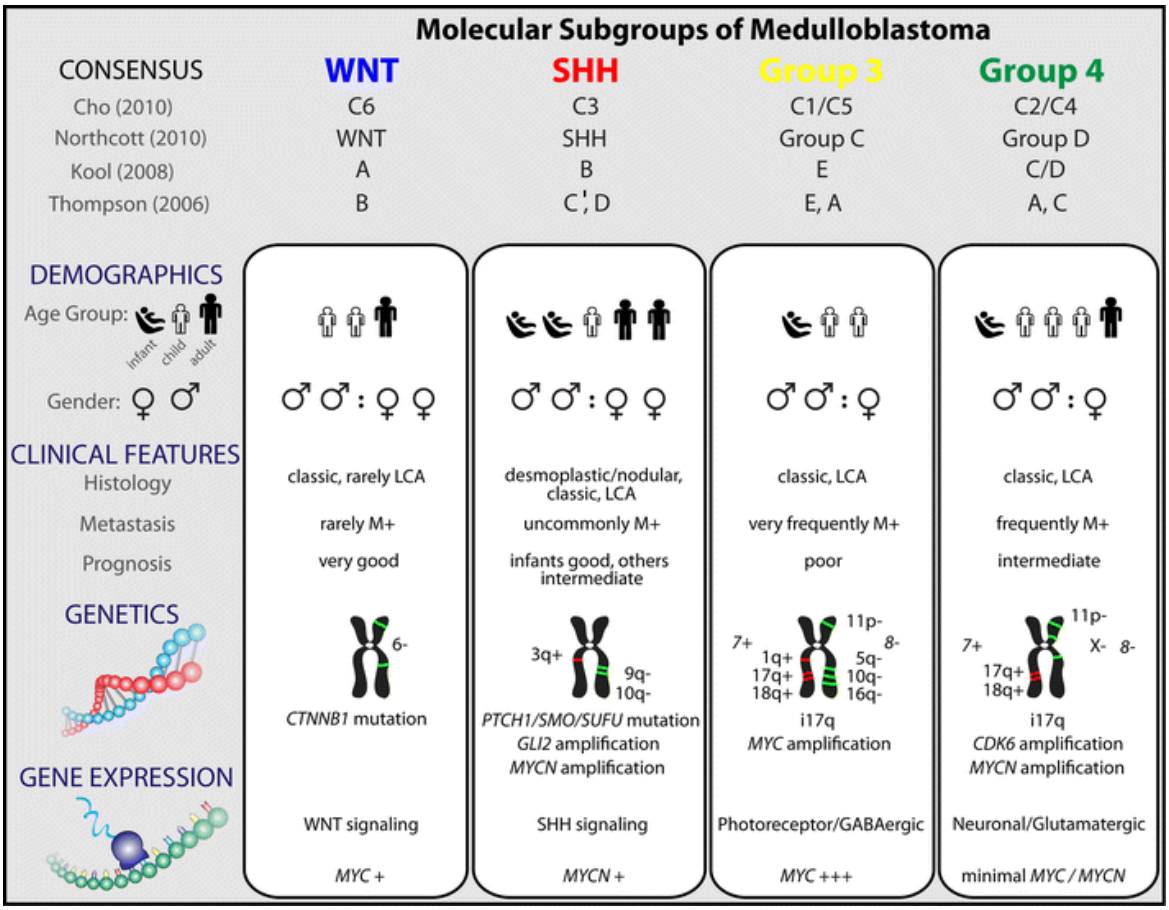

Figure 2 Comparison of the various subgroups of medulloblastoma including their affiliations with previously published papers (with outdated nomenclature of groups) on medulloblastoma molecular subgrouping (Taylor et al. 2012; with permission of Springer, copyright (2011), license number 3967660344265).

The WNT subgroup shows a very good long-term prognosis in comparison to other subgroups (Ellison et al. 2005, Clifford et al. 2006, Rogers et al. 2009, Ellison et al. 2011). WNT-associated tumors, which occur in children and teenagers as well as in adults, normally have disrupted WNT signalling genes, including activating mutations in *CTNNB1* (ß-catenin), which activates canonical WNT signalling, and inactivating mutations in the adenomatous polyposis coli (*APC*) gene, a negative regulator of the WNT pathway (Hamilton et al. 1995, Zurawel et al. 1998). Other common features of the WNT subgroup are chromosome 6 loss and expression of the WNT-gene *DKK1* (Thompson et al. 2006, Northcott et al. 2011). WNT MBs typically have classic histology (Rogers et al. 2009).

Analogous to the WNT subgroup, MBs of the SHH subtype show a characteristic activation of the Sonic hedgehog signalling pathway (Kool et al. 2008, Northcott et al. 2011, Schwalbe

et al. 2011, Kool et al. 2012). Medulloblastoma of the SHH subtype (about 25% of all MBs) are the best analysed subgroup (Hatten and Roussel 2011). Common are somatic mutations in genes of this signalling pathway like inactivating mutations in the negative regulators PATCHED1 (PTCH1) or Suppressor of Fused (SUFU), activating mutations in the signal transducing molecule SMOOTHENED (SMO), but also amplifications of the SHH-target genes GLI1 and GLI2 transcription factor can lead to the constitutive activation of the pathway (Johnson et al. 1996, Hahn et al. 1999, Northcott et al. 2009, Adamson et al. 2010, Pfister et al. 2010, Northcott et al. 2011, Taylor et al. 2012). Many SHH-associated MBs have desmoplastic/nodular histology, although classic and LCA histologies are also observed (Taylor et al. 2012). SHH MB occurs in infants, where the prognosis is favourable, as well as in adults, where the prognosis is more variable (Kool et al. 2012). In this subgroup, there is a special age distribution. Mainly infants and adults develop SHH medulloblastoma, children quite rarely (Northcott et al. 2011). This biphasic age distribution presumes a huge heterogeneity in clinical, molecular and developmental biological parameter in this group. In addition, localization of human SHH MBs differs depending on the age of the patient. For so far unknown reasons, adult SHH MBs are almost exclusively located in cerebellar hemispheres, whereas infant SHH MBs often grow in the vermis (Wefers et al. 2014). It is known that an activation of the SHH pathway in granule cell precursors of the rhombic lip and the external granule cell layer (EGL) can lead to the development of Shh-associated Medulloblastoma (Schüller et al. 2008). Recently, it was shown that SHH-associated MB can also arise from granule neuron precursors of the cochlear nucleus of the brainstem (Grammel et al. 2012).

The majority of MBs do not exhibit activation of the WNT or SHH pathways, and these tumors can be divided into at least two subtypes – Group 3 and Group 4 – based on gene expression, DNA copy number changes and mutations. Group 3 MB patients commonly exhibit amplification or overexpression of the MYC oncogene and have gene signatures resembling those of photoreceptors and gamma-aminobutyric acid expressing (GABAergic) neurons (Taylor et al. 2012). In contrast, Group 4 tumors often exhibit amplification of CDK6 and MYCN or duplication of the Parkinson's Disease-associated gene synuclein alpha interacting protein (SNCAIP), and have expression profiles reminiscent of glutamate-expressing (glutamatergic) neurons (Northcott et al. 2012).

These four subgroups are highly distinct in tumor histology and biology, and in addition show divergent clinical phenotypes such as differences in patient demographics, tumor dissemination, and patient outcome (Kool et al. 2012, Northcott et al. 2012, Taylor et al. 2012). Recently, a large series of pediatric MB was analysed using next generation sequencing technologies to map the genomic landscape of MB and to identify novel driver mutations in each molecular subgroup (Parsons et al. 2011, Jones et al. 2012, Northcott et al. 2012, Northcott et al. 2012, Pugh et al. 2012, Rausch et al. 2012, Robinson et al. 2012). As there are still many MB, for which a clear driver mutation is not identified yet, it was also analysed the epigenome of a large series of MB using whole genome bisulfite sequencing and ChIP-seq for various histone modifications to investigate, to what extent epigenetics plays a role in MB tumorigenesis and whether epigenetic alterations may explain the formation of tumors, in which a clear driver mutation was not found (point mutations, small insertions or deletions or focal copy-number aberrations) by WGS (Hovestadt et al. 2014).

1.3.2 Symptoms, diagnostics and therapy of medulloblastoma

First clinical symptoms are typically unspecific symptoms of an increased intracranial pressure: head ache, impaired vision, morning sickness and vomiting (Alston et al. 2003). Very young patients can develop a hydrocephalus due to the blockade of the circulation of the cerebrospinal fluid (CSF). This means that the increased fluid pressure in the ventricular system of the whole brain leads to the deformation of the still flexible calvaria. The primary localization of the medulloblastoma in the cerebellum causes the increased appearing ataxia in the course of the disease. Dizziness and problems with coordination as well as a general impairment of motor function are typical for progressive tumor growth. Neurological deficits, which are typical for the secondary affected brain structures can be observed at infiltrating growth and metastases. Diagnosis is made with imaging techniques (magnetic resonance imaging, MRI), where you can evaluate localization, size and extent of the tumor. For validation of the diagnosis and for therapeutic approach the dissected tumor tissue is examined by histology, immunohistochemistry and molecular methods. Independent of the subgroup, the treatment consists of a combination of resection, irradiation and chemotherapy (Evans et

al. 1990, Tait et al. 1990, Kortmann et al. 2000, Taylor et al. 2003). For very young patients you have to balance the chance of success of the irradiation and the psychomotor and cognitive disturbances in the early infantile development and the coincided postnatal development of the cerebellum (Duffner et al. 1993). Despite of substantial progress, actual therapy approaches still show unwanted secondary effects and hence resulting significant death rate. Due to the detailed characterisation of the subgroups of medulloblastoma and the analysis of the cell of origin of the different subtypes, therapies can be fitted to the proteins or cell populations involved. Due to the well-known influence of the SHH pathway on the development of medulloblastoma, many low-molecular connections were discovered, which can repress the activity of the SHH pathway as inhibitors of the transmembrane receptor Smoothened. The efficacy of these inhibitors could already be proven in allografts and mouse models for medulloblastoma (Berman et al. 2002, Romer et al. 2004, Romer and Curran 2005) and are analysed in clinical studies at the moment for the benefit in the human system (Coon et al. 2010). Molecular analyses of primary medulloblastoma promise much progress with regard to targeted cancer therapies, which have the molecular, cytological and developmental biological characteristics of the tumors as basis.

Targeted therapies as a novel treatment modality for MB patients are especially intriguing for primary and relapsed SHH-MB. As more drugs targeting the Hh pathway become available and enter clinical trials, it is important to know how to stratify the patients for different drugs in order to maximize response rates and to prevent unnecessary treatment failures. Current clinical trials targeting SHH-MB with SMO antagonists (such as LDE225) use a five-gene signature to identify SHH-MB. However, this signature is not sufficient as a predictive biomarker for response to SMO antagonists, since it detects all SHH-MB with Hh activation regardless of their underlying genetic makeup (Kool et al. 2014). Indeed, it is clear from clinical trials using SMO antagonists that the response appears to be highly variable with a large proportion of striking durable responders, but also with a lot of non-responders. Recent data have shown that SHH-MB are genetically very heterogeneous and the response to drugs antagonizing the Hh pathway strongly depends on the type of mutation that activates the pathway. To understand the mechanism(s) of primary resistance and to identify pathways co-operating with aberrant Hh signalling, a large cohort of SHH-MB (n = 133) was sequenced and profiled. Hh

pathway mutations identified in this study involved *PTCH1* (found across all age groups), *SUFU* (mainly found in infants, including many in the germline), and *SMO* (mainly in adults) (Figure 3).

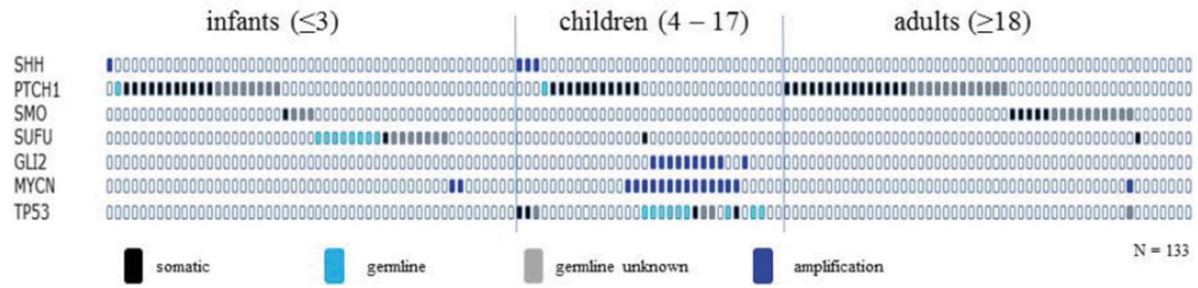

Figure 3 Hh pathway mutations in 133 sequenced SHH-MB. Cases have been split up in infants, children and adults, and are sorted based on the type of mutation in the Hh pathway. Results show that SHH-MB are genetically heterogeneous and the different age groups harbor different predominant mutations activating the Hh pathway (reprinted from with permission of Elsevier (Kool et al. 2014), copyright (2014), license number 3967660794571).

Older children harbored an excess of downstream *MYCN* and *GLI2* amplifications and frequent *TP53* mutations, often in the germline, all of which were exceedingly rare in infants and adults.

1.3.2.1 Resistance to SMO inhibition

Functional assays in different patient-derived SHH-MB xenograft models demonstrated that SHH-MB harboring a *PTCH1* mutation were responsive to SMO inhibition, whereas tumors harboring *SUFU* mutations or *MYCN* amplifications were primarily resistant. SHH-MBs with alterations in downstream SHH pathway genes, however, such as *SUFU*, *GLI2*, or *MYCN*, demonstrated primary resistance to SMO inhibition (Lee et al. 2007). These data showed for the first time that most adults, but only half of the pediatric patients with SHH-MB will likely be responsive to SMO inhibition as predicted by molecular analysis of the primary tumor and tested in the SHH-xenografts. SHH-MB patients resistant to SMO inhibitors need to be treated with other inhibitors targeting the pathway, for instance, at

the level of GLI. Furthermore, as has been shown in both humans and mice, tumors may also rapidly acquire secondary resistance to treatment (Rudin et al. 2009, Yauch et al. 2009, Dijkgraaf et al. 2011), suggesting that such inhibitors might be ineffective as a curative option when administered as monotherapy. It is strongly advocated that the next generation of SMO inhibitor trials should be based on underlying tumor genetics because many patients with SHH-MB will not respond to these inhibitors. Alternative treatment options could include arsenic trioxide (ATO) targeting GLI transcription factors by degrading the protein (Kim et al. 2013). ATO and the antifungal agent itraconazole (which acts on SMO) have also been suggested in preclinical experiments for use in SHH-MBs that become resistant after treatment with SMO antagonists (Kim et al. 2013) or in combination with SMO inhibitors upfront knowing that *GLI2* amplifications comprise a common mechanism of secondary resistance to SMO inhibition in preclinical models (Buonamici et al. 2010, Dijkgraaf et al. 2011). Recurrent mutations in additional pathways also suggested rational combination therapies including epigenetic modifiers and PI3K/AKT inhibitors, especially in adults. Other options for combination therapies to avoid or delay the development of resistance include drugs targeting PI3K/AKT/mTOR- or PKA-signalling pathways, both mutated in a subset of patients with SHH and both also leading to GLI activation (Milenkovic and Scott 2010, Wang et al. 2012, Metcalfe et al. 2013), or epigenetic drugs. Most MB molecular data have been generated for primary resected tumors, but patients usually die of relapses/metastases that do not respond anymore to therapy. Therefore, it is of utmost importance to gain insight in the molecular alterations that are present in these relapses and/or metastases to improve the survival of these relapsed patients.

1.3.3 Altered signalling pathways

The dysregulation of two evolutionary highly conserved signalling pathways can lead to disturbances of postnatal development of the cerebellar cortex and to the development of medulloblastoma. These pathways are the WNT- and the Sonic hedgehog (SHH)- pathway (Figure 4).

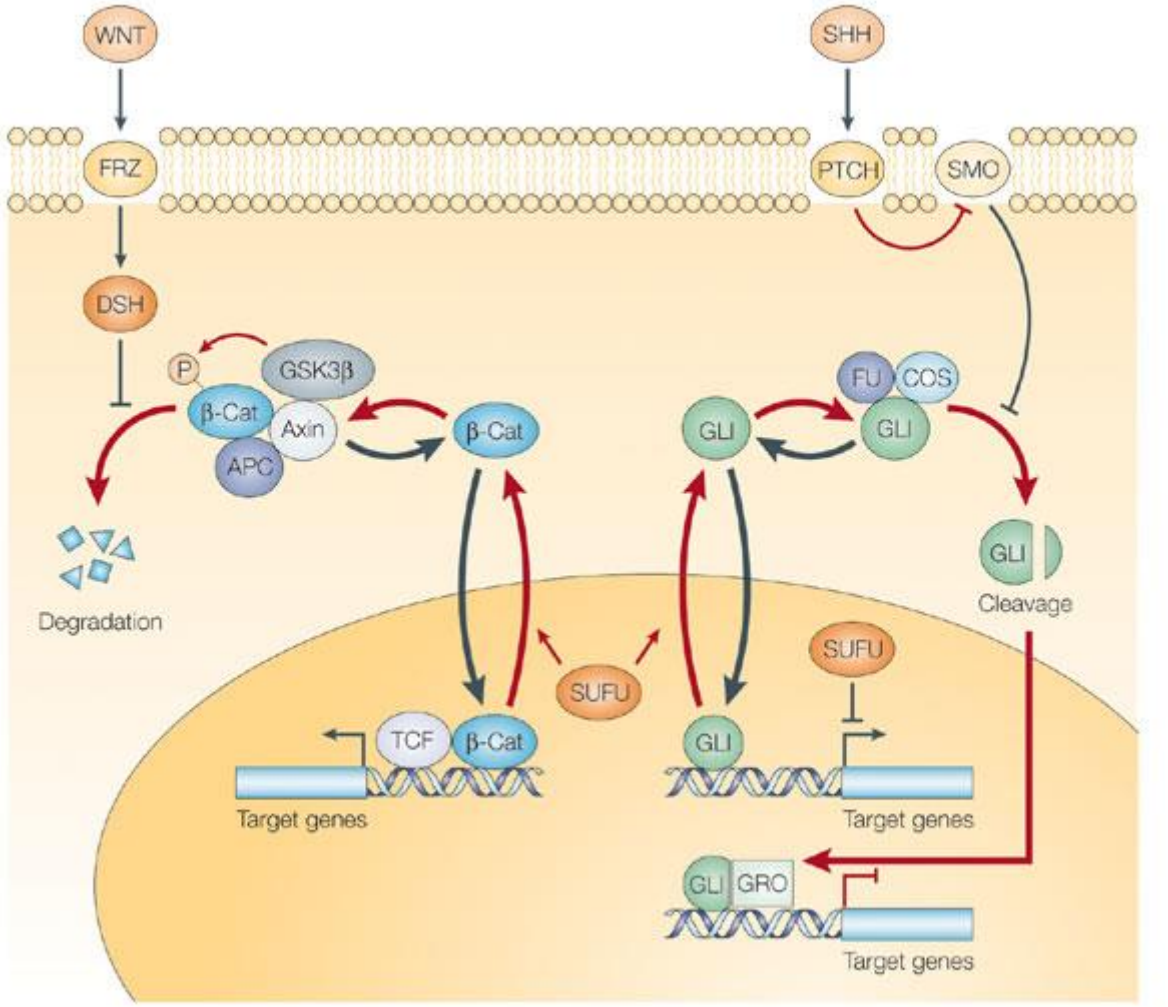

Figure 4 The WNT and SHH pathway. These two major signalling pathways regulate a wide range of developmental events, particularly the proliferation of cerebellar granule cells by sonic hedgehog (SHH). Both pathways have been implicated as targets for disruption in childhood solid tumors (CSTs), including medulloblastoma, a granule-cell-derived brain tumor. WNT and SHH bind to the cell-surface receptors frizzled (FRZ) and patched (PTCH), respectively. Binding of WNT activates its receptor, which then blocks the phosphorylation-activated (by glycogen synthase kinase-3ß (GSK3ß) in a complex with APC and axin) degradation of ß-catenin (ß-Cat). As a consequence, ß-catenin translocates to the nucleus and activates transcriptional events that, in some contexts, promote proliferation. Binding of SHH inhibits PTCH function and so releases smoothened (SMO) to activate intracellular events. SMO represses the cleavage of GLI (the cleaved form has a transcriptional-repressor role in the nucleus), resulting in its release from a complex including fused (FU) and costal (COS). GLI is subsequently translocated to the nucleus and, as a result, activates target genes that, in some contexts, produce a pro-proliferative response. So, there is a great deal of similarity between these two pathways. Furthermore, suppressor of fused (SUFU) represses both pathways by promoting nuclear export of both ß-catenin and GLI. SUFU can also directly repress the transcriptional activity of intact GLI. Mutations in SUFU, ß-catenin, PTCH and SMO have all been implicated as causative events in medulloblastoma. Black steps are activating and red steps are inhibitory. Large arrows indicate movements within the cell, whereas thin arrows represent activating molecular targets. Thin T-bars indicate inhibiting molecular targets. DSH, dishevelled; TCF, T-cell factor; GRO, groucho. (reprinted by permission from Macmillan Publishers ltd: Nature Reviews Cancer (Scotting et al. 2005), copyright (2005), license number 3967661323110)

1.3.3.1 The Wnt pathway

The Wnt (Wingless related integration site) pathway is a highly conserved signalling pathway, which was first discovered due to its role in carcinogenesis (Nusse and Varmus 1982) and body axis formation during embryonic development (Klaus and Birchmeier 2008).

In the inactive state of the WNT signalling pathway, ß-catenin, which is coded by the gene *CTNNB,* is phosphorylated in the cytoplasma of the cell (Amit et al. 2002). ß-catenin is ubiquitinated by a protein complex of APC, Axin, Ck1α and kinase GSK-3ß and thus degraded by the proteasomal route of degradation (Aberle et al. 1997, Behrens et al. 1998, Itoh et al. 1998). After binding of a WNT-agonist to the transmembrane receptor Frizzled, an intracellular signalling cascade leads to the inactivation of the protein kinase GSK-3ß whereby ß-catenin is not phosphorylated anymore (Bhanot et al. 1996, Salic et al. 2000). Hence ß-catenin can't be ubiquitinated anymore and therefore is not degraded. In consequence, ß-catenin reaches the nucleus where it functions as primary effector of the WNT-signalling and leads to the transcription of target genes as *Dkk1, MYC, Axin2* and *CD44* (He et al. 1998, Wielenga et al. 1999, Jho et al. 2002, Chamorro et al. 2005). The WNT pathway is pathologically altered in 10-15% of all medulloblastoma cases which led to the name of the WNT subgroup due to the characteristic activation (Roussel and Hatten 2011). First indications for the involvement of this pathway in the development of medulloblastoma were made due to the fact that patients with the Turcot syndrome, which is caused by mutations in the tumor suppressor gene *APC,* tend to develop colon carcinoma and neuroepithelial brain tumors including medulloblastoma (Hamilton et al. 1995, Marino 2005). In addition, sporadic mutations in the *CTNNB1* gene can often be found in this subgroup, which lead to stabilization of ß-catenin und therefore to the activation of the WNT pathway (Zurawel et al. 1998).

1.3.3.2 The Sonic hedgehog pathway

In the inactive state of the hedgehog pathway, the transmembrane receptor Patched (*PTCH1*) inhibits the G-protein coupled receptor Smoothened (*SMO*) which leads to the inhibition of the whole signalling pathway. Ligands for the Patched receptor in mammals are three different proteins (sonic hedgehog, indian hedgehog, desert hedgehog) (Echelard et al. 1993). Through binding of SHH-ligands to the extracellular domain of the Patched receptor, the inhibition of Smoothened by Patched is removed and the signal is transmitted. Therefore Smoothened migrates into the primary cilium of the cell and causes the dissociation of the protein complex consisting of SUFU (*Suppressor of fused homolog*) and the transcription factors Gli2 and Gli3 (Corbit et al. 2005, Huangfu and Anderson 2006, Wang et al. 2009). After dissociation of SUFU, the transcriptions factors move into the nucleus and there regulate the gene expression (Aza-Blanc et al. 1997, Bai et al. 2002). The Sonic hedgehog pathway is significantly involved in the development of the cerebellum. During the postnatal development of the cerebellum, granule cell precursors move transversally out of the upper rhombic lip over the surface of the cerebellum and there build the external granular layer (EGL) (Altmann 1997). Sonic hedgehog, which is produced by Purkinje cells serves as growth factor for these granule cell precursors and leads to a rapid expansion of this cell population during the postnatal development (Hatten 1999, Wechsler-Reya and Scott 1999). In this context it is not surprising that mutations in genes of this signalling pathway which is important for the proliferation of granule cell precursors were early associated with the development of medulloblastoma. Thus, in patients with a germline mutation in the SHH-receptor *PTCH1* the Gorlin-syndrome is manifested which is featured among other things by a predisposition for medulloblastoma (Bale et al. 1998, Taylor et al. 2000). In a similar way, germline mutations in the SHH-inhibitor *SUFU* also lead to an increased development of medulloblastoma (Taylor et al. 2002, Pastorino et al. 2009, Brugieres et al. 2010). Somatic mutations in genes of the SHH pathway like *PTCH, SMO* and *SUFU*, but also amplifications of the SHH target genes *GLI1* and *GLI2,* were identified in sporadic medulloblastoma and are said to be the reason for the constitutive activation of this signalling pathway (Johnson et al. 1996, Hahn et al. 1999, Northcott et al. 2009, Adamson et al. 2010, Northcott et al. 2011). This spectrum of mutations together with the fact that a subgroup of medulloblastoma show a pathological activation of the SHH pathway indicates that a

dysregulation of this pathway plays an important role in the development of medulloblastoma. Furthermore, dysregulation of the Shh pathway plays a role in the induction of tumors occurring in different human tissues, such as Basal cell carcinoma (Athar et al. 2014) or Pancreatic ductal carcinoma (Lauth and Toftgard 2011). Molecules targeting different components of the Sonic hedgehog pathway, such as the Smoothened inhibitor Vismodegib, have already been subject of clinical trials aiming at the consolidation of novel therapeutic approaches against Shh-driven neoplastic pathologies (Sekulic et al. 2012).

In addition to the molecular distinctions among MB subtypes, a number of signalling pathways are found to be activated across multiple subtypes of the disease. For example, the phosphatidylinositol 3-kinase (PI3K) pathway is activated in WNT (Robinson et al. 2012), SHH (Northcott et al. 2012), and Group 3 MB (Pei et al. 2012), and genes responsible for histone methylation and chromatin remodelling (MLL2, MLL3, KDM6A, EZH2, ZMYM3) are deregulated in both Group 3 and Group 4 MBs (Pugh et al. 2012, Robinson et al. 2012).

1.3.3.3 Interaction of Wnt and Shh signalling

It has been reported that sonic hedgehog (SHH) signalling and Wnt signalling interact in tumors. For example, in colorectal cancer, overexpression of Gli1 (a downstream component of the SHH signalling pathway) inhibits Wnt signalling and colorectal cancer cell proliferation, even in cells possessing the stabilizing mutation of ß-catenin (Akiyoshi et al. 2006). In neural progenitors, Wnt signalling and SHH signalling coordinately regulate cell cycle progression, with SHH signalling activation required upstream (Alvarez-Medina et al. 2009). The Wnt/beta-catenin and the Hedgehog (Hh) pathway interact in various cell types while eliciting opposing or synergistic cellular effects. Both pathways are known as exclusive drivers of two distinct molecular subtypes of MB. In sonic hedgehog (Shh)-driven MB, activation of Wnt signalling has been shown to suppress tumor growth by either beta-catenin-dependent or -independent inhibition of Shh signalling (Anne et al. 2013, Peng et al. 2013, Pöschl et al. 2014). However, neither mechanistic insight into β-catenin-mediated inhibition of the Hh pathway, nor the

therapeutic potential of Wnt/β-catenin-activating drugs has been examined specifically in MB. Recently, Zinke et al. propose that beta-catenin stabilization increases its physical interaction with Gli1, leading to Gli1 degradation and inhibition of Hh signalling, thereby promoting tumor cell senescence and suppression of "tumor take" in mice (Zinke et al. 2015).

1.3.4 Mouse models

In order to better understand and analyse genetic, molecular and cytological influences on the development of medulloblastoma, different mouse models are available, which are based on different mutations and genetic systems depending on the group of tumor.

It is currently thought that tumor cells of the SHH type of medulloblastoma originate from the granule cell progenitors in the external granular layer. Indeed the vast majority of these cells express markers of the proliferating external granular layer, the most common of which is ATOH1 (MATH1). More recently, it was demonstrated that Atoh1 protein expression was crucial for the progression of this type of tumor (Flora et al. 2009) because this transcription factor potently regulates the proliferation of granule cell progenitors in mice (Klisch et al. 2011). This likely occurs by Atoh1 maintaining the sensitivity of progenitor cells to Shh signalling through transcriptional activation of the Gli2 gene. Moreover, several groups have generated mouse models for key elements of the SHH subgroup of human medulloblastomas.

One of the first and most used genetically engineered mouse model (GEMM) for the Shh-associated medulloblastoma is based on a conventional knockout of the Shh-repressor Patched (Ptch1). This first *Ptch*$^{+/-}$ mouse model was generated by homologous recombination in embryonic stem cells, in which part of *Ptch* exon 1 (including the putative start codon) and all of exon 2 were replaced with *lacZ* and a neomycin resistance gene (Goodrich et al. 1997). Homozygous deletion of *Ptch1* (*Ptch1*$^{-/-}$) in the mouse is embryonic lethal, but 20% of mice with a heterozygous *Ptch1*-knockout (*Ptch1*$^{+/-}$) develop tumors in the cerebellum, which are molecularly very similar to human medulloblastoma (Goodrich et al. 1997, Hahn et al. 2000). Simultaneous loss of the tumor suppressor *p53* (*Tp53*$^{-/-}$) leads to a tumor incidence of 100% and illustrates cooperative functional

mechanisms in tumor development (Wetmore et al. 2001). Similar effects were observed in knockouts of cell cycle regulators p18-Ink4c and p27-Kip in *Ptch1*$^{+/-}$ mice (Uziel et al. 2005, Uziel et al. 2006, Ayrault et al. 2009). A disadvantage of the Ptch1 mouse model for development of medulloblastoma is the simultaneous appearance of soft tissue tumors (Wetmore et al. 2001, Lee et al. 2006).

Activation of other components of the Shh pathway can also lead to the development of medulloblastoma. It has been shown via RCAS/TVA-systems that Nestin-positive precursor cells can develop medulloblastoma in 10-15% of cases after transduction with RCAS-based retrovirus which are coding for Shh (Rao et al. 2003, Broderick et al. 2004, Browd et al. 2006, Binning et al. 2008). Here RCAS (replication competent ASLV long terminal repeat with Splice acceptor)-based retrovirus can just transduce cells which express TVA (avian retrovirus receptor) under the Nestin promoter and therefore enables a cell-specific activation of the Shh pathway.

A very robust mouse model for Shh-associated medulloblastoma was generated by expression of a constitutive activated form of the *Smoothened* gene (SmoA1) under the granule cell precursor specific promoter ND2 (Hallahan et al. 2004, Hatton et al. 2008). Almost 100% of the animals developed a tumor which also metastasizes in the leptomeningeal region, a characteristic of many human tumors. Analogous to RCAS-based mouse model mentioned above, tumor development outside the CNS can be avoided.

At the moment the most popular mouse models for Shh-associated medulloblastoma are based on conditional systems like the Cre/loxP-recombination system, which allows a tissue- and cell type-specific recombination and therefore manipulation. Independent of the temporal activity of the promoter, mutations are activated cell type specifically by injection of an oestrogen analogue (Tamoxifen) (Leone et al. 2003, Erdmann et al. 2007, Arnold et al. 2011). The cell type specific activation of the Shh pathway with special Cre mouse strains (*Math1-cre* for granule cell precursors, *hGFAP-cre* for neural precursors) increased the tumor penetrance up to 100% without a simultaneous knockout of further tumor suppressors. Therefore the Shh-repressor *Ptch1* is promoter specifically deleted or a constitutive activated form of *Smoothened* gene (SmoM2-YFP) is transcribed, what is leading, in both cases, to an activation of Shh signalling and a subsequent development of medulloblastoma (Mao et al. 2006, Schüller et al. 2008, Yang et al. 2008).

While all mouse models mentioned above imitate human SHH-associated medulloblastoma, the number of mouse models for WNT-, Group 3- and Group 4-subgroups are very limited. Recently a mouse model for human WNT-associated medulloblastoma was described (Gibson et al. 2010). Here tumors were generated through activation of the Wnt pathway in cell populations of the dorsal brainstem with a simultaneous knockout of the tumor suppressor p53, which are molecularly similar to human WNT-medulloblastoma. For the first time it was shown that the cell of origin of WNT medulloblastoma lies not necessarily in the cerebellum. Interestingly, the comparison of the model for Shh- and Wnt-associated medulloblastoma showed that they really develop from different cell of origins (Gibson et al. 2010). Shh-medulloblastoma develop from the upper part of the rhombic lip, or in the auditory part of the lower rhombic lip, whereas Wnt-tumors develop in the precerebellar part of the lower rhombic lip (Grammel et al. 2012).

Limited data from two different mouse models for Group 3 medulloblastoma were generated through expression of *c-MYC* in cerebellar precursor cells and an additional knockout of p53 (Kawauchi et al. 2012, Pei et al. 2012). The fact that Group 3 medulloblastoma are the most aggressive subgroup with the least survival rate, illustrates the need to generate appropriate mouse models for this subgroup with regard to preclinical studies.

For Group 4 medulloblastoma no reliable mouse model exists at the moment.

1.4 Aim of the study

My focus of research is the development, diagnosis and therapy of medulloblastoma, the most malignant brain tumor in children. Medulloblastoma possibly develop very early, already during embryonic development.

Recent clinical trials for SHH-MB using SMO antagonists showed highly variable clinical responses including a large proportion of striking durable responders, but also a lot of non-responders. Recent sequencing data from an unprecedented series of SHH-MB (n=133) showed that about half of pediatric SHH-MB are predicted to be primarily resistant to these drugs because of mutations downstream of SMO. Moreover, it is known that some initially responsive tumors may also rapidly acquire secondary resistance to treatment, whereas other patients keep in remission for several years on a single targeted drug.

One part of this study deals with the localization of SHH MBs. Since we know that the localization of human SHH MBs differs depending on the age of the patient, we wanted to analyse this statement more precisely at different ages in an already existing mouse model for SHH MBs. The aim is to determine if such murine SHH MBs develop at special time points and/or at defined localizations.

Another point of this study intends to investigate the diverging role of synchronistic Wnt and Shh activation and deals with the question whether the physiological roles of Wnt/ß-catenin signalling can be utilized to treat Shh-medulloblastomas. *In vitro* experiments were carried out, aiming at the possible use of Lithium, a Wnt activator, in the therapy of Shh-driven medulloblastoma.

Finally, we aimed at a better understanding of the mechanisms in MB of primary and secondary resistance to various drugs targeting the hedgehog pathway. To this end, we generated, characterized and used genetically engineered mouse models (GEMMs) of SHH-MB. We aimed to further expand our pre-existing repertoire of murine SHH-activated MB models in order to have a spectrum of tumors that are driven by mutations at different levels of the Hh pathway, such as in *PTCH1, SMO* or *MYCN,* and with different combinations of other mutations in additional pathway that may co-operate with Hh

signalling (e.g. *TP53* or *PIK3CA*). We treated some of these models with drugs targeting the Hh pathway. We tested LDE225, a SMO inhibitor that already have entered clinical trials. Mice were monitored for treatment response, development of secondary drug resistance, and overall survival. Tumors will be molecularly characterized by sequencing and gene expression profiling, and data will be compared to untreated tumors.

2 Materials and methods

2.1 Experimental animal studies

2.1.1 Mouse strains

In this work wild type mice of the strains *C57/Bl6* and *FVB* and a number of transgenic mouse models were used. *SmoM2-YFP*$^{Fl/Fl}$ (Mao et al. 2006), *aiTdTomato* (Madisen et al. (2010), *Ptch1*$^{+/-}$ (Goodrich et al. 1997, Oliver et al. 2005), *Ctnnb1(ex3)*$^{Fl/Fl}$ (Harada et al., 1999; Pöschl et al., 2013), *GSK3ß*$^{Fl/Fl}$ (Jaworski et al., 2011), *Math1-GFP* (Lumpkin et al., 2003), *Ptch1*$^{Fl/Fl}$ (Uhmann et al., 2007), *Pik3ca*^{H1047R} (Adams et al., 2011), *P53* (Marino et al., 2000), *lsl-Mycn* (Althoff et al., 2015).

In addition, the driver lines *Math1-cre* (Matei et al., 2005; Schüller et al., 2007) and *Math1-creER*^{T2} (Machold and Fishell, 2005) were used.

Mice were hold in a SPF-animal facility (specific-pathogen-free) in individually ventilated cages (IVC) with a constant light-dark rhythm of 12/12 hours. Food and water were given *ad libitum*. For preparation of the brain adult mice were sacrificed by cervical dislocation. Animals under 10 days were sacrificed by decapitation. For removal of the brain the cranial bone was opened and removed until the surface was laid open from the olfactory bulb anterior till the hindbrain. The brain was lifted out of the skull by cutting through the optical nerve at the optic chiasm and the brain nerves under the brain stem.

All experimental procedures were approved by the Government of Upper Bavaria, Germany (Reference number 55.2-1-54-2532-10-14 and 55.2-1-55-2532-56-15).

2.1.1.1 Conditional knockout mice

By mating a cre-driverline with one or more transgenic mouse strains, conditional Cre-loxP-systems are created. This means that the cre-recombinase is expressed under the promoter (here *Math1-cre*), which is able to initiate recombination between so called *lox-P-Sites* on the DNA and therefore delete everything located between the *lox-P-Sites.*

2.1.1.2 Inducible knockout mice

By induction with the oestrogen analogue tamoxifen mutations can be created under the *Math1*-promoter (*Math1-creER^{T2}*) at defined time points. Mice with this genetic background express the transgene after successful recombination promoter-specific. Under the *Math1*-promoter a transgenic oestrogen receptor is expressed which allows the translocation of the cre-recombinase from the cytoplasm into the nucleus only after binding of tamoxifen. Here the enzyme can remove the STOP-sequences in front of the genes by recombination. Thus the expression of the transgene depends on the activity of the *Math1*-promoter and the time point of the tamoxifen induction.

2.1.2 Tamoxifen induction and BrdU pulse

The tamoxifen-inducible mouse model *Math1-creER^{T2}* makes it possible to activate the cre recombinase specifically during the postnatal development in Math1-positive granule cell precursors of the cerebellum. The fusion protein of the cre recombinase and a mutated form of the human oestrogen receptor is expressed under the Math1-promoter in this mouse line, but it is retained in the cytoplasm of the cell. Only after tamoxifen induction it reaches the nucleus and became active (Feil et al., 1997; Helms et al., 2000; Machold and Fishell, 2005). Mice with this inducible cre system were induced by tamoxifen (Sigma Aldrich) either at postnatal day 3 or 5 or pregnant dams were induced at embryonic day 14.5. Therefore 1 mg tamoxifen (in cornoil) is administered intraperitoneal (i.p.).

For analysis of the proliferation rate of cerebellar granule cells *in vivo* in different mouse models a bromodesoxyuridine (BrdU)–pulse was performed and mice were sacrificed 2 hours later. Therefore the animals were administered 25 µg/g body weight intraperitoneal. BrdU is integrated in the DNA as a chemical analogue of the nucleoside thymidine and can be verified immunohistochemically afterwards. After a 2 hour BrdU-pulse, cells which were in the S–phase of the cell cycle can be verified.

2.1.3 Treatment of mice with LDE225 *in vivo*

Mice (*Math1creER^{T2}::lsl-SmoM2$^{Fl/+}$, Math1-creER^{T2}::lsl-SmoM2$^{Fl/+}$ lsl-Pik3ca$^{Fl/+}$ and Math1creER^{T2}::Ptch1$^{Fl/Fl}$)* were treated with the hedgehog inhibitor (via smoothened antagonism) LDE225, also known as Sonidegib/Erismodegib (sponsored by Novartis; marketed as Odomzo). Treatment start was at postnatal day 30 or 20. Each mouse was treated 5 times per week for three weeks long with a dose of 30 mg/kg/day (i.p.). LDE225 was dissolved in DMSO and this solution was then mixed with 40% polyethylene glycol (PEG). Each injection was 100 µl i.p. (5 µl LDE225 dissolved in DMSO + 95 µl 40% PEG were mixed directly before usage). The vehicle group was treated with 5 µl DMSO + 95 µl 40% PEG.

2.1.4 DNA extraction and genotyping

DNA for genotype verification through PCR and electrophoresis was extracted from mouse tail (early postnatal stages) or ear biopsies (older than 3 weeks). Each biopsy was first treated with 500 µl Laird´s lyses buffer (200 mM NaCl, 100 mM Tris buffer (pH 8.5), 5 mM EDTA, 0.2% SDS) and 10 µl Proteinase K (10 mg/ml) on a thermo-shaker at 56°C for at least 2 hours. Samples were than centrifuged (14.000 U) at room temperature for 5 minutes. The supernatant containing the DNA was then extracted into a new tube and 500 µl Isopropanol were added. After mixing, the precipitated DNA became visible. Centrifugation at room temperature with 14.000 U for 5 minutes was repeated. Finally, the remaining Isopropanol was discarded and the DNA pellet was resuspended in TE-Buffer (20 nM Tris-HCl pH 8.3, 1 mM EDTA in ddH_2O) and then stored at 4°C.

The genomic DNA (gDNA) is the starting material for genotyping. Therefore genotype-specific regions of the genome were amplified by polymerase chain reaction (PCR). Primers are listed in Table 1 according to primary descriptions of the mouse strains in original publications.

Primer name	Sequence 5' – 3'	Product length
Cre-Fw	TCCGGGCTGCCACGACCAA	
Cre-Rv	GGCGCGGCAACACCATTTT	448 bp
SmoM2-YFP Mut-Fw	GAACGGCATCAAGGTGAA	
SmoM2-YFP Mut-Rv	CGATGGGGGTGTTCTGCT	109 bp
SmoM2-YFP WT-Fw	GGAGCGGGAGAAATGGATATG	
SmoM2-YFP WT-Rv	CGTGATCTGCAACTCCAGTC	410 bp
tdTomato Mu-Fw	GGCATTAAAGCAGCGTATCC	
tdTomato Mu-Rv	CTGTTCCTGTACGGCATGG	196 bp
tdTomato WT-Fw	AAGGGAGCTGCAGTGGAGTA	
tdTomato WT-Rv	CCGAAAATCTGTGGGAAGTC	297 bp
Ctnnb1(ex3)$^{Fl/Fl}$ Fw	CGTGGACAATGGCTACTCAA	330 bp (wildtype),
Ctnnb1(ex3)$^{Fl/Fl}$ Rv	TGTCCAACTCCATCAGGTCA	500 bp (mutant)
GSK3ß Fw	TCTGGGCTATAGCTATCTAG	302 bp (wildtype),
GSK3ß Rv	CGAAAGTGATTGGAAATGGA	488 bp (mutant)
Math1 GFP Mut Rv	AGGGTCAGCTTGCCGTAGGT	
Math1 GFP Fw	GCGATGATGGCACAGAAGG	200 bp (wildtype),
Math1 GFP WT Rv	GAAGGGCATTTGGTTGTCTCAG	314 bp (mutant)
MYCN MU Fw	ACCACAAGGCCCTCAGTACC	
MYCN MU Rev	TGGGACGCACAGTGATGG	168 bp
MYCN WT Fw	CTCTTCCCTCGTGATCTGCAACTCC	
MYCN WT Rev	CATGTCTTTAATCTACCTCGATGG	299 bp
P53 Fw	CACAAAAAACAGGTTAAACCCAGC	288 bp (wildtype),
P53 Rv	GCACCTTTGATCCCAGCACATA	370 bp (mutant)
Ptch1 Fl Fw	TTCATTGAACCTTGGGGAAC	216 bp (wildtype),
Ptch1 Fl Rv	AGTGCGTGACACAGATCAGC	269 bp (mutant)
Ptch1 ko Fw	TTCACTGGCCGTCGTTTTACAACGTCGTGA	
Ptch1 ko Rv	ATGTGAGCGAGTAACAACCCGTCGGATTCT	364 bp
Pik3ca 1	AAAGTCGCTCTGAGTTGTTAT	600 bp (wildtype),
Pik3ca 2	GCGAAGAGTTTGTCCTCAACC	310 (mutant),
Pik3ca 3	GGAGCGGGAGAAATGGATATG	410 bp (Pi3k)

Table 1 List of primers for genotyping.

Standard conditions the genotyping PCR are as follows (Table 2):

step	temperature [°C]	time [s]	
pre-incubation	95	120	
denaturation	95	30	
primer hybridisation	60	30	35 cycles
elongation	72	60	
stop	4	∞	

Table 2 PCR conditions for genotyping.

Analysis of the amplified DNA-fragments was carried out by 1% agarose gels and the Syngene gel documentation system (Synoptics Limited).

2.1.5 Primary cell culture

2.1.5.1 Cerebellar granule neuron precursor cells

Well plates were coated with 1x poly-L-ornithine (PLO) (Sigma) from a 100x stock (10 mg/ml). Dilution was carried out in H_2O and 0.2 µM sterile filters were used in order to preserve poly-L-ornithine. The plates were than incubated at 37°C during mouse preparation allowing poly-ornithine to polymerise. Mouse cerebella were dissected at postnatal day 5-7 and put on ice in 15 ml Hanks buffered saline solution (Gibco, pH 7.4 Glucose 6 mg/L). After centrifugation at 4°C for 5 minutes with 800 rpm, HBSS was discarded. 1 ml of 1x Trypsin/EDTA/DNAse (100 µg DNAse/ml, both Trypsin/EDTA and DNAse were from Sigma) was added and the cerebella were left 10 minutes in water bath for incubation. Trypsin was then inactivated with 2 ml of DMEM-F12 +10% fetal bovine serum (fetal bovine serum was inactivated at 56°C for 30 minutes prior to usage). Next, the cerebella were centrifuged at 4°C with 1500 g for 5 minutes. The fetal bovine serum medium was aspirated and substituted with 5 ml HBSS solution. The pellets were dissolved by pipetting gently and a new centrifugation step (as above) was conducted. After discarding supernatant HBSS, the pellets were resuspended in 1 ml HBSS and spun

as above. The HBSS remnant was extracted and the cells were put into suspension with culture medium with supplements (DMEM-F12, 1% N2 Supplement, 1% Penicillin/Streptomycin, 0.25 mM KCl with 10% FCS. All reagents were from Invitrogen). The poly-L-ornithine solution was removed and each well was washed with PBS once. Granule neuron precursors were then plated in serum-free culture medium with supplements at a concentration of 1 million cells/well and grown at 37°C and 5% CO_2. After 6-12 hours the medium was removed and culture medium with Shh-protein (3 µg/ml) was added. Due to culturing with this medium for at least 24 hours, all cells except cerebellar granule cells leave the cell cycle and a homogeneous proliferating granule cell population remained. For transduction of granule cells with *IRES-GFP* and *Cre-IRES-GFP* virus, the medium was removed and the virus supernatant (see 2.5.3 production of retroviral particles) was added to the cells for 4 hours. Due to the fact that retrovirus just transduce proliferating cells and culturing in selective Shh-medium, it was prevented that other cell types than granule cells could be transduced with the virus. After virus transduction cells were again cultured in culture medium with Shh-protein for 24 hours. For analysis of the proliferation rate bromodesoxyuridin (BrdU, 25 µg/ml) was added to the medium, and cells were fixed after two hours with 4% paraformaldehyde.

2.1.5.2 Tumor cells

Tumor cell culture was performed as described for culturing GNPs with the following exceptions: tumor cells were maintained in Neurobasal medium containing B27 supplement, human FGF (20 ng/ml), mouse EGF (20 ng/ml), glutamin (2 mM) and Pen/Strep (100 µg/ml). Here no Shh-protein was added to the medium because cultured tumor cells from our mouse strains for Shh-associated medulloblastoma have a constitutive activated Shh signalling pathway anyway.

2.2 Histology and immunohistochemistry

For all histological methods, brains were dissected, fixed overnight in 4% paraformaldehyde, embedded in paraffin, and sectioned at 5 µm according to standard protocols. Paraffin sections were deparaffinised with xylene and rehydrated in a graded alcohol series. In general morphology was analysed with Hematoxylin and eosin (H&E) stains. H&E stains were performed according to standard protocols.

All histological photomicrographs were taken digitally using an Olympus BX50 microscope in combination with the ColorView (Soft Imaging System).

For immunohistochemistry, paraffin sections were subjected to heat antigen retrieval at 100°C for 20 min in 10 mM sodium citrate buffer for all antibodies. For inactivation of the endogene peroxidase all slides were incubated in 5% H_2O_2 in methanol. Then the slides were washed in PBS, blocked for 30 min in I-Block reagent (Invitrogen) and incubated over night with the primary antibody at 4°C.

All primary antibodies for immunohistochemistry and immunocytochemistry are listed in Table 3.

antibody	species	Catalog #	vendor/provider
BrdU	mouse	10198	Bioscience Products
BrdU	rat	ab6326	Abcam
GFP	rabbit	sc-9334	Santa Cruz
Ki67	rabbit	ab16667	Abcam
RFP	rabbit	AA234	Antibodies online
Sox2	mouse	ab79352	Abcam
Sox2	rabbit	ab97959	Abcam

Table 3 Primary antibodies for immunohistochemistry and immunocytochemistry.

Staining was performed using the HRP/DAB staining system (DAKO) according to the manufacturer's specifications. For immunofluorescence staining slides were washed with

PBS after incubation with the first antibody and incubated with a species-specific, fluorophore-coupled secondary antibody (Alexa 488 and Alexa 546, Invitrogen). Staining of the nuclei was done by 4',6-Diamidin-2-phenylindol (DAPI; Roth). For fluorescent staining of cell culture the same protocol was used as for immunofluorescence staining, but without deparaffination and rehydration. Pictures of fluorescent staining were taken with an Olympus IX50 microscope.

2.2.1 BrdU staining

The immunohistochemical detection of the incorporation of the base analogue BrdU in the DNA instead of the physiological nucleoside thymidine requires another pre-treatment before the incubation with the first antibody. To permit the access for the BrdU-specific antibody to the antigene, DNA has to be denaturated with 2N HCl for 10 min and then the acid has to be neutralized with 0.1 M sodium borat buffer (pH 8.5), not to impair the structure of the primary antibody.

2.3 Molecular biological methods

2.3.1 RNA extraction, cDNA synthesis and qRT-PCR

Both cultured cells and tissue samples were first put into Eppendorf tubes and homogenised with 750 µl TRlzol® (Invitrogen) reagent using a pipette, before proceeding with RNA extraction. The homogenised samples were let sit at room temperature for about 5 min. 150 µl of chloroform were added to each tube. After mixing for 15 sec, the samples were incubated at room temperature for 3 min. A centrifugation step with 14.000 rpm at 4°C was conducted for 15 min, after which the supernatant, RNA-containing top layer was extracted into a new Eppendorf tube. The RNA was then precipitated with cold (4°C) isopropanol and incubated at room temperature for 10 min. A centrifugation step was repeated as described above. Eventually, the RNA pellet became visible at the bottom of the tubes. The supernatant liquid was discarded and the RNA pellet was washed with 75% ethanol. After brief shaking, each sample was centrifuged for 5 min at 4°C with 7500 rpm. Ethanol was discarded, and the RNA pellets were resuspended in 24 µl DEPC water each. The RNA concentration was determined through Nanodrop 3300 technology (Thermo Fischer Scientific). cDNA synthesis for RT-PCR was performed using SuperScript® III First-Strand Synthesis Supermix (Invitrogen). Each component was mixed and centrifuged before use. For each RNA sample the reaction mix consisted of the following reagents: 6 µl of RNA (in DEPC water, up to 5 µg RNA), 0.5 µl oligo(dT)$_{20}$ primer (50 µM), 0.5 µl of random hexamers (50 ng/µl), 1 µl annealing buffer, RNAse/DNAse-free water to bring the total volume up to 8 µl. After heating at 65°C for 5 min in a thermo-cycler, the tubes were put on ice for 1 min. Leaving the tubes on ice, the following solutions were added to each reaction mix: 10 µl First-Strand Reaction Mix (2x), 2 µl SuperScript® III/ RNaseOUT™ Enzyme Mix. The tubes were than mixed by vortexing and centrifuged briefly. The samples were incubated in a thermo-cycler for 5 min at 25°C, 50 min at 50°C and finally at 85°C for 5 min. Finally, the cDNA was cooled down on ice and stored at -20°C.

Quantitative real-time PCR (qRT-PCR) was carried out using the LightCycler® 480 (Roche) technology and the LightCycler® 480 SYBR Green I Master Mix (Roche). SYBR Green is a fluorescent cDNA-intercalating dye, which is detected and quantified after each elongation step, therefore allowing cDNA quantification in real time. Each reaction mix

contained the following agents: FastStart Taq DNA Polymerase and SYBR Green dye (Roche), 3 µl of cDNA, 1 µl forward primer and 1 µl reverse primer (primer stocks concentration: 100 pmol/µl). Before usage, each primer was diluted 1:10 in DNAse free water. A RT-PCR program was conducted, which included the following steps: heat shock at 95°C for 5 min, then 45-cycles containing the following steps: denaturation at 95°C for 10 seconds, annealing at 57-62°C for 10 seconds, elongation at 72°C for 15 seconds. Relative quantification was achieved by comparing cDNA levels between target genes and housekeeper genes (*β2-Microglobulin* (*β2M*)). Besides this, a calibrating sample was used for each LightCycler® run within a single experiment, in order to compensate variations of the reaction mix composition. All samples were analysed in triplicates. The following formula was applied for relative quantification:

$$NR = E_T^{\,CpT(C) - CpT(S)} \times E_R^{\,CpR(S) - CpR(C)}$$

NR=normalized ratio, E=primer efficiency, T=target gene, C=calibrating sample, R=housekeeper gene, S=sample, Cp=crossing point (number of cycles after which the SYBR Green detection threshold is reached).

All primers were designed using the Primer3 software and ordered from Eurofins Genomics. Amplicon melting curves were analysed to determine the presence of a single PCR product, primer quality and primer efficiencies were calculated based on standard curves. Table 4 shows primer pairs sequences and efficiencies.

gene	sequence	efficiency	annealing
β2M Fw	CCTGGTCTTTCTGGTGCTTG	2.23	60°C
β2M Rv	TATGTTCGGCTTCCCATTCT		
Axin2 Fw	GCTGGTTGTCACCTACTTTTTCT	1.81	62°C
Axin2 Rv	ATTCGTCACTCGCCTTCTTG		
Gli1 Fw	CGCCCCGACGGAGGTCTCTT	1.964	60°C
Gli2 Rv	GCTGGCCGTCCCAACTGCTT		

Table 4 Primers for qRT-PCR.

Standard conditions for RT-PCR are summarized in Table 5.

step	detection mode	temperature [°C]	time [s]	
preincubation		95	300	
denaturation		95	10	
primer hypridisation	single	60	10	45 cycles
elongation		72	20	
melting curve analysis	continuous	40-95	300	
stop		4	∞	

Table 5 Conditions for qRT-PCR.

2.3.2 Production of retroviral particles

Retroviral particle for transduction of primary mouse cells were produced by transfection of human HEK293T cells (*American Type Culture Collection*, ATCC). The work with eukaryotic cells was done with sterile vessels and solutions in a sterile environment (HERAsafe, Thermo). HEK293T cells were cultured in incubators at 37°C and 5% CO_2. For production of retroviral particles, HEK239T cells were transfected in a triple-transfection with two helper plasmids (pCMV-VsVg and pCMV-gag-pol) and each with a retroviral construct with only IRES (internal ribosome entry-site)-GFP or with a Cre (Cre-recombinase)-IRES-GFP sequence using the transfection reagent X-tremeGENE HP (Roche). The medium was replaced after 24 hours with normal culture medium (DMEM medium, 10% foetal calf serum, 1% Glutamax). The supernatant of the retroviral medium was taken up to 4 days after transfection and cleaned with 0.45 mm filters and stored at -80°C.

2.3.3 Colorimetric MTT-assay

The colorimetric MTT (3-(4,5-dimethylthiazol-2-yl)-2,5-diphenyltetrazolium bromide)-assay is a spectrophotometer-based method used to quantify cell growth or cytotoxicity rates (Finlay et al. 1986, Vistica et al. 1991). The tetrazolium salt MTT is chemically

reduced by ribosomes in metabolic active cells, forming formazan crystals. The resulting change of solution colour is than quantified through spectrophotometric absorbance measure. For this work, the Cell Proliferation Kit I (MTT) from Roche was used. Cells were first seeded in 100 µl in 96-well plates at a concentration of $2x10^4$/well and incubated (37°C) in neurobasal culture medium with supplements (see also 2.1.5 Primary cell culture) for 16 hours. Spectrophotometric absorbance was determined using the FLUOstar Optima (BMG labtech) system. For lithium chloride treatment, start point of therapy was defined by adding 10 µl of the MTT reagent to at least three wells and adding the Solubilisation solution (100 µl) after 4 hours, in order to quantify cell viability at time point 0 (T_0). After 24 hours (T_1), 10 µl of the MTT reagent were put into the remaining wells (at least in triplicates) for 4 hours, after which, the Solubilisation solution (100 µl) was added into each well. One well was left without MTT and served as a blank sample. The plates were let sit in the incubator overnight and the optical density (OD) at T_0 and T_1 was determined as follows: $OD_T - OD_{blank}$. Cell viability after 24 hours (T_1) was calculated using the following formula: $OD_{T0}/OD_{T1} = 100\%/x$.

2.3.4 Cell Lines

HEK 293T cells arise from human embryonic kidney cells, which were originally transformed with Adenovirus 5 DNA (Graham et al. 1977). UW473 are a human medulloblastoma cell line obtained from a pediatric tumor sample (Bobola et al. 2005, Castro-Gamero et al. 2013). GL261 cells derive from the GL261 mouse glioma model. This murine model was first developed through application of a chemical carcinogen into the brain of C57BL/6 mice and then perpetuated by means of syngeneic transplantation (Maes et al. 2011). All three cell lines proliferated as adherent monolayers and were cultured in DMEM medium with 10% fetal calf serum, 1% Glutamax (Invitrogen), 1% Penicillin/Streptomycin (Invitrogen) and 1% HEPES buffer (Sigma).

2.3.5 Lithium chloride treatment *in vitro*

In our *in vitro* setting, lithium chloride was balanced with NaCl in order to achieve equal salt concentrations of 25 mM in every well.

2.4 Statistical analyses

The Prism5.02 software (GraphPad) was used for statistical analysis. Survival data were obtained through Kaplan-Meier curves and the Log-rank test served as significance test. P-values < 0.05 were considered as significant. When comparing two groups with assumed Gaussian distribution and equal variances, the unpaired t-test was conducted. In case of not equal variances or an expected non-Gaussian distribution, the non-parametric Mann-Whitney test was used. For testing distributions for their significance between two groups, the χ^2 test was used. For RT-PCR and MTT-assays a number of at least three samples was analysed for each experimental condition or mouse genotype.

3 Results

3.1 Establishment and characterisation of mouse models for SHH medulloblastoma

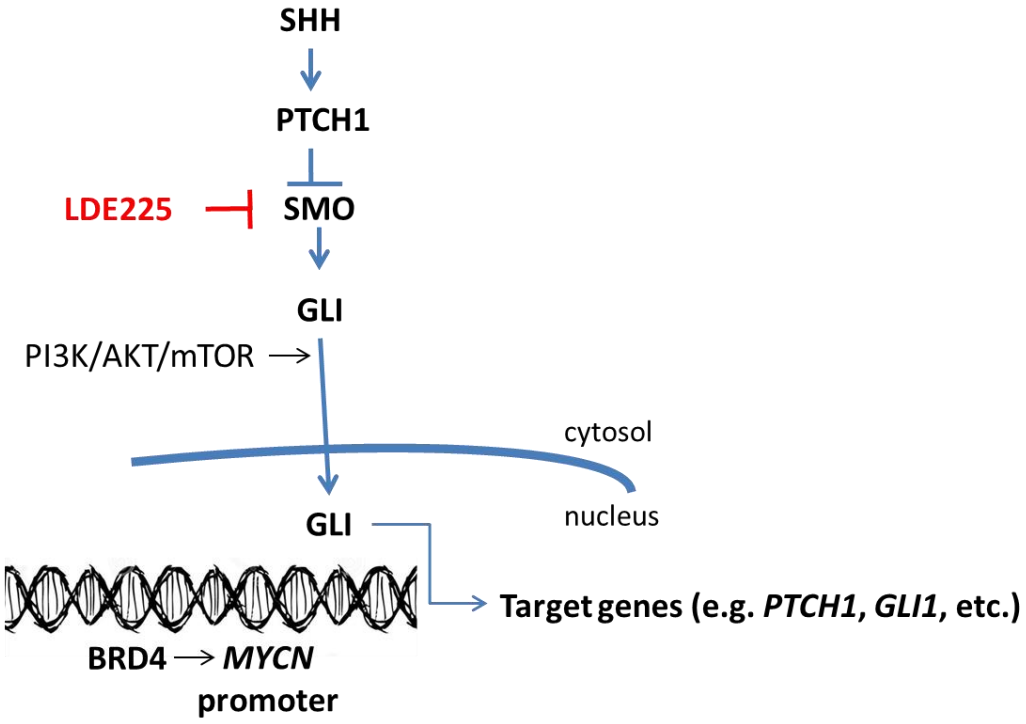

Figure 5 Hh signalling pathway. Binding of SHH to PTCH1 releases PTCH1-mediated inhibition of SMO, resulting in activation of GLI transcription factors and expression of target genes. PI3K/AKT/mTOR enhance GLI1 activity. BRD4 (bromodomain 4) binds to the *MYCN* promoter. The pharmacological inhibitor LDE225 is indicated in red.

Components of the canonical Hh signalling pathway are Hh ligands such as sonic hedgehog (SHH), the transmembrane protein PTCH1 that acts as a receptor for Hh ligands, SMO, a transmembrane protein and signalling partner of PTCH1, and the family of GLI transcription factors (Zibat et al. 2010). In the absence of SHH, PTCH1 inhibits SMO. Binding of SHH to PTCH1 suspends this PTCH1-mediated inhibition of SMO, which in turn activates GLI transcription factors, resulting in the expression of target genes including GLI1. GLI1 activity is increased upon its phosphorylation by e.g. PI3K/AKT/mTOR (Figure 5).

Recent clinical trials for SHH-MB using SMO antagonists showed highly variable clinical responses including a large proportion of striking durable responders, but also a lot of non-responders. Recent sequencing data (Kool et al. 2014) from an unprecedented series of SHH-MB (n = 133) showed that about half of pediatric SHH-MB are predicted to be primarily resistant to these drugs because of mutations downstream of SMO. Moreover, it is known that some initially responsive tumors may also rapidly acquire secondary resistance to treatment, whereas other patients keep in remission for several years on a single targeted drug.

In order to establish novel therapies that are based on the individual genetic and molecular profile of a patient's SHH-MB, we wanted to expand our battery of genetically engineered mouse models (GEMMs) based on mutations at different levels of the Hh signalling cascade. Apart from using already established mice with mutations in *PTCH1* and *SMO* we wanted to generate novel additional models that faithfully model human SHH-MB with amplifications of e.g. *MYCN*. All these models are also be modified with respect to additional mutations in *TP53* or *PIK3CA*, strictly representing the findings in human SHH-MB.

All mice were exposed to tamoxifen and monitored for symptoms of tumor growth, head growth, drinking behaviour, movements, weight and neurological symptoms, such as ataxia, paralysis or seizures. Animals that developed symptoms were sacrificed and one half of the cerebella were subjected to histological analysis to confirm the presence of tumors, and of the other half of the cerebella tumor tissue was harvested for further analysis.

3.1.1 Mouse model with *SMO* mutation

Here we used the Cre-LoxP-recombination system to ensure the constitutive activation of the Shh pathway. Therefore the enzyme cre-recombinase is able to cut out so called floxed sequences in the genome of mice, which are framed by loxP-sequences *in vivo*. For the constitutive activation of the Shh pathway a floxed mouse strain was available which allows a cre-mediated, conditional expression of a mutated *Smo*-allele (*SmoM2-YFP*) together with YFP-sequences (Mao et al. 2006). Mice with a mutation in the *Smoothened*

receptor (*SmoM2*) under the tamoxifen-inducible *Math1-creER^{T2}*-promoter (MATH1 is a marker for cerebellar granule precursor cells) were generated. Through administration of tamoxifen at postnatal day 3 (P3), the Shh pathway can be constitutively activated in cerebellar granule cell precursors which leads to the development of SHH-associated medulloblastoma and often to the development of a hydrocephalus. The tumor incidence is 100%. Here the heterozygosity (one activated *SmoM2* allele) is sufficient for tumor development (*Math1-creER^{T2}::lsl-SmoM2$^{Fl/+}$)*. The median survival of these mice is 65 days (Figure 6 i). Tumor mice developed symptoms like abnormal head growth, ataxia and loss of weight. All tumors display classic histology (Supplementary Figure 25).

3.1.2 Mouse model with *SMO* and *PIK3CA* mutations

The phosphoinositide 3-kinase (PI3K) signalling pathway is one of the most frequently mutated pathways in cancer and plays an important role for proliferation in human tumors. The *Pik3ca^{H1047R}* model was first described by (Adams et al. 2011). H1047R mutations in the kinase domain account for approximately 40% of breast cancer *PIK3CA* mutant alleles (Saal et al. 2005). Although PIK3CA mutations are common in adult cancers (Samuels et al. 2004) and reported in medulloblastoma (Broderick et al. 2004), their role in tumorigenesis remains controversial. In particular it is not known if these mutations initiate or progress cancer.

Math1-creER^{T2}::Pik3ca$^{Fl/+}$ and *Math1-creER^{T2}::Pik3ca$^{Fl/Fl}$* mice were induced at P3 and analysed. No abnormalities in brain development, no tumor development or abnormalities in survival could be observed.

Analogous to the previous mouse model, mice with an additional constitutive activated form of *PIK3CA* were generated. Tumor incidence after tamoxifen administration was 100%. *Math1-creER^{T2}::lsl-SmoM2$^{Fl/+}$ lsl-Pik3ca$^{Fl/+}$* mice showed a faster tumor development and first symptoms (e.g. head growth or ataxia) occurred earlier compared to *Math1-creER^{T2}::lsl-SmoM2$^{Fl/+}$* mice (Figure 6). Kaplan-Meier analysis of these two mouse models show that mice with both (*SMO* and *PIK3CA*) mutations have a significantly ($p < 0.0001$) worse survival rate than mice with only a *SMO* mutation. The median survival of *Math1-creER^{T2}::lsl-SmoM2$^{Fl/+}$ lsl-Pik3ca$^{Fl/+}$* mice is 48 days. All tumors display classic

histology (Supplementary Figure 25). MBs in this mouse strain often have contact to the brainstem (13/18) (e.g. Figure 6 j, k).

Here, heterozygous as well as homozygous PIK3CA mutations alone are not enough to generate a tumor in our mouse model, but leads to a faster tumor progression in *Math1-creER^{T2}::lsl-SmoM2$^{Fl/+}$* mice.

Figure 6 (a-l) shows an overview of *Math1-creER^{T2}::lsl-SmoM2$^{Fl/+}$*, *Math1-creER^{T2}::Pik3ca$^{Fl/+}$*, *Math1-creER^{T2}::Pik3ca$^{Fl/Fl}$* and *Math1-creER^{T2}::lsl-SmoM2$^{Fl/+}$ lsl-Pik3ca$^{Fl/+}$* mice: sagittal section H&E and proliferation (Ki67).

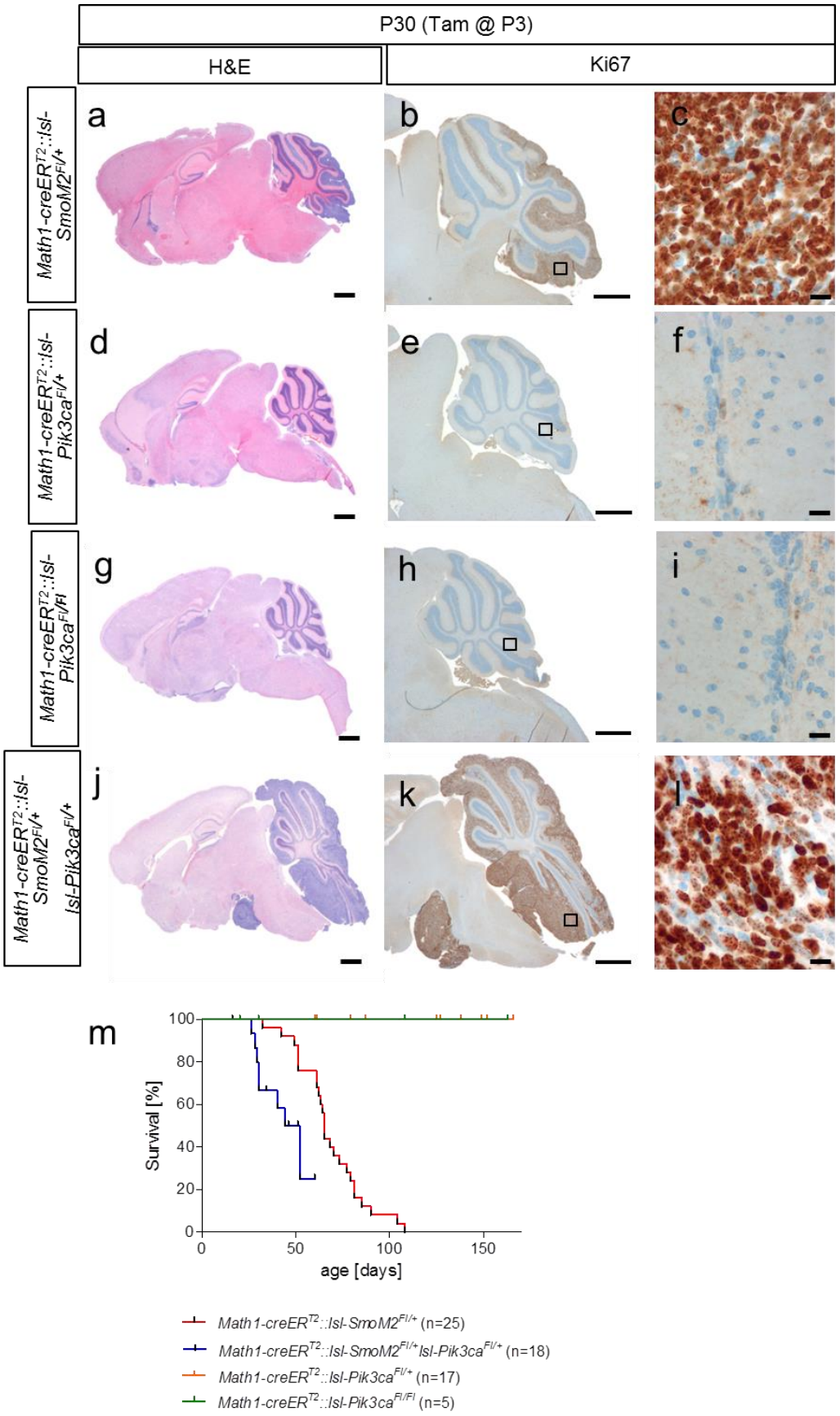

Figure 6 Overview *Math1-creER^{T2}::lsl-SmoM2$^{Fl/+}$*, *Math1-creER^{T2}::lsl-Pik3ca$^{Fl/+}$*, *Math1-creER^{T2}::lsl-Pik3ca$^{Fl/Fl}$* and *Math1-creER^{T2}::lsl-SmoM2$^{Fl/+}$ lsl-Pik3ca$^{Fl/+}$ mice.* Mice were induced with Tamoxifen at P3 and sacrificed

at P30. Left column (a, d, g, j) shows sagittal H&E stains of the whole brain (*scale bar* 1 mm), middle column (b, e, h, k) shows proliferation (Ki67 stains) of the cerebellum (*scale bar* 500 µm); *Scale bar* is 10 µm for higher magnifications (c, f, I, l). The Kaplan-Meier analysis (m) shows a sig. lower survival rate for *Math1-creER^{T2}::lsl-SmoM2$^{Fl/+}$ lsl-Pik3ca $^{Fl/+}$* mice (n = 18) compared to *Math1-creER^{T2}::lsl-SmoM2$^{Fl/+}$* mice (n = 25) ($p < 0.0001$). No *Math1-creER^{T2}::lsl-Pik3ca$^{Fl/+}$* (n = 17) or *Math1-creER^{T2}::lsl-Pik3ca$^{Fl/Fl}$* (n = 5) mice died because of any symptoms.

3.1.3 Mouse model with *PTCH1* mutation

Math1-creER^{T2}::Ptch1$^{Fl/Fl}$ mice show after administration of tamoxifen in all Math1-positive cells and their progeny a homozygous deletion of the Ptch1 gene and a constitutive activation of the SHH pathway. Depending on the time of tamoxifen administration these mice can develop medulloblastoma. Administration between embryonic day E14.5 and postnatal day P8 leads to a tumor incidence of 100% (Yang et al. 2008). The median survival of *Math1-creER^{T2}::Ptch1$^{Fl/Fl}$* mice is 127 days (Figure 7m). All tumors display classic histology (Supplementary Figure 25).

Heterozygous deletion (Tamoxifen induction at P3) of the Ptch1 gene (*Math1-creER^{T2}::Ptch1$^{Fl/+}$)* has no effect on brain development, there is no tumor formation and no abnormalities in survival could be observed (Figure 7).

3.1.4 Mouse model with *PTCH1* and *PIK3CA* mutations

In a sequencing study of Robinson and collegues (Robinson et al. 2012) the identification of the co-occurrence of mutations in *PTCH1* and *PIK3CA* in medulloblastoma was first described.

Analogous to the previous mouse model, mice with an additional constitutive activated form of *PIK3CA* were generated. *Math1-creER^{T2}::Ptch1$^{Fl/Fl}$ lsl-Pik3ca$^{Fl/+}$* and *Math1-creER^{T2}::Ptch1$^{Fl/Fl}$ lsl-Pik3ca$^{Fl/Fl}$* mice showed a faster tumor development compared to *Math1-creER^{T2}::Ptch1$^{Fl/Fl}$* mice. *Math1-creER^{T2}::Ptch1$^{Fl/Fl}$ lsl-Pik3ca$^{Fl/+}$* and *Math1-creER^{T2}::Ptch1$^{Fl/Fl}$ lsl-Pik3ca$^{Fl/Fl}$* mice showed no differences in survival. Kaplan-Meier analysis show that mice with both (*Ptch1$^{Fl/Fl}$* and *PIK3CA*) mutations have a worse survival rate than mice with only a *Ptch1$^{Fl/Fl}$* mutation (Figure 7). Heterozygous or homozygous

mutation of *PIK3CA* alone under the *Math1* promoter has no effect on survival. All tumors display classic histology (Supplementary Figure 25).

Heterozygous deletion of the Ptch1 gene and a simultaneous constitutive activated form of PIK3CA (homo- or herterozygous) (*Math1-creER^{T2}::Ptch1$^{Fl/+}$ lsl-Pik3ca$^{Fl/+}$* and *Math1-creER^{T2}::Ptch1$^{Fl/+}$ lsl-Pik3ca$^{Fl/Fl}$*) has no effect on survival rate and did not show any symptoms of tumor development.

Figure 7 (a-l) shows an overview of *Math1-creER^{T2}::Ptch1$^{Fl/+}$*, *Math1-creER^{T2}::Ptch1$^{Fl/Fl}$*, *Math1-creER^{T2}::Ptch1$^{Fl/Fl}$ lsl-Pik3ca$^{Fl/+}$* and *Math1-creER^{T2}::Ptch1$^{Fl/Fl}$ lsl-Pik3ca$^{Fl/Fl}$* mice: sagittal section H&E and proliferation (Ki67).

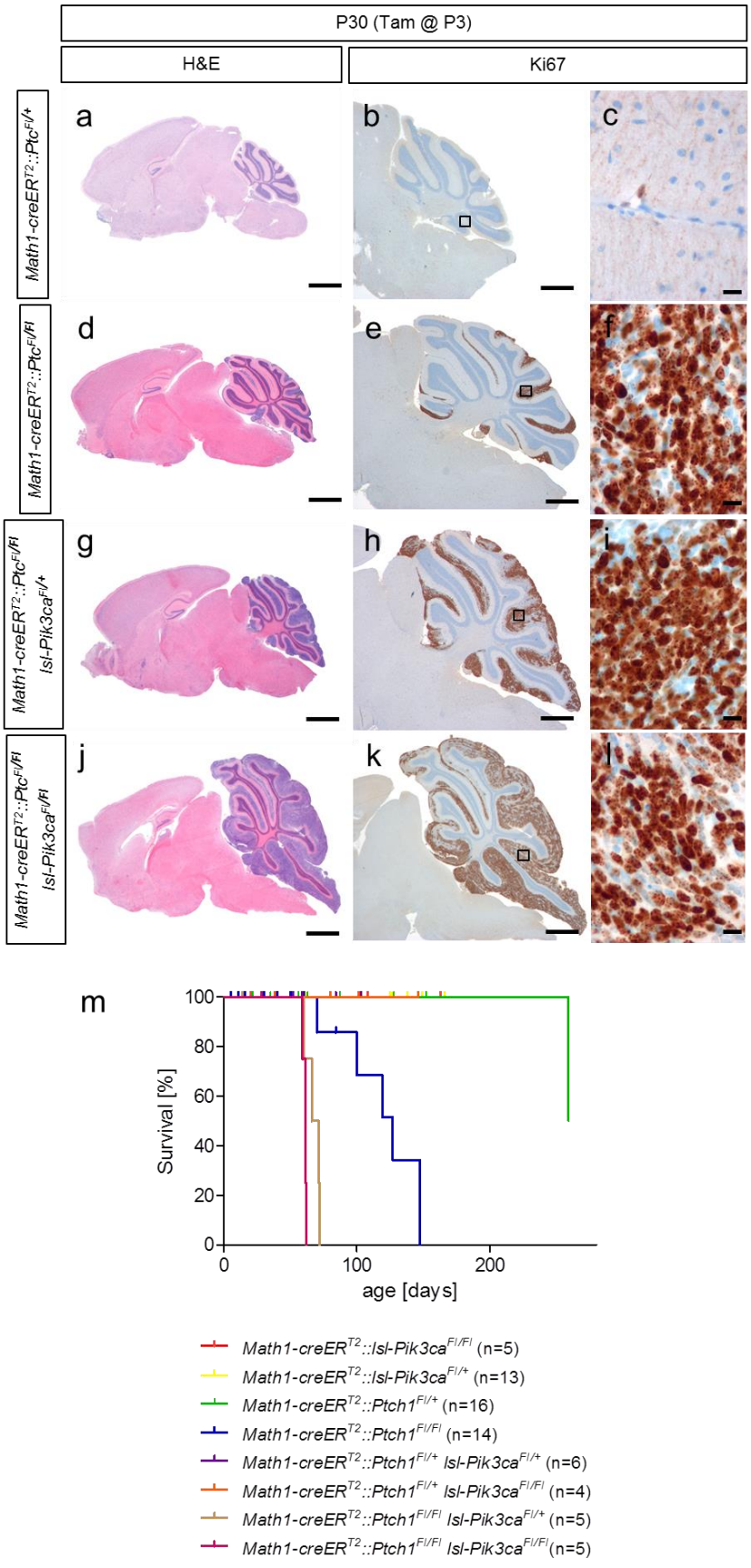

Figure 7 Overview *Math1-creER^{T2}::Ptch1$^{Fl/+}$*, *Math1-creER^{T2}::Ptch1$^{Fl/Fl}$*, *Math1-creER^{T2}::Ptch1$^{Fl/Fl}$ lsl-Pik3ca$^{Fl/+}$*, *Math1-creER^{T2}::Ptch1$^{Fl/Fl}$ lsl-Pik3ca$^{Fl/Fl}$*, *Math1-creER^{T2}::lsl-Pik3ca$^{Fl/+}$* and *Math1-creER^{T2}::lsl-*

Pik3ca$^{Fl/Fl}$ mice. Mice were induced with Tamoxifen at P3 and sacrificed at P30. Left column (a, d, g, j) shows sagittal H&E stains of the whole brain (*scale bar* 1 mm), middle column (b, e, h, k) shows proliferation (Ki67 stains) of the cerebellum (*scale bar* 500 µm) and right column shows higher magnification of Ki67 stains (c, f, i, l) (*scale bar* 10 µm). The Kaplan-Meier analysis (m) shows a sig. lower survival rate for *Math1-creER^{T2}::Ptch1$^{Fl/Fl}$ lsl-Pik3ca$^{Fl/+}$* ($p = 0.0040$; n = 5), *Math1-creER^{T2}::Ptch1$^{Fl/Fl}$ lsl-Pik3ca$^{Fl/Fl}$* ($p = 0.0005$; n = 5) compared to *Math1-creER^{T2}::Ptch1$^{Fl/Fl}$* mice ($p < 0.0001$; n = 6). No *Math1-creER^{T2}:: lsl-Pik3ca$^{Fl/+}$* (n = 17) or *Math1-creER^{T2}:: lsl-Pik3ca$^{Fl/Fl}$* (n = 5) mice died because of any symptoms.

3.1.5 Mouse model with *MYCN* amplification

A number of observations suggest a role for the proto-oncogene *MYCN* in the pathogenesis of MB. Amplification of *MYCN*, a relatively rare event in MB, correlates with poor outcome (Pfister et al. 2009). Shh promotes the expression and post-transcriptional stabilization of N-Myc in mice (Kenney et al. 2003, Thomas et al. 2009). Brain-specific deletion of murine *N-myc* results in cerebellar dysplasia, suggesting that *N-myc* is critical to proliferation in the developing cerebellum, and that other myc family members cannot compensate for loss of *N-myc* (Knoepfler et al. 2002). Experiments in genetically engineered mice demonstrate that *N-myc* is required for MB development (Hatton et al. 2006), suggesting that human tumors could also arise, in part, through misexpression of *MYCN* (Kenney et al. 2003, Oliver et al. 2003, Hatton et al. 2006, Kessler et al. 2009, Thomas et al. 2009). To date, however, N-myc overexpression (alone or in combination with Gli1, IGF-II, or Bcl-2) has failed to initiate MB in any experimental model (Browd et al. 2006, McCall et al. 2007).

In this work *Math1-creER^{T2}::lsl-Nmyc$^{Fl/+}$* and *Math1-creER^{T2}::lsl-Nmyc$^{Fl/Fl}$* were generated These mouse strains enable an overexpression of Nmyc in cerebellar granule precursors after administration of tamoxifen (at P5). This overexpression did not lead to any tumor formation in our mice (Figure 8) and no symptoms or other abnormalities in the brain could be observed.

3.1.6 Mouse model with *MYCN* amplification and *TP53* mutation

The *TP53* gene provides instructions for making a protein called tumor protein p53 (or p53). This protein acts as a tumor suppressor, which means that it regulates cell division by keeping cells from growing and dividing too fast or in an uncontrolled way.

Combined MYC family amplifications and P53 pathway defects (*TP53* mutation) commonly emerged at relapse, and all patients in this group died of rapidly progressive disease postrelapse (Hill et al. 2015). These clinical observations and previous modelling of medulloblastoma in mice suggested that aberrant activation of the *MYC* gene family synergizes with inactivation of p53 or Rb in the genesis of biologically aggressive medulloblastoma (Shakhova et al. 2006, Kawauchi et al. 2012, Pei et al. 2012).

For this project mouse strains with an overexpression on Nmyc and a simultaneous p53 loss of function in cerebellar granule precursors after administration of tamoxifen (at P5) were generated (*Math1-creER^{T2}::lsl-Nmyc$^{Fl/+}$p53$^{Fl/+}$*, *Math1-creER^{T2}::lsl-Nmyc$^{Fl/+}$p53$^{Fl/Fl}$*, *Math1-creER^{T2}::lsl-Nmyc$^{Fl/Fl}$p53$^{Fl/+}$* and *Math1-creER^{T2}::lsl-Nmyc$^{Fl/Fl}$p53$^{Fl/Fl}$* mice). Mice with only a p53 loss of function (hetero- and homozygous) were completely inconspicuous.

Recently, the group of Wechsler-Reya developed a similar mouse model with *MYCN* amplifications. These mice did not develop medulloblastoma, but they developed choroid plexus tumors (personal communication). These tumors arise from brain tissue called the “choroid plexus.” They commonly invade nearby tissue and spread widely via the cerebrospinal fluid. Due to this information we also looked at the choroid plexus.

All these mouse models did neither develop a tumor in the cerebellum, nor abnormalities could be found in the choroid plexus of these animals (Figure 8).

Figure 8 shows an overview of the different genotypes of sagittal sections H&E and proliferation (Ki67).

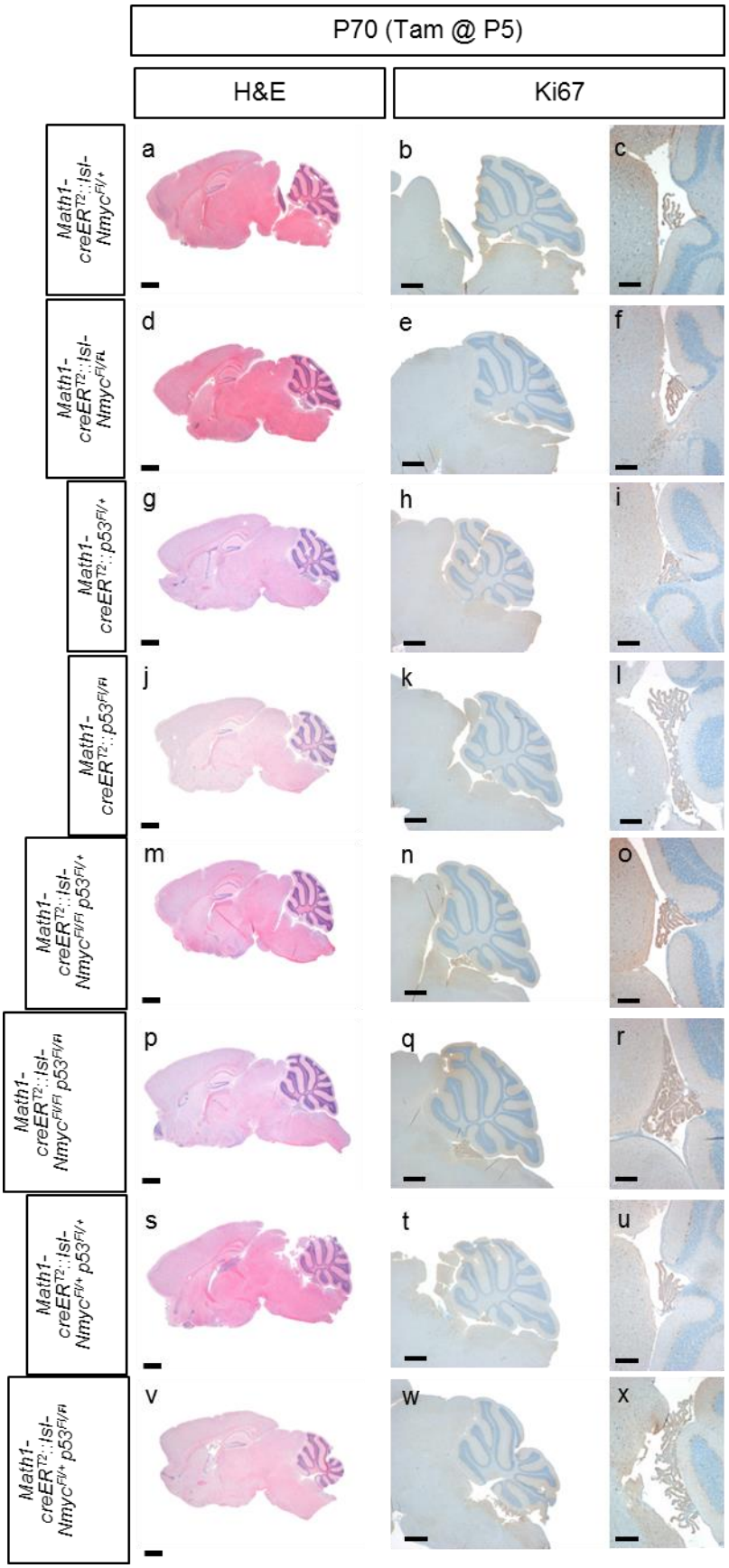

Figure 8 Overview *Math1-creER^{T2}::lsl-Nmyc$^{Fl/+}$*, *Math1-creER^{T2}::lsl-Nmyc$^{Fl/Fl}$*, *Math1-creER^{T2}::p53$^{Fl/+}$*, *Math1-creER^{T2}::p53$^{Fl/Fl}$*, *Math1-creER^{T2}::lsl-Nmyc$^{Fl/+}$p53$^{Fl/+}$*, *Math1-creER^{T2}::lsl-Nmyc$^{Fl/+}$p53$^{Fl/Fl}$*, *Math1-creER^{T2}::lsl-*

Nmyc$^{Fl/Fl}$p53$^{Fl/+}$ and *Math1-creER^{T2}::lsl-Nmyc$^{Fl/Fl}$p53$^{Fl/Fl}$ mice.* All mice were induced with Tamoxifen at P5 and sacrificed at P70. Left column (a, d, g, j, m, p, s, v) shows sagittal H&E stains of the whole brain (*scale bar* 1 mm), right column shows proliferation (Ki67 stains) of the cerebellum (b, e, h, k, n, q, t, w) (*scale bar* 500 µm) and choroid plexus (c, f, I, l, o, r, u, x.) (*scale bar* 200 µm).

Survival analysis for *Math1-creER^{T2}::lsl-Nmyc$^{Fl/+}$* (n = 22), *Math1-creER^{T2}::lsl-Nmyc$^{Fl/Fl}$* (n = 11), *Math1-creER^{T2}::p53$^{Fl/+}$* (n = 9), *Math1-creER^{T2}::p53$^{Fl/Fl}$* (n = 8), *Math1-creER^{T2}::lsl-Nmyc$^{Fl/+}$p53$^{Fl/+}$* (n = 12), *Math1-creER^{T2}::lsl-Nmyc$^{Fl/+}$p53$^{Fl/Fl}$* (n = 2), *Math1-creER^{T2}::lsl-Nmyc$^{Fl/Fl}$p53$^{Fl/+}$* (n = 11) and *Math1-creER^{T2}::lsl-Nmyc$^{Fl/Fl}$p53$^{Fl/Fl}$* (n = 4) *mice* shows no significant difference in prognosis over the different genotypes (Figure 9).

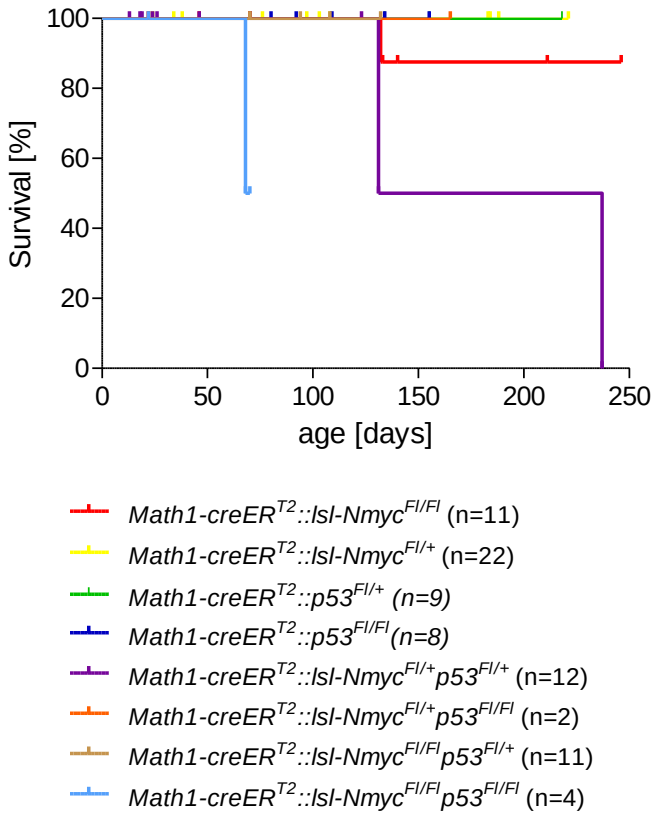

.

Figure 9 Kaplan-Meier analysis for *Math1-creER^{T2}::lsl-Nmyc$^{Fl/+}$* (n = 22), *Math1-creER^{T2}::lsl-Nmyc$^{Fl/Fl}$* (n = 11), *Math1-creER^{T2}::p53$^{Fl/+}$* (n = 9), *Math1-creER^{T2}::p53$^{Fl/Fl}$* (n = 8), *Math1-creER^{T2}::lsl-Nmyc$^{Fl/+}$p53$^{Fl/+}$* (n = 12), *Math1-creER^{T2}::lsl-Nmyc$^{Fl/+}$p53$^{Fl/Fl}$* (n = 2), *Math1-creER^{T2}::lsl-Nmyc$^{Fl/Fl}$p53$^{Fl/+}$* (n = 11) and *Math1-creER^{T2}::lsl-Nmyc$^{Fl/Fl}$p53$^{Fl/Fl}$* (n = 4) *mice*.

3.2 Localization of SHH medulloblastoma in mice depends on the age at its initiation

Approximately, 30% of MBs belong to the SHH subgroup. This subgroup shows a two-peak age distribution, making up the majority of infant (≤ 3 years) and adult (≥ 16 years) MBs, but only a small fraction of childhood (4-15 years) tumors (Kool et al. 2012). Global methylation and gene expression profiles of infant and adult SHH MBs are clearly distinct, although, overall, they belong to the same molecular subgroup (Northcott et al. 2011, Kool et al. 2014). In addition, localization of human SHH MBs differs depending on the age of the patient. For so far unknown reasons, adult SHH MBs are almost exclusively located in cerebellar hemispheres, whereas infant SHH MBs often grow in the vermis (Wefers et al. 2014). Since the genetic makeup is known to be different in infant and adult MB (Kool et al. 2014), it appears possible that the anatomical localization is dependent on the tumor's driver mutations. On the other hand, it appears possible that the susceptibility of different cell types for oncogenic transformation is dependent on a distinct developmental time frame, but independent of the tumor-initiating driver mutation. To test this hypothesis in a systematic way, we used *Math1-GFP,Ptc*$^{+/-}$ mice, which develop green fluorescent SHH MB (Goodrich et al. 1997, Oliver et al. 2005). Importantly, in contrast to SUFU or SMO mutations that predominantly occur in SHH MB of infants and adults, respectively, PTCH1 mutations are equally detected in both age groups of human SHH MB (Kool et al. 2014, Pöschl et al. 2014). So, PTCH1 mutations per se do not appear to predispose for a specific tumor localization.

First, we analysed the localization of *Math1-GFP,Ptc*$^{+/-}$ MBs in the cerebellum at different time points. The localization of a tumor (as defined as >2 mm in size) was categorized according to the involvement of vermis and hemispheres, the involvement of rostral and caudal cerebellar regions, and its growth into the fourth ventricle (Figure 10).

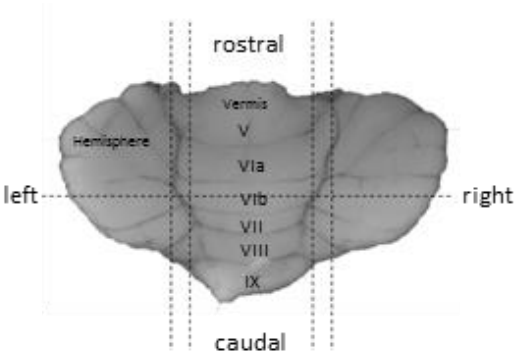

Figure 10 Anatomical compartments of the murine cerebellum.

We confirmed expression of Sox2 in all tumors that were included in our statistics, as preneoplastic lesions and real tumors have quite different gene expression profiles, and Sox2 is at the top of the list of the genes that are expressed in tumors, but not in normal granule cell precursors or preneoplastic lesions (Oliver et al. 2005) (Figure 11).

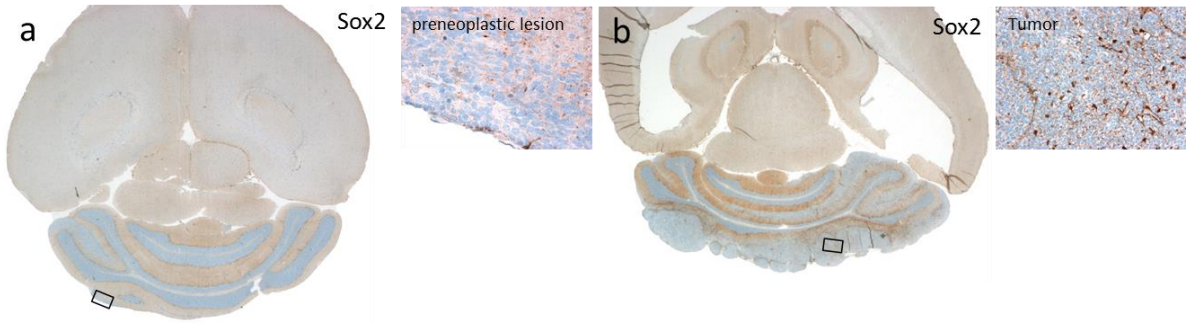

Figure 11 Sox2 expression in *Math1-GFP,Ptc*$^{+/-}$ mice. (a) Sox2 expression is not detectable in small preneoplastic lesions of *Math1-GFP,Ptc*$^{+/-}$ mice. (b) On the contrary, large tumors that are visible in older mice display strong Sox2 expression.

We analysed 81 5-week-old and 34 10-week-old *Math1-GFP,Ptc*$^{+/-}$ mice (Figure 13a). In the 5-week-old group, 44/81 animals (54%) had no MB, 23/81 (29%) developed one tumor, 13/81 (16%) developed two separable tumors, and 1/81 (1%) developed three separable tumors within the cerebellum. Only 7/34 animals (20%) in the 10-week-old group did not develop any MB, 4/34 (12%) had 2 separable tumors, and 23/34 (68%) developed one tumor ($p < 0.001$). Hence, the overall tumor incidence was 46 % in 5-week-old mice and 80% in 10-week-old mice. This implies that a good number of tumors

develop after 5 weeks of age. Representative examples of MB in 5- or 10-week-old *Math1-GFP,Ptc*$^{+/-}$ mice are given in Figure 12.

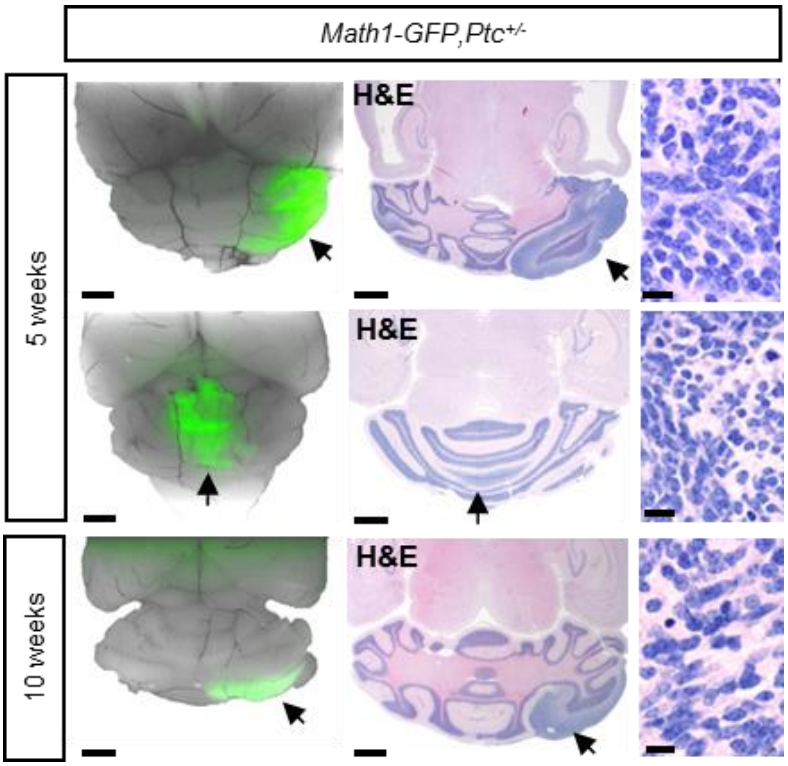

Figure 12 Representative fluorescent images and H&E stains of MB in *Math1-GFP,Ptc*$^{+/-}$ mice at different time points. *Arrows* point to tumors, which display classic histology at both ages. High magnifications are shown on the *right. Scale bars* correspond to 2 mm for low-power images and 10 µm for high-power images.

Every tumor was then categorized according to its main localization in the cerebellum (Figure 13 b). 31/52 MBs of the 5-week-old *Math1-GFP,Ptc*$^{+/-}$ mice (60 %) exclusively grew in the hemispheres, but 9/52 tumors (17 %) were restricted to the vermis. In contrast, all 31 tumors in the 10-week-old group grew in the hemispheres with 15/31 (48 %) being exclusively in the hemispheres ($p < 0.01$). This implies that tumors in the vermis do not develop at later stages and must develop in embryonic or early postnatal stages. Otherwise, one would clearly expect MBs that exclusively occupy the vermis at 10 weeks of age (Ohli et al. 2015).

Furthermore, we analysed the main vertical MB localization (Figure 13 c).

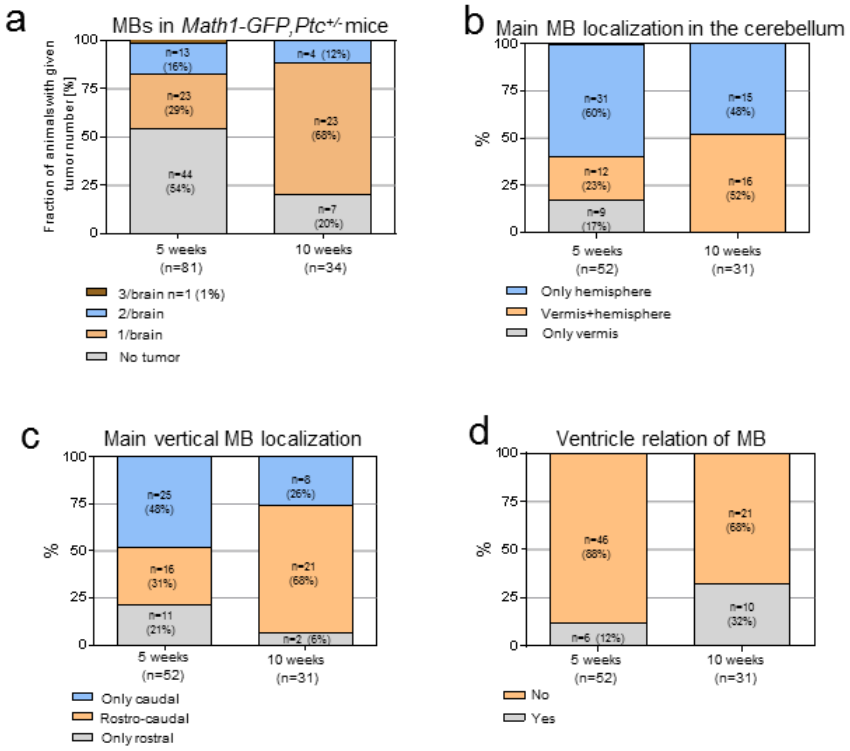

Figure 13 (a) MB incidence in *Math1-GFP,Ptc*$^{+/-}$ mice. (b) Main localization in the cerebellum of *Math1-GFP,Ptc*$^{+/-}$ mice. (c) Main vertical MB localization. (d) Ventricle relation of MB.

Almost half of the tumors of the 5-week-old mice (25/52, 48%) grew only caudal, whereas only 11/52 (21%) grew exclusively rostral. In the 10-week old group, 8/31 (26%) grew only caudal, 2/31 (6%) grew only rostral, but the majority of these tumors extended rostro-caudal (21/31, 68%) ($p < 0.01$). Moreover, 6/52 (12%) of the 5-week-old MBs and 10/31 (32%) of the 10-week old MBs expanded into the fourth ventricle (Figure 13 d, $p = 0.02$).

To confirm the time-dependent localization of SHH medulloblastoma in an independent model, we used *Math1-creER*^{T2}*::lsl-SmoM2*$^{Fl/+}$ mice that were Tamoxifen-induced at E14.5 or P5. To make sure that the targeted cells under both conditions are comparable, we first performed lineage tracing analyses using *Math1-creER*^{T2}*::tdTomato* mice and found an equal distribution of *creER*^{T2}-mediated recombination, as indicated by RFP staining throughout the vermis and the hemispheres for both time points of Tamoxifen induction (Figure 14 a). Therefore mice from the *Math1-creER*^{T2} strain were paired with mice which carry a sequence for a red fluorescent protein (tdTomato, variant of RFP). With the Cre-LoxP-system it is possible through, the cre-mediated recombination, to cut out specific

sequences lying between two loxP-sequences. In the system used here, the sequence which is cut out is a polyadenylation sequence, thus a stop-codon. After the loss of the stop-codon, the expression of the coding reporter genes could take place. This induced modification in the protein expression also manifest after the cell divison and independent of further differentiation of progeny. Thus, every daughter cell of a primary recombinated cell further on express RFP. Due to the traceability of the fate of a single cell and populations with this system, it is called fate-mapping or lineage tracing analysis.

Tumor growth in *Math1-creER^{T2}::lsl-SmoM2$^{Fl/+}$* mice was then analysed in the vermis and hemispheres at P14 or P26, i.e., 3 weeks after Tamoxifen induction (Figure 14 b). In agreement with the data above, we did not find anatomical differences in the tumor growth when induced at E14.5. However, animals induced postnatally (P5) developed tumors, the growth of which was clearly pronounced in the hemispheres (Figure 14 c). There was significantly less tumor burden in the vermis of P5-induced animals compared to embryonically induced mice. Together, these results fit well to the distribution of SHH MBs in humans (Wefers et al. 2014) and indicate that the localization of SHH MBs is dependent on the time-restricted susceptibility of granule cell precursors in defined cerebellar compartments, and independent of the type of tumor-initiating driver mutation.

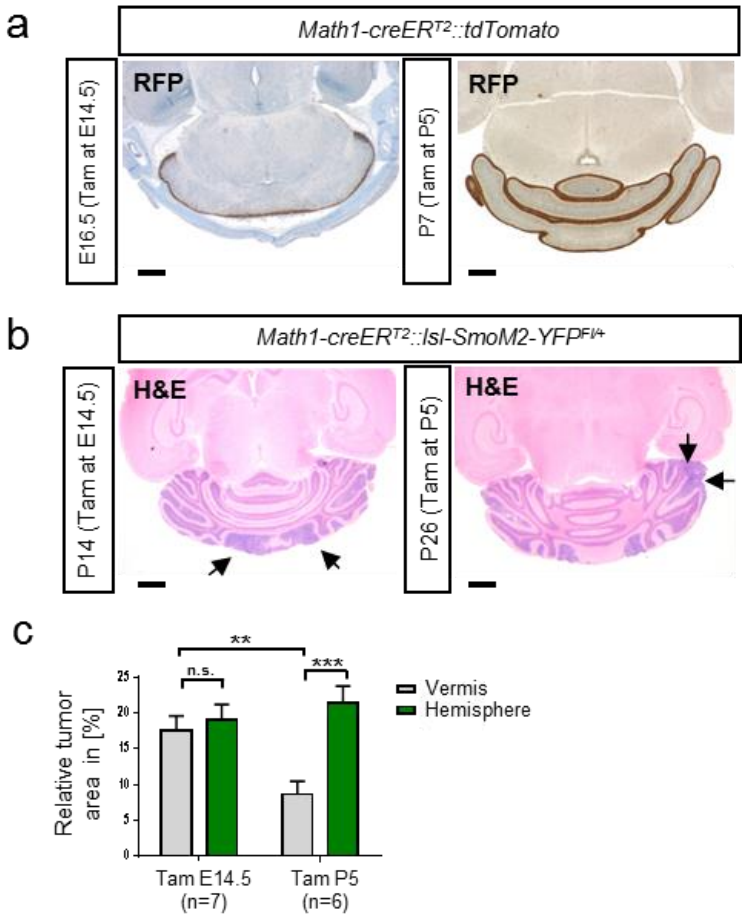

Figure 14 (a) RFP stainings indicating equally distributed recombination in granule cells of *Math1-creER^{T2}::tdTomato* mice. (b) H&E stainings of embryonically and postnatally induced *Math1-creER^{T2}::lsl-SmoM2$^{Fl/+}$* mice. Arrows indicate tumor areas in the vermis and hemisphere. (c) Quantification of the relative tumor area of embryonically and postnatally induced *Math1-creER^{T2}::lsl-SmoM2$^{Fl/+}$* mice in different cerebellar compartments. Scale bars correspond to 2 mm for low-power image (*right image* in a and *both images* in b), 500 µm (*left image* in a). Bars show mean with SEM. *ns* not significant, ** $p < 0.01$, *** $p < 0.001$.

3.3 Effects of Wnt/β-catenin signalling on Shh-dependent medulloblastoma formation

Shh is crucial for the proliferation of cerebellar granule neuron precursors (GNPs) (Wechsler-Reya and Scott 1999), but constitutive activation of the Shh pathway in GNPs leads to medulloblastoma (Schüller et al. 2008). In contrast, canonical Wnt/ß-catenin signalling is required for the maturation of GNPs, and constitutive activation of this pathway causes significant proliferation deficits (Lorenz et al. 2011). To develop new therapeutic strategies for patients with Shh-medulloblastoma, we asked whether the physiological roles of Wnt/ß-catenin signalling can be utilized to treat Shh-medulloblastomas that have developed from GNPs.

To analyse the effect of Wnt/ß-catenin-activation, primary cell culture experiments were performed. At the time point of the biggest clonal expansion of the granule cell precursors (p5-p7) the Shh-activating *SmoM2*-mutation and the Wnt-activating form of ß-catenin were introduced by viral inserted cre-recombinase. $SmoM2^{Fl/+}$, $Ctnnb1(ex3)^{Fl/+}$, or $SmoM2^{Fl/+}$ $Ctnnb1(ex3)^{Fl/+}$ cerebellar GNPs were cultured as described (Lorenz et al. 2011) and transduced with *Cre-IRES-GFP* viruses. Cre treatment of $SmoM2^{Fl/+}$ cerebellar GNPs led to a 2.6-fold proliferation increase due to active Shh signalling (Figure 15, $p = 0.008$). Here, proliferation is the fraction of $BrdU^+$ cells among GFP^+ granule cells [%].

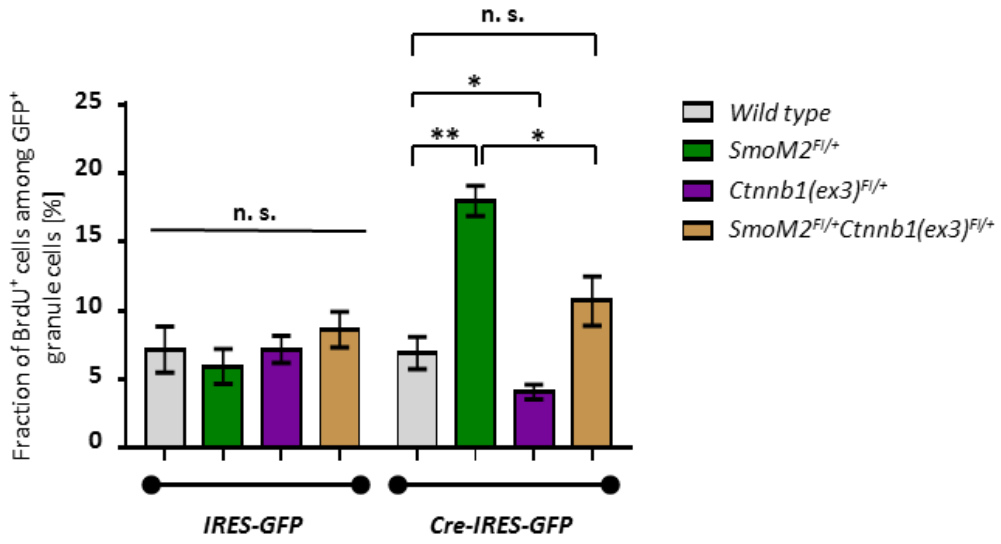

Figure 15 Cultured cerebellar GNPs from mice of indicated genotypes were transduced with control *IRES-GFP* virus or *Cre-IRES-GFP* virus to recombine alleles. Wnt/ß-catenin-activation significantly reduced proliferation of both normal GNPs and *SmoM2*$^{Fl/+}$ -transformed GNPs. Bars show mean with SEM. *ns* not significant. * $p < 0.05$, ** $p < 0.01$.

Wnt pathway activation in *Ctnnb1(ex3)*$^{Fl/+}$ GNPs reduced proliferation to 52% (Figure 15, $p = 0.029$). Importantly, Wnt-activation significantly decreased oncogenic GNP proliferation driven by *SmoM2 (SmoM2*$^{Fl/+}$ *Ctnnb1(ex3)*$^{Fl/+}$ condition, $p = 0.028$), and cells reached proliferation levels similar to the wild type. Thus, the proliferation of Shh-medulloblastoma cells may be blocked through canonical Wnt signalling. These results extend previous studies showing inhibitory effects of Wnt3a through non-canonical Wnt signalling on GNPs (Anne et al. 2013).

Next, we introduced a *Ctnnb1(ex3)*$^{Fl/+}$ allele into *Math1-cre::SmoM2*$^{Fl/+}$ mice, a model for Shh-medulloblastoma (Schüller et al. 2008). Activation of the Shh pathway in *Math1*-positive GNPs resulted in a thickened external granule cell layer (EGL) and medulloblastoma (Figure 16 a, b; Supplementary Figure 26). Additional activation of the Wnt-pathway (*Math1-cre::SmoM2*$^{Fl/+}$*Ctnnb1*(*ex3*)$^{Fl/+}$ mice) notably reduced growth of medulloblastoma and resulted in decreased cerebellar size (Figure 16 a, c; Supplementary Figure 26). Importantly, *Math1-cre::SmoM2*$^{Fl/+}$*Ctnnb1*(*ex3*)$^{Fl/+}$ mice ($n = 16$) survived significantly longer than *Math1-cre::SmoM2*$^{Fl/+}$ animals ($n = 53$, $p < 0.0001$, (Figure 16 d)).

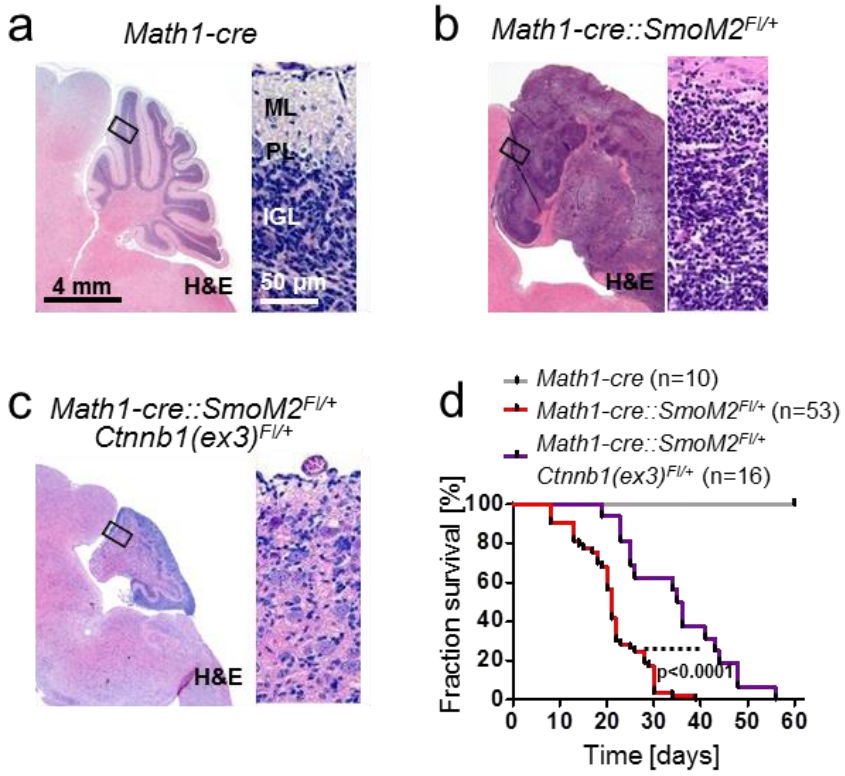

Figure 16 (a-c) Sagittal cerebellar sections. Shh pathway activation in *Math1*-positive cerebellar GNPs resulted in the formation of medulloblastoma (b). Co-activation of the Wnt/β-catenin signalling pathway [*Math1-cre::SmoM2*$^{Fl/+}$*Ctnnb1(ex3)*$^{Fl/+}$ mice] reduced growth of medulloblastoma and led to a decreased cerebellar size (c). (d) *Math1-cre::SmoM2*$^{Fl/+}$*Ctnnb1(ex3)*$^{Fl/+}$ mice displayed a significantly prolonged survival. *ML* molecular layer, *PL* Purkinje cell layer, *IGL* internal granule cell layer

In order to just analyse cells, that were transduced with *Cre-IRES-GFP* virus, we used FACS (fluorescence-activated cell sorting) to isolate GFP$^+$ cells from *SmoM2*$^{Fl/+}$ or *SmoM2*$^{Fl/+}$*Ctnnb1*(*ex3*)$^{Fl/+}$ GNP cultures after *Cre-IRES-GFP* virus treatment. Looking at different targets of the Shh and the Wnt pathway, quantitative RT-PCR analysis was performed. It could be confirmed that the mRNA level of *Axin2,* a direct target of the Wnt pathway, was upregulated in *SmoM2*$^{Fl/+}$*Ctnnb1*(*ex3*)$^{Fl/+}$ GNPs, whereas the mRNA level of *Gli1*, a downstream target of the Shh pathway, was downregulated (Figure 17).

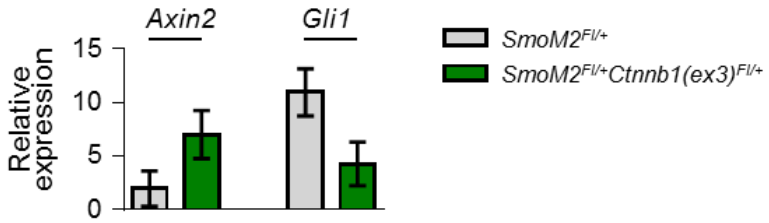

Figure 17 Relative quantification of *Axin2* and *Gli1* in GFP⁺ *SmoM2*$^{Fl/+}$ and *SmoM2*$^{Fl/+}$*Ctnnb1(ex3)*$^{Fl/+}$ GNPs after Cre-IRES-GFP transduction. Bars show mean with SEM.

Hence, active canonical Wnt signalling is a potent inhibitor of the Shh pathway in medulloblastoma. Pharmacologically, activation of Wnt/β-catenin signalling can be achieved via inhibition of GSK3β, an upstream player of the pathway (Rubinfeld et al. 1996). Primary cell culture was used for cre treatment of cerebellar *GSK3β*$^{Fl/Fl}$ GNPs (Jaworski et al. 2011). A significant decrease in proliferation was achieved when GSK3ß was knocked out *in vitro* (Figure 18, p = 0.041).

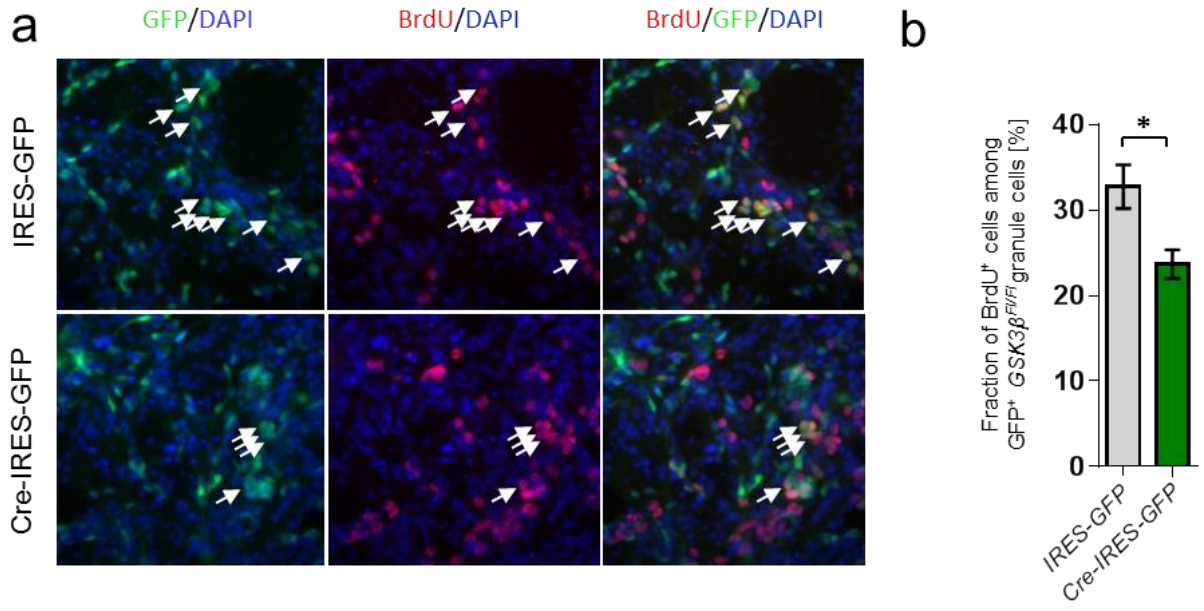

Figure 18 GSK3ß knockout resulted in significantly reduced proliferation of GNPs. (a) Cultured cerebellar granule neuron precursors (GNPs) from GSK3ß mice (P5-P7) were transduced with IRES-GFP (control) and Cre-IRES-GFP virus to recombine alleles. GFP staining (green) shows recombined cells, BrdU staining (red) shows proliferating cells. Knockout of GSK3ß led to decreased proliferation of transduced cerebellar GNPs (arrows point to proliferating cells that have undergone successful recombination).(b) Quantifications for

results shown in (a) including control experiments with IRES-GFP virus. Bars show mean of three individual experiments. Knockout of GSK3ß significantly reduced proliferation of cerebellar GNPs ($p = 0.041$). Bars show mean with SEM. *ns* not significant, * $p < 0.05$ (t-test).

3.3.1 *In vitro* treatment with the Wnt agonist lithium chloride

Lithium is a chemical element with psychotropic properties, which is commonly used to treat bipolar disorder as well as other psychiatric diseases (Geddes et al. 2004, Storosum et al. 2007), although the underpinnings of its biochemical effects remain only partially understood (Alda 2015). Among others, Lithium has been shown to act as an inhibitor of Glycogen synthase kinase 3 beta, a serine/threonine kinase also known as GSK3B (Klein and Melton 1996, Stambolic et al. 1996, O'Brien and Klein 2009). GSK3B is part of the so-called cytoplasmic destruction complex together with Axin, Adenomatosis polyposis coli (APC), Dishevelled (Dvl), the CK1-Kinase group and GSK3A (Clevers 2006). This protein complex leads to phosphorylation, ubiquitination, and therefore proteasomal degradation of β-Catenin in the cytoplasm (Aberle et al. 1997, Willert et al. 1999). Hence, Lithium is able to activate the Wnt/ β-Catenin pathway by inhibiting GSK3B and therefore preventing phosphorylation and subsequent degradation of β-Catenin (Stambolic et al. 1996). Previous results demonstrated an inhibitory effect of constitutional Wnt/ β-Catenin activation on Shh-dependent medulloblastoma formation in *Math1-cre::SmoM2$^{Fl/+}$::Ctnnb1(ex3)$^{Fl/+}$* mice (Pöschl et al. 2014). In order to examine, whether a Wnt agonist might represent a suitable treatment option for patients with Shh-dependent medulloblastoma, a series of *in vitro* experiments was conducted, in order to inquire a possible inhibitory effect of lithium chloride (LiCl), a highly soluble lithium salt, which has been suggested to act as a Wnt/ β-Catenin activator in the cerebellum (Lancaster et al. 2011). MTT (3-(4,5-dimethylthiazol-2-yl)-2,5-diphenyltetrazolium bromide) assays were carried out to investigate, whether the treatment of medulloblastoma tumor cells with LiCl would result in a decrease of cell viability *in vitro (*Figure 19).

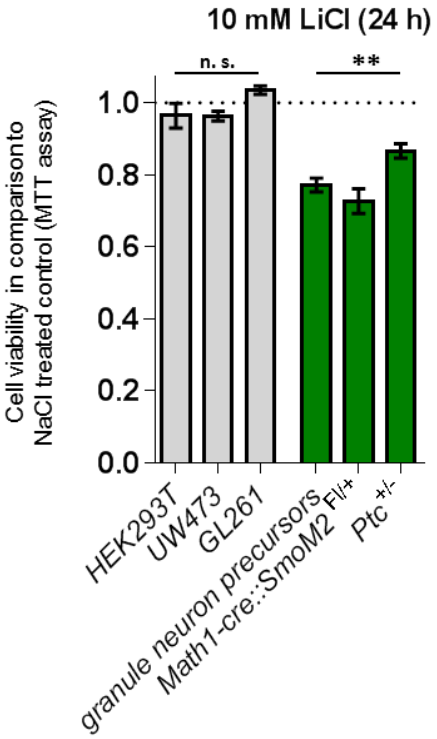

Figure 19 Lithium chloride (LiCl) reduces medulloblastoma cell viability *in vitro.* Colorimetric MTT assays after 24h *in vitro* treatment with 10 mM LiCl decreased cell viability of granule neuron precursor cells and medulloblastoma tumor cells from *Math1-cre::SmoM2$^{Fl/+}$* and *Ptch1$^{+/-}$* mice, when compared to HEK293T, UW473 and GL261 control cells. $p < 0.01$, t-test. Bars show mean with SEM. *ns* not significant. ** $p < 0.01$.

Granule neuron precursor cells (GNPs), from which Shh-dependent medulloblastoma arise (Schüller et al. 2008), as well as medulloblastoma tumor cells from *Math1-cre::SmoM2$^{Fl/+}$* and *Ptch1$^{+/-}$* mice, two well-known murine models for Shh-induced medulloblastoma (Goodrich et al. 1997, Schüller et al. 2008), were isolated and put into primary culture for 16 hours. These cells were than treated with 10 mM LiCl for 24 hours in parallel with the fibroblast line HEK293T, the (non-SHH) medulloblastoma cell line UW473 and the glioma cell line GL261 cell lines, which served as Shh-independent control cells. As a result, LiCl lead to a significant decrease of cell viability in Shh-dependent GNPs and tumor cells from *Math1-cre::SmoM2$^{Fl/+}$* and *Ptch1$^{+/-}$* mice when compared to control cells ($p < 0.01$) (Figure 19). Thus, LiCl is able to inhibit proliferation of Shh-associated medulloblastoma cells *in vitro*.

3.4 Preclinical treatment of mouse models of SHH medulloblastoma with Hh inhibitors

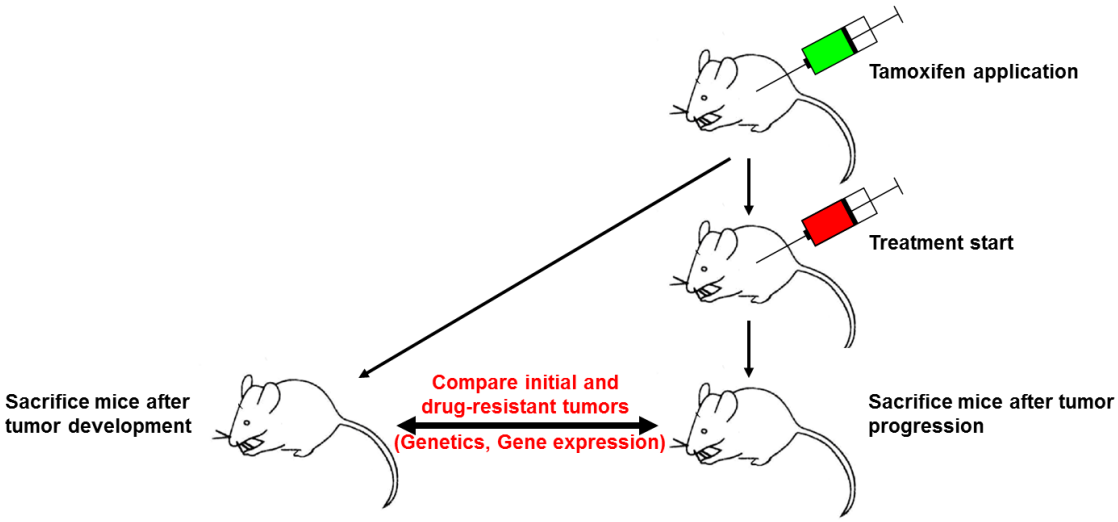

Figure 20 Overview over treatment of Shh-associated mouse models. Using *CreERT2* systems, recombination will be induced by a single i.p. shot of 1 mg Tamoxifen at postnatal day 3 or 5. The inducible conditional transgenic mice will receive primary treatment starting at day 30 using LDE225 (30 mg/kg/day i.p., 5 days per week, treatment duration 21 days). Once mice become symptomatic they will be sacrificed. One half of the brain will be processed for histology and tumor tissue will be harvested from the other second half for molecular analyses. Tumor samples with and without LDE225 treatment will be analysed and compared.

Targeted therapies as a novel treatment modality for MB patients are especially intriguing for primary and relapsed SHH-MB. As more drugs targeting the Hh pathway become available and enter clinical trials, it is important to know how to stratify the patients for different drugs in order to maximize response rates and to prevent unnecessary treatment failures.

Mouse models for medulloblastoma can be treated with SMO inhibitors that have already entered clinical trials and drugs targeting at the level of GLI, such as arsenic trioxide (ATO), bromodomain inhibitors like JQ1 or other more recently developed specific GLI inhibitors, such as GANT61.

Transgenic mice are induced with tamoxifen and then randomly divided in two groups (vehicle/with treatment). After tumor development, mice were sacrificed und tumor tissue was harvested for molecular analyses (Figure 20).

3.4.1 LDE225 treatment

Here we focus on the SMO antagonist LDE225. LDE225 (also known as Sonidegib; Novartis Pharma) is as synthetic, highly potent and selective, small molecule clinical SMO inhibitor resulting from the optimisation as a hit arising from a high throughput screening phenotypic assay designed to identify SMO inhibitors. LDE225 interacts directly with SMO, in a similar fashion to cyclopamine, to reduce expression of downstream Hh signalling targets (Pan et al. 2010). LDE225 is effective in various Hh-dependent tumor models and inhibits downstream expression of Hh targets in cell lines, *in vivo* animal models and in patients, and is currently under clinical trial investigation both as a single agent (Rodon et al. 2014) and in combination (reviewed in (Brechbiel et al. 2014)).

All mice are monitored for treatment response, development of resistance, and overall survival.

3.4.1.1 LDE225 treatment in *Math1-creER^{T2}::lsl-SmoM2$^{Fl/+}$* mice

To determine the effects of LDE225 treatment on tumor growth *in vivo, Math1-creER^{T2}::lsl-SmoM2$^{Fl/+}$* mice at P30 were randomized to receive either vehicle or LDE225 (30 mg/kg/day) five times per week for three weeks and assessed for tumor development. Tumor size was substantially reduced in LDE225-treated *Math1-creER^{T2}::lsl-SmoM2$^{Fl/+}$ mice* compared to the control condition. LDE225 treatment resulted in a significantly extended lifespan of *Math1-creER^{T2}::lsl-SmoM2$^{Fl/+}$* mice (Figure 21 a). After three weeks of LDE225 treatment there is a significant reduction in proliferation or BrdU^{+} cells in LDE225-treated tumors of *Math1-creER^{T2}::lsl-SmoM2$^{Fl/+}$* mice (Figure 21 b). There is no change in morphology after treatment compared to untreated *Math1-creER^{T2}::lsl-SmoM2$^{Fl/+}$* tumors (data not shown).

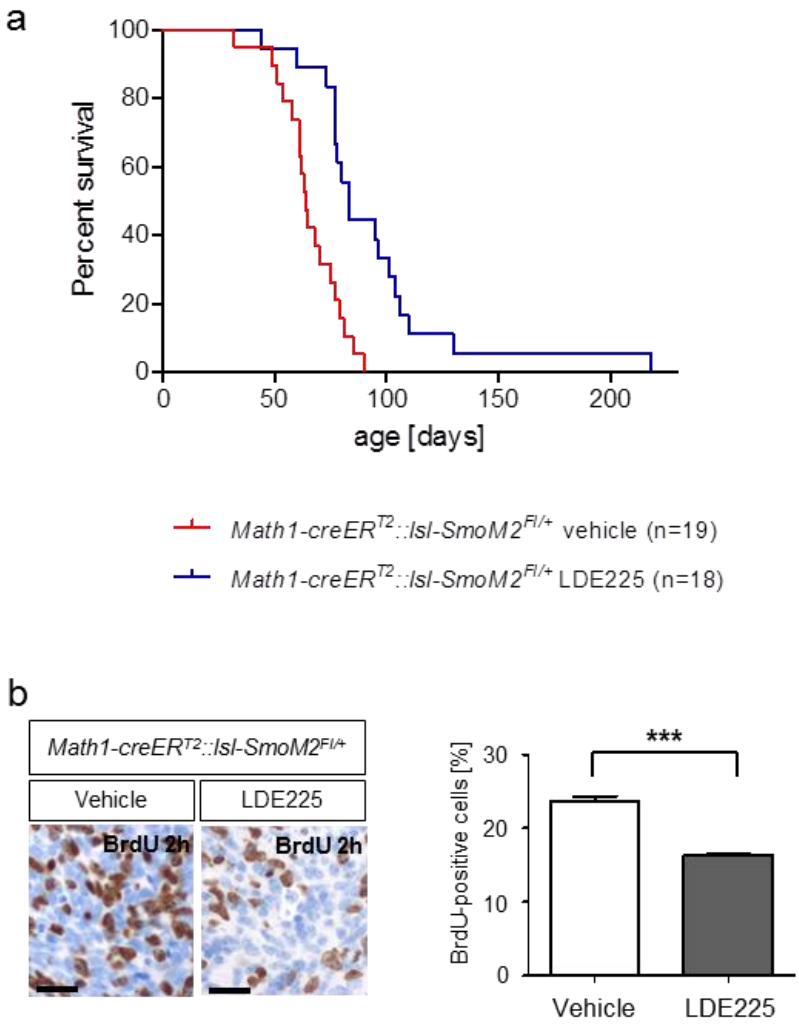

Figure 21 (a) Kaplan-Meier survival curve illustrating overall survival of *Math1-creER^{T2}::lsl-SmoM2$^{Fl/+}$* mice in LDE225 treatment cohort. All mice were induced to tumor formation at P3 by tamoxifen and treated with vehicle or LDE225 from P30 to P51. LDE225 treatment leads to a significant improvement of survival rate (log rank test, $p < 0.0001$); (b) Quantification of the fraction of BrdU$^+$ tumor cells at P51 in *Math1-creER^{T2}::lsl-SmoM2$^{Fl/+}$* mice treated with vehicle or LDE225 for 21 days (n = 3, mean ± SEM, *t-test*), *scale bar* 20 µm. *** $p < 0.001$.

3.4.1.2 LDE225 treatment in *Math1-creER^{T2}::lsl-SmoM2$^{Fl/+}$ lsl-Pik3ca$^{Fl/+}$* mice

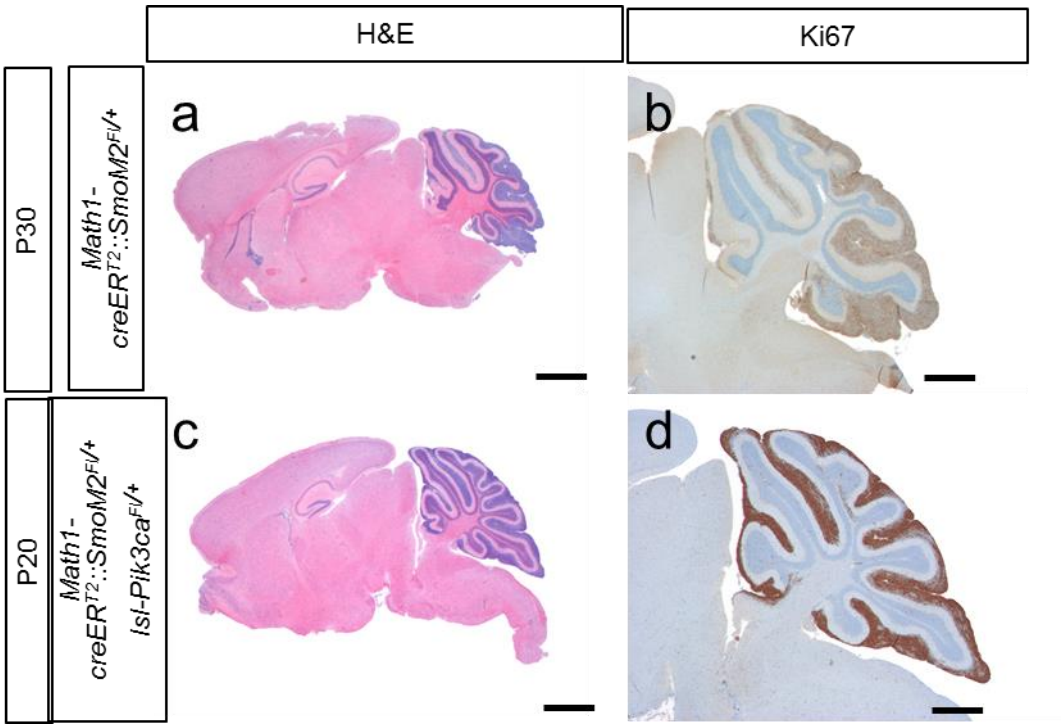

Figure 22 Comparison of *Math1-creER^{T2}::lsl-SmoM2$^{Fl/+}$* and *Math1-creER^{T2}::lsl-SmoM2$^{Fl/+}$ lsl-Pik3ca$^{Fl/+}$* mice. H&E (a, c) *scale bar* 1 mm; Ki67 (b, d) *scale bar* 500 µm.

To determine the effects of LDE225 treatment on tumor growth in a similar mouse model (described above) with an additional mutation in *Pik3ca, Math1-creER^{T2}::lsl-SmoM2$^{Fl/+}$ lsl-Pik3ca$^{Fl/+}$* mice were treated in a similar way like *Math1-creER^{T2}::lsl-SmoM2$^{Fl/+}$* mice. As *Math1-creER^{T2}::lsl-SmoM2$^{Fl/+}$ lsl-Pik3ca$^{Fl/+}$* mice had a lower median survival and much faster tumor growth than *Math1-creER^{T2}::lsl-SmoM2$^{Fl/+}$* mice, *Math1-creER^{T2}::lsl-SmoM2$^{Fl/+}$ lsl-Pik3ca$^{Fl/+}$* mice often died during the 3 week long treatment phase. Therefore treatment start was moved up from P30 to P20 (Figure 22). As first symptoms normally occurred around P20 in *Math1-creER^{T2}::lsl-SmoM2$^{Fl/+}$ lsl-Pik3ca$^{Fl/+}$* mice and in *Math1-creER^{T2}::lsl-SmoM2$^{Fl/+}$* mice around P30, this shifted time point of treatment start makes the treatment of this two mouse strains more comparable (Figure 22). Both treatment groups had no significant improvement of survival compared to the control group. However, *Math1-creER^{T2}::lsl-SmoM2$^{Fl/+}$ lsl-Pik3ca$^{Fl/+}$* mice with an earlier treatment start (P20) have a better prognosis than *Math1-creER^{T2}::lsl-SmoM2$^{Fl/+}$ lsl-Pik3ca$^{Fl/+}$* mice with a

later treatment start (P30) (p = 0.0065)(Figure 23 a). However, after three weeks of LDE225 treatment there is a significant reduction in BrdU⁺ cells in LDE225-treated tumors of *Math1-creER^{T2}::lsl-SmoM2$^{Fl/+}$ lsl-Pik3ca$^{Fl/+}$* mice with treatment start at P20 as well as with treatment start at P30 compared to the control group (Figure 23 b). LDE225 treatment does not change the morphology of *Math1-creER^{T2}::lsl-SmoM2$^{Fl/+}$ lsl-Pik3ca$^{Fl/+}$* tumors compared to untreated tumors (data not shown).

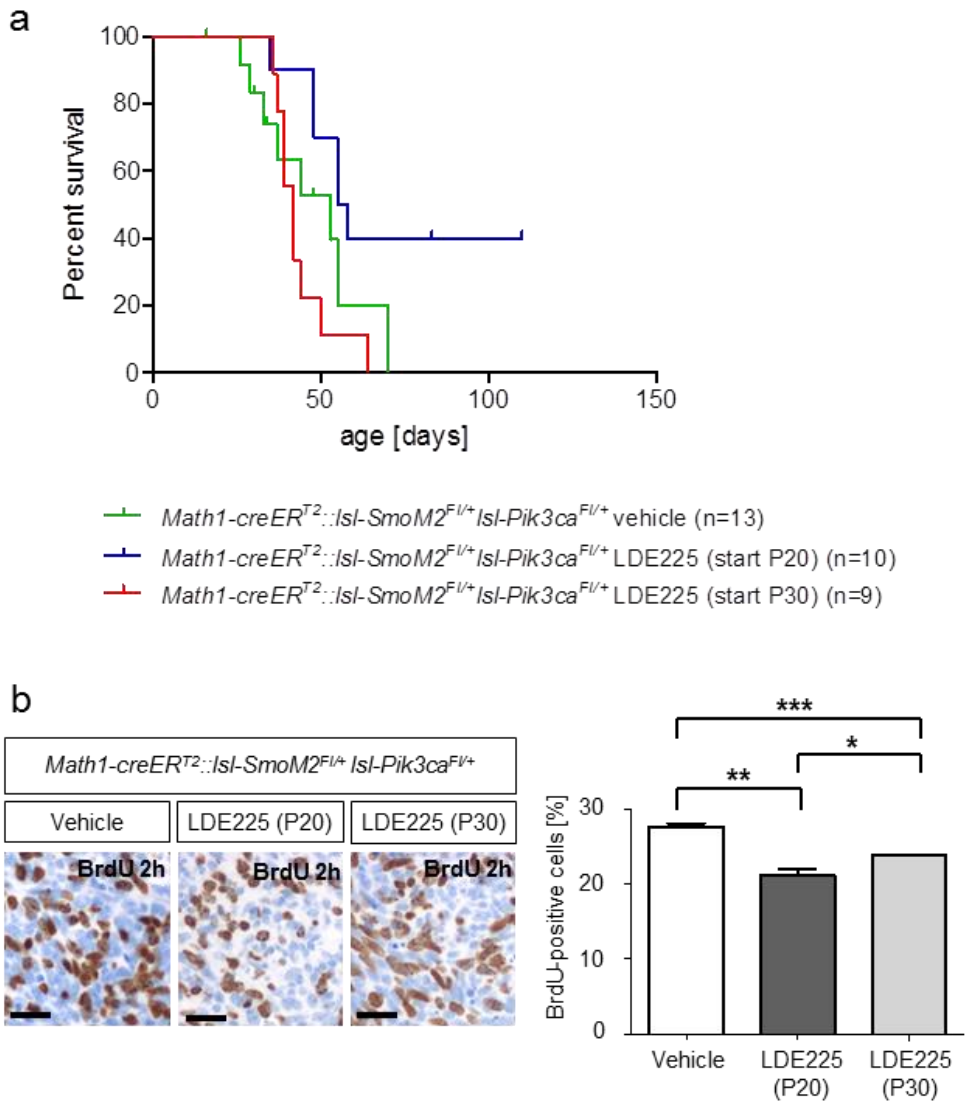

Figure 23 (a) Kaplan-Meier survival curve illustrating overall survival of *Math1-creER^{T2}::lsl-SmoM2$^{Fl/+}$ lsl-Pik3ca$^{Fl/+}$* mice in LDE225 treatment cohort. All mice were induced to tumor formation at P3 by tamoxifen and treated with vehicle or LDE225 from P30 to P51 or P20 to P41. *Math1-creER^{T2}::lsl-SmoM2$^{Fl/+}$ lsl-Pik3ca$^{Fl/+}$* LDE225 (treatment start P20) (n = 10) vs *Math1-creER^{T2}::lsl-SmoM2$^{Fl/+}$ lsl-Pik3ca$^{Fl/+}$* vehicle (n = 13) (p = 0.0651); *Math1-creER^{T2}::lsl-SmoM2$^{Fl/+}$ lsl-Pik3ca$^{Fl/+}$* LDE225 (treatment start P30) (n = 9) vs *Math1-creER^{T2}::lsl-SmoM2$^{Fl/+}$ lsl-Pik3ca$^{Fl/+}$* vehicle (n = 13) (p = 0.2982); *Math1-creER^{T2}::lsl-SmoM2$^{Fl/+}$ lsl-Pik3ca$^{Fl/+}$*

LDE225 (treatment start P20) (n = 10) vs *Math1-creER^{T2}::lsl-SmoM2$^{Fl/+}$ lsl-Pik3ca$^{Fl/+}$* LDE225 (treatment start P30) (n = 9) (p = 0.0065); (b) Quantification of the fraction of BrdU^{+} tumor cells at P51 (for vehicle and LDE225 (P30)) and at P41 (for LDE225 (P20)) in *Math1-creER^{T2}::lsl-SmoM2$^{Fl/+}$ lsl-Pik3ca$^{Fl/+}$* mice treated with vehicle or LDE225 for 21 days (n = 3, mean ± SEM, *t-test*), *scale bar* 20 µm. * p < 0.05, ** p < 0.01, *** p < 0.001.

3.4.1.3 LDE225 treatment in *Math1-creER^{T2}::Ptch1$^{Fl/Fl}$* mice

This mouse strain was also treated with the same dosage (30 mg/kg/day) and duration (5 times per week, for 3 weeks) of LDE225. Here treatment start was P30. LDE225 treatment leads to a significant better survival rate (p = 0.0198) compared to the control group (Figure 24 a). After three weeks of LDE225 treatment there is a significant reduction in BrdU^{+} cells in LDE225-treated tumors of *Math1-creER^{T2}::Ptch1$^{Fl/Fl}$* mice (Figure 24 b). The treatment has no effect on the morphology of *Math1-creER^{T2}::Ptch1$^{Fl/Fl}$* tumors compared to untreated tumors (data not shown).

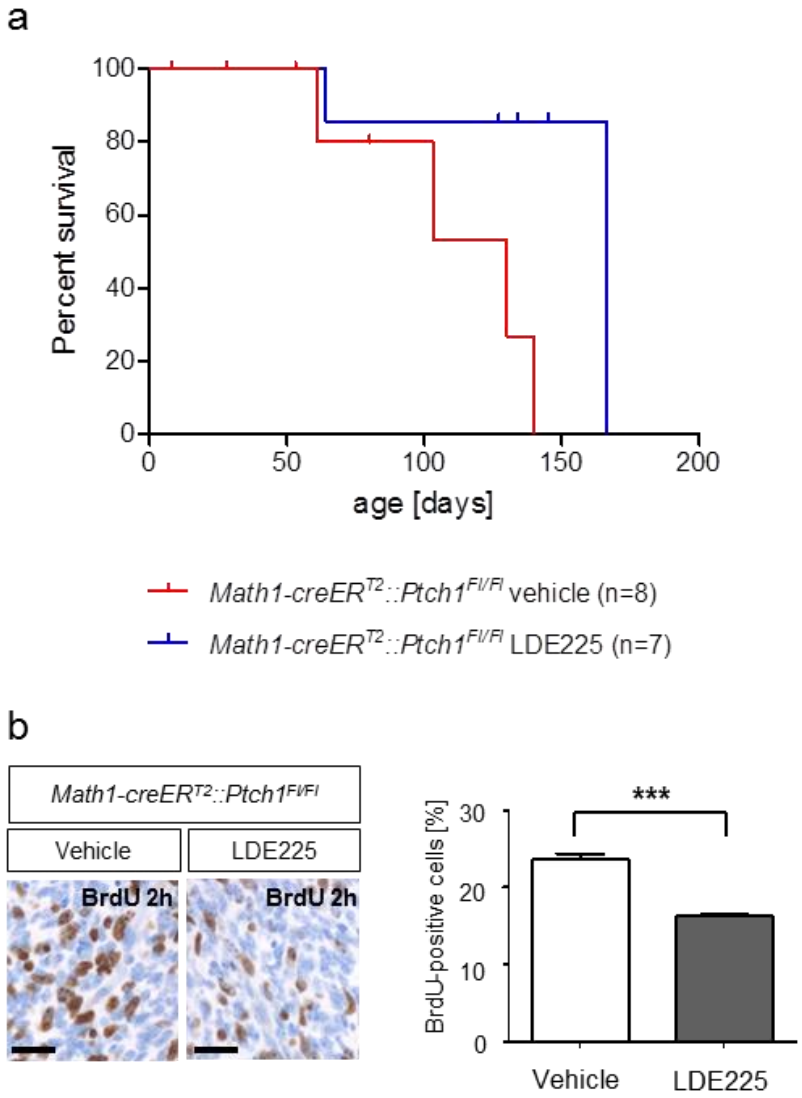

Figure 24 (a) Kaplan-Meier survival curve illustrating overall survival *of Math1-creER^{T2}::Ptch1$^{Fl/Fl}$* mice in LDE225 treatment cohort. All mice were induced to tumor formation at P3 by tamoxifen and treated with vehicle or LDE225 from P30 to P51. *Math1-creER^{T2}::Ptch1$^{Fl/Fl}$* vehicle (n = 14) vs *Math1-creER^{T2}::Ptch1$^{Fl/Fl}$* LDE225 (n = 7) (p = 0.0198); (b) Quantification of the fraction of BrdU^{+} tumor cells at P51 in *Math1-creER^{T2}::Ptch1$^{Fl/Fl}$* mice treated with vehicle or LDE225 for 21 days (n = 3, mean ± SEM, *t-test*), *scale bar* 20 µm. *** $p < 0.001$.

4 Discussion

MB is a collection of clinically and molecularly distinct tumor subgroups that arise either in the cerebellum or brainstem (Louis et al. 2007, Schüller et al. 2008, Grammel et al. 2012, Taylor et al. 2012). In children they comprise the most frequent embryonal brain tumor, whereas in adults the disease is relatively rare, accounting for about 1% of all intracranial malignancies (Louis et al. 2007). Current therapy regimens including surgery, cranio-spinal radiotherapy, and chemotherapy, may cure 70-80% of patients with MB. Most survivors, however, suffer from long-term sequelae as a result of the intensive treatment, demonstrating that less toxic treatments are urgently needed. Molecular analyses have shown that there are four major MB subgroups (WNT, Sonic Hedgehog (SHH), Group 3, Group 4) (Taylor et al. 2012). But this is just a rough classification as a considerable amount of heterogeneity was already described within a single molecular subgroup. Specifically for human SHH-associated MB, differences on the molecular level and also in clinical parameters were described for infants and adult patients (Northcott et al. 2011). Curiously, Shh-MB occur in a bimodal distribution, making up the majority of infant (≤ 3 years) and adult (≥ 16 years) MBs, but only a very small fraction of childhood (4-15 years) tumors. This unusual bimodal age distribution also suggests the existence of Shh-subgroup heterogeneity.

As targeted therapies for MB patients are novel strategies for treatment, this project focused on different mouse models for analysing Shh-associated MBs in more detail.

4.1 Localization of SHH medulloblastoma in mice

In order to unravel a possible relation between MB biology and localization, and to provide novel hints regarding the cellular origin of MB, *Math1-GFP,Ptc*$^{+/-}$ mice, which develop green fluorescent SHH MBs, were analysed regarding tumor localization. MB occurring in *Ptc*$^{+/-}$ mice or Smo-based mouse models resemble the human counterparty in an excellent manner (Pöschl et al. 2014). For so far unknown reasons, human adult SHH MBs are almost exclusively located in cerebellar hemispheres, whereas human infant SHH

MBs often grew in the vermis (Wefers et al. 2014). Here we show in mice that 60% of the younger group (5-week-old) had tumors that exclusively grew in the hemispheres, but 17% were restricted to the vermis. In contrast, in the older group (10-week-old) all tumors grew in the hemispheres and no single tumor was restricted to the vermis (Figure 13). This leads to the suggestion that tumors in the vermis do not develop at later stages and must develop in embryonic or early postnatal stages. Otherwise, one would clearly expect MBs that exclusively occupy the vermis also in the older group. To confirm the time-dependent localization of SHH MB, another Shh-associated mouse model (*Math1-creER^{T2}::lsl-SmoM2$^{Fl/+}$*) was used (Figure 14). It could be demonstrated that there is less tumor burden in the vermis of postnatal-induced mice compared to embryonically induced mice. Using well established mouse models we showed here that oncogenic transformation of granule cell precursors at early developmental time points may result in the formation of midline and hemispheric medulloblastoma. On the other side, oncogenic transformation at later developmental time points exclusively results in the formation of hemispheric medulloblastoma. These results perfectly match to the recently published distribution of SHH MBs in humans (Wefers et al. 2014) and indicate that the localization of SHH MBs is dependent on the time-restricted susceptibility of granule cell precursors in defined cerebellar compartments, and independent of the type of tumor-initiating driver mutation.

The tumor incidence of the *Math1-GFP,Ptc$^{+/-}$* mice used here was clearly higher as described before (Figure 13 a). The 5-week old group show a tumor incidence of 46% and 10-week old mice 80%, whereas Oliver and colleagues only described a tumor incidence of 14-20% of *patched* heterozygotes (Oliver et al. 2005). The rather high incidence in this study here could be explained as it is known that the tumor incidence (and spectrum) in *Ptc$^{+/-}$* mice may vary from colony to colony.

The time point of tumor analysis (as for *Math1-GFP,Ptc$^{+/-}$* mice) and tumor induction (as for *Math1-creER^{T2}::lsl-SmoM2$^{Fl/+}$* mice) is a crucial point with some limitations. Apart from tumors that eventually develop, normal granule neuron precursors also express Math1 and will hence shine green in *Math1-GFP* mice. Thus, mice with 3 weeks of age or even younger are not suited for our experiments, because granule neuron precursors are still present and one would detect green fluorescence all over the cerebellum. Furthermore, SHH MB occur either in infancy (predominantly in midline structures) or in adulthood

(predominantly in cerebellar hemispheres). 1 year in humans approximately corresponds to 3 weeks of age in mice (ten Donkelaar et al. 2006, Manto et al. 2013). While 3 weeks is too early for tumor analysis in mice, 5 weeks of age appears appropriate and still corresponds to human infancy. 10 weeks of age in mice were chosen, since this is well after mice become fertile, which corresponds to the age of 16-20 years of humans. This exactly covers the second peak of incidence for human SHH medulloblastoma. Mice older than 10 weeks of age appear inappropriate, since we would lose too many mice, which die between 10 and 20 weeks of age. Furthermore, tumors may have become huge, so that it is very hard, if not impossible to judge, whether a tumor started in the vermis or in one of the hemispheres. For the tamoxifen application in *Math1-creER^{T2}::lsl-SmoM2$^{Fl/+}$* mice, there is a theoretical time frame between E14.5 and P8 with 100% tumor incidence (Yang et al. 2008). While it is very hard to estimate, at which time point tumor initiation occurs in humans, we thought that choosing time points for tamoxifen induction that are far away from each other would be good to detect any possible differences in tumor localization.

4.2 Wnt/ß-catenin signalling and Shh-dependent medulloblastoma

Survival of children with relapsed or refractory MB remains remarkably poor despite aggressive treatment protocols and cure is a rare exception for these patients (Jones et al. 2012). This highlights the urgent medical need to identify and validate novel molecular targets that can be exploited for the treatment of these patients in order to improve their dismal prognosis. Since conventional therapies and risk stratification have already been optimized in recent years, molecular targeted therapies are currently considered to open promising perspectives for more efficient therapies.

The SHH pathway interacts with different other pathways. The Wnt/beta-catenin and the Hedgehog (Hh) pathway interact in various cell types while eliciting opposing or synergistic cellular effects (see 1.3.3.3). Previous studies showed that Wnt/β-Catenin activation is able to inhibit the Shh-driven proliferation of cerebellar granule neuron precursor cells (CGNPs) (Lorenz et al. 2011) as well as tumor growth in Shh-dependent medulloblastoma (Pöschl et al. 2014). Our *in vitro* analyses in GNPs of *SmoM2$^{Fl/+}$*, *Ctnnb1(ex3)$^{Fl/+}$* and *SmoM2$^{Fl/+}$ Ctnnb1(ex3)$^{Fl/+}$* mice could demonstrate that Shh signalling

leads to an increase of proliferation, Wnt signalling to a decrease of proliferation, and Wnt signalling decreases the proliferation in the increased condition of Shh signalling. Thus, the proliferation of Shh-medulloblastoma cells may be blocked through canonical Wnt signalling. These results extend previous studies showing inhibitory effects of Wnt3a through non-canonical Wnt signalling on GNPs (Anne et al. 2013). Furthermore, we could demonstrate that the Wnt target *Axin2* is upregulated and the Shh target *Gli1* is downregulated in GFP^{+} cells of *SmoM2*$^{Fl/+}$*Ctnnb1*(*ex3*)$^{Fl/+}$ GNP cultures. In addition, β-catenin was identified as a GSK3 substrate: GSK3-mediated phosphorylation triggers β-catenin destabilization (Peifer et al. 1994, Yost et al. 1996). This finding thus established a central role for GSK3 in Wnt/ß-catenin signalling. Studies since then have revealed multifaceted roles of this kinase in Wnt signal transduction. Although the detailed mechanisms for GSK3 regulation during Wnt signal transduction remain incompletely understood, it is clear that Wnt-mediated GSK3 regulation does not utilize the same phosphorylation events as in AKT signalling (Yuan et al. 1999, Ding et al. 2000). Recent advances indicate that GSK3 also plays a positive role in Wnt signal transduction by phosphorylating the Wnt receptors low density lipoprotein receptor-related protein (LRP5/6) and provide new mechanisms for the suppression of GSK3 activity by Wnt in β-catenin stabilization. Furthermore, GSK3 mediates crosstalk between signalling pathways and β-catenin-independent downstream signalling from Wnt. Hence, active canonical Wnt signalling is a potent inhibitor of the Shh pathway in medulloblastoma. Pharmacologically, activation of Wnt/β-catenin signalling can be achieved via inhibition of GSK3β. Cre treatment of cerebellar *GSK3β*$^{Fl/Fl}$ GNPs significantly decreased proliferation (Figure 18).

With the intent of investigating, whether the newly discovered inhibitory effect of Wnt over Shh might represent a novel approach in the therapy of Shh-associated medulloblastoma, *in vitro* experiments on medulloblastoma cells were conducted using Lithium, a well-known Wnt activator (Stambolic et al. 1996, Lancaster et al. 2011). Results showed that Lithium is able to reduce cell viability of CGNPs and medulloblastoma tumor cells from *Math1-cre::SmoM2*$^{Fl/+}$ and *Ptch1*$^{+/-}$ mice *in vitro* (Figure 19). Therefore, considering the encouraging in vitro results, it is possible to propose the hypothesis that Wnt activators may represent a valuable therapeutic option for Shh-associated medulloblastoma. Further investigations adopting different dosages of Lithium and other Wnt-activating substances appear therefore to be required.

4.3 Establishment and characterization of mouse models

Besides the Wnt pathway, there are some other pathways that interact with the SHH pathway and components of these pathways may represent venues for further investigation, especially in the context of combination therapy with the SHH pathway. P53 is one of it. In the light of the observation from Kool et al. 2014 that TP53 was enriched in pediatric (ages 4-17) MBs, the role of p53 in MB should be examined closely. P53 status is important in the prognosis of patients with SHH-medulloblastoma, as well as disease incidence. A cohort study suggested that TP53 status plays a critical role in survival status of patients, with five-year survival rates differing significantly between 41% and 81%, respectively, for SHH-medulloblastoma patients with and without TP53 mutations (Zhukova et al. 2013). In this study we tried to develop a tumor model based on *MYCN* amplification and *TP53* mutation in cerebellar granule precursors, as this combination commonly occurred in the human system at relapse of MB patients (Hill et al. 2015). As no tumor development or any other lesions in the brain could be observed (Figure 8), one explanation could be that the tumor incidence of our mouse model is so low, that we could not detect one tumor, compared to our *Math1-creER^{T2}::lsl-SmoM2$^{Fl/+}$* model, in which penetrance was 100%. This suggests that, in general, Cre-mediated excision should be sufficient to achieve a tumor penetrance of 100%, but also that MYCN and P53 expression may be variable and that a threshold sufficient for tumor development may not be reached in tumor-free *Math1-creER^{T2}::lsl-Nmyc p53* (homo- and heterozygous) mice. Alternatively, additional hits that have not occurred in tumor-free mice may be required for tumor development. However, a potential "second hit" could not be identified yet.

MYC family oncogenes are amplified in ~10% of medulloblastoma tumors and amplifications correlates with poor survival (Huse and Holland 2010, Kool et al. 2012, Korshunov et al. 2012). *MYCN* is highly expressed in two of the medulloblastoma subgroups (SHH group and Group 4 tumors) (Taylor et al. 2012). To date, however, N-myc overexpression (alone or in combination with Gli1, IGF-II, or Bcl-2) has failed to initiate MB in any experimental model (Browd et al. 2006, McCall et al. 2007). Interestingly, a model of MB where murine-derived allografted cells are implanted into

nude mice could be developed (Cage et al. 2015). Since PI3K stabilizes MYCN, PI3K inhibitors were used to drive degradation. It could be shown that these inhibitors can drive apoptosis in MYCN-driven cancers.

PI3K/AKT signalling is also shown to crosstalk with Hh signalling. The activity of Gli1 is crucial determined by its protein stability and localization. Several kinases were known to modulate Gli1 protein stability and localization. Treatment of melanoma cells with AKT1 inhibitors decreased the number of cells with nuclear Gli1 labelling, while increasing the number of cells with cytoplasmic Gli1 labelling, suggesting that AKT1 may be required for Gli1 nuclear localization and transcriptional activity (Stecca et al. 2007). However, as shown in neuroblastoma, Gli1 activity is suppressed by AKT2 which phosphorylates GSK3ß, leading to GSK3ß stabilizing the inhibitory SUFU/GLI1 complex (Paul et al. 2013). As Gli1 represents downstream SHH signalling, it is an attractive target for specific SHH mediated MB. Inhibition of its activating kinases or activation of its inhibitory kinases can be explored. Here, we combined the already existing and well described SHH mouse models *Math1-creER^{T2}::lsl-SmoM2$^{Fl/+}$* (see 3.1.1) and *Math1-creER^{T2}::Ptch1$^{Fl/Fl}$* (see 3.1.3) with a PIK3CA mutation (*Math1-creER^{T2}::lsl-SmoM2$^{Fl/+}$ lsl-Pik3ca$^{Fl/+}$*, *Math1-creER^{T2}::Ptch1$^{Fl/Fl}$ lsl-Pik3ca$^{Fl/+}$* and *Math1-creER^{T2}::Ptch1$^{Fl/Fl}$ lsl-Pik3ca$^{Fl/Fl}$ mice).* To analyse the effect of an acute PIK3CA mutation in the view of oncogenic transformation, these inducible tumor models were generated, which enable a conditional activation of the Shh pathway in postnatal granule cell precursors and a simultaneous constitutive activated form of *PIK3CA.* The additional PIK3CA mutation shows an increase in proliferation, leads to a faster tumor development and therefore a significantly worse survival prognosis (Figure 6, Figure 7). Hh and PI3K signalling appear to synergize in promoting proliferation of cerebellar neuronal precursors and the formation of medulloblastoma tumors. Furthermore, looking at the localization of the *Math1-creER^{T2}::lsl-SmoM2$^{Fl/+}$ lsl-Pik3ca$^{Fl/+}$* tumors it was striking that 13/18 (~72%) had contact to the brainstem. For further analysis it would be interesting if these tumors grow into the brainstem or also develop out of it. These newly developed mouse models can be used for further analysis, e.g treatment studies.

4.4 LDE225 treatment of Shh-associated mouse models

Inhibition of the Hh pathway is considered as promising therapeutic avenue and small-molecule Hh inhibitors are currently evaluated in early clinical trials for Hh-driven cancers (Low and de Sauvage 2010, Amakye et al. 2013). Hh-driven childhood tumors besides MB are rhabdomyosarcoma (RMS) and rhabdoid tumors (RTs). SMO inhibitors are the leading Hh inhibitors in clinical development, examples are LDE225 and Vismodegib. The remarkable clinical response of a patient with MB to Vismodegib emphasizes the great potential of targeting the Hh pathway in Hh-driven pediatric cancers (Rudin et al. 2009). Based on this proof-of-concept, a phase I/II clinical trial with the SMO inhibitor LDE225 in pediatric advanced solid cancers has been launched (Geoerger et al. 2012). So far, LDE225 turned out to be well-tolerated and clinical responses were observed in patients with documented Hh activation. Recently, a phase III clinical trial with LDE225 in MB has been launched (www.clinicaltrials.gov).

Although a patient with Hh-driven MB initially showed a remarkable response to the SMO inhibitor Vismodegib (Rudin et al. 2009), persistent therapy rapidly led to acquired resistance (Yauch et al. 2009). This indicates that, like other targeted therapies, secondary resistance to SMO inhibitors is a potential hurdle to durable responses in the clinic. In the context of resistance to kinase inhibitors, the elucidation of mechanisms of resistance has enormously accelerated the design of alternative strategies to avoid or overcome resistance. Thus, a better understanding of the molecular mechanisms of resistance against Hh inhibitors is a top priority.

Several other substances for the treatment of MB have already been analysed. Cyclopamine suppresses MB development in *Ptch1*$^{+/-}$ mice (Sanchez and Ruiz i Altaba 2005). Unfortunately, cyclopamine is not proper for clinical development because of its low oral solubility (Lipinski et al. 2008). More SMO inhibitors are currently being evaluated, including vismodegib (GDC-0449), sonidegib (LDE225), BMS-833923, PF-04449913 and LY2940680, in clinical trials in advanced cancers (Amakye et al. 2013). Among these, vismodegib became the first U.S. Food and Drug Administration (FDA) approved SMO antagonist for the treatment of advanced or metastatic BCC in 2012 (Fellner 2012). Vismodegib significantly lessens the rate of appearance of new BCCs in

patients (Sekulic et al. 2012). Nonetheless, reports showed that most BCCs regrow after vismodegib is stopped (Tang et al. 2012).

GANT61 and HPI-1 are potential therapeutics for MB that target the Hh signalling pathway; both target Gli1 and Gli2 (Lauth et al. 2007, Hyman et al. 2009, Mazumdar et al. 2011). Recent evidence has shown that ATO can inhibit the Hh pathway via mechanisms distinct from that of SMO inhibitors via inhibition of GLI proteins, i. e. by blocking ciliary accumulation of GLI2 and by direct binding and inhibition of GLI1/2 proteins (Kim et al. 2010, Beauchamp et al. 2011). Thus, ATO, a Food and Drug administration (FDA)-approved drug for the treatment of acute promyelocytic leukemia, may offer an alternative treatment option to overcome resistance to SMO inhibitors. Indeed, ATO was recently shown in preclinical models to retain antitumor activity in SMO inhibitor-refractory tumors (Kim et al. 2013). Since concomitant perturbations in additional pathways, which interact with Hh signalling or which become activated as compensatory mechanisms, have been reported in Hh inhibitor-resistant cases, rational drug combinations have been suggested, including PI3K/AKT/mTOR or RAS/MEK/ERK inhibitors or epigentically acting drugs (Stecca et al. 2007, Buonamici et al. 2010, Wang et al. 2012, Filbin et al. 2013).

LDE225, BMS-833923 and saridegib target SMO (Buonamici et al. 2010, Lee et al. 2012, Lin and Matsui 2012). Here we used LDE225 for the treatment of our Shh-associated mouse models.

Several Smo antagonists including LDE225 are currently being evaluated in clinical trials in patients with advanced solid tumors including medulloblastoma (Tremblay et al. 2009). However, acquired resistance has emerged as a challenge to targeted therapeutics and may limit their anti-cancer efficacy (Engelman and Settleman 2008). Indeed, evidence of resistance to Smo inhibition has recently been reported in a medulloblastoma patient who progressed during therapy with the Smo antagonist GDC0449 (Rudin et al. 2009). Here, mouse strains with an activation of the Shh pathway - *Math1-creER^{T2}::lsl-SmoM2$^{Fl/+}$*, *Math1-creER^{T2}::lsl-SmoM2$^{Fl/+}$ lsl-Pik3ca$^{Fl/+}$*, and *Math1-creER^{T2}::Ptch1$^{Fl/Fl}$* - were treated with LDE225 (Figure 21, Figure 23, Figure 24). In both mouse strains with only one mutation (*Math1-creER^{T2}::lsl-SmoM2$^{Fl/+}$* and *Math1-creER^{T2}::Ptch1$^{Fl/Fl}$*) LDE225 treatment led to a significant better survival rate and to a decrease of proliferation of the tumor.

Finally these mice died of tumor symptoms anyway. Here we suggest that after the 3-week long treatment phase, tumor cells of *Math1-creER^{T2}::lsl-SmoM2$^{Fl/+}$* and *Math1-creER^{T2}::Ptch1$^{Fl/Fl}$* mice developed resistance mechanisms. It is conceivable that genetic alterations (mutations, copy-number changes) or changes in gene expression profile appeared after the drug treatment that could explain the acquired resistance. Current evidence suggests that treatment response to SMO inhibitors may only be transient, while resistance rapidly emerges (Kool et al. 2014). Some initially responsive tumors may also acquire secondary resistance to treatment, whereas other patients keep in remission for several years on a single targeted drug. This indicates that, like other targeted therapies, secondary resistance to SMO inhibitors is a potential hurdle to durable responses in the clinic.

Whereas the additional PIK3CA mutation in *Math1-creER^{T2}::lsl-SmoM2$^{Fl/+}$ lsl-Pik3ca$^{Fl/+}$* mice led to an inhibition of the positive effect of LDE225 treatment. The Smo inhibiton effect of LDE225 is here not enough. The survival prognosis for LDE225 treated *Math1-creER^{T2}::lsl-SmoM2$^{Fl/+}$ lsl-Pik3ca$^{Fl/+}$* mice does not differ compared to the control group. This upregulation of PI3K signalling could be a mechanism to evade Smo inhibition. Therefore a combination therapy of this Smo inhibitor and an additional PI3K/Tor inhibitor would be useful. A recent study demonstrated that Igf2, through PI3K signalling, potentiates Gli activation induced by low levels of Hh ligand (Riobo et al. 2006). It is possible that under conditions of continuous Hh pathway inhibition, the PI3K pathway compensates for the loss of Hh signalling and thus becomes a major mediator of resistant tumor growth. A combination of the selective PI3K inhibitor BKM120 (also known as Buparlisib), which is already used in clinical trials, and LDE225 constitutes a potential strategy to delay or prevent resistance to Smo antagonists and has important implications for future treatment strategies in medulloblastoma and also other Smo-dependant human cancers.

Interestingly, the earlier treatment start at P20 in *Math1-creER^{T2}::lsl-SmoM2$^{Fl/+}$ lsl-Pik3ca$^{Fl/+}$* mice led to a significant better survival prognosis compared to the later treated mice which started at P30 (Figure 23 a). This concludes how important it is to start treatment of tumor as soon as possible. It is conceivable that an even earlier starting point can lead to an even better prognosis.

For future experiments it is planned that the mouse models which were treated with LDE225 (*Math1-creER^{T2}::lsl-SmoM2$^{Fl/+}$*, *Math1-creER^{T2}::lsl-SmoM2$^{Fl/+}$ lsl-Pik3ca$^{Fl/+}$*, and *Math1-creER^{T2}::Ptch1$^{Fl/Fl}$* mice) will be molecularly analysed in detail. These molecular analyses include whole exome sequencing of tumor DNA and low-coverage WGS of tumor DNA. All samples will be analysed by the mentioned methods before any drug treatment in order to fully characterize these models and identify mutations and copy-number aberrations that could explain any primary drug resistance present in the tumors at the time of biopsy. After drug treatment we will sequence and profile those tumors that became resistant to drug treatment to see whether any genetic alterations (mutations, copy-number changes) or changes in gene expression profiles will appear that could explain the acquired resistance.

Smoothened inhibitors are now available clinically to treat medulloblastoma. However, resistance to these inhibitors rapidly develops thereby limiting their efficacy. The determination of Smoothened crystal structures enables structure-based discovery of new ligands with new chemotypes that will be critical to combat resistance. In a current study 3.2 million available, lead-like molecules against Smoothened were docked, looking for those with high physical complementarity to its structure; this represents the first such campaign against the class Frizzled G-protein coupled receptor family. Twenty-one high-ranking compounds were selected for experimental testing, and four, representing three different chemotypes, were identified to antagonize Smoothened with IC_{50} values better than 50 μM. A screen for analogs revealed another six molecules, with IC_{50} values in the low micromolar range (Lacroix et al. 2016). Importantly, one of the most active of the new antagonists continued to be efficacious at the D473H mutant of Smoothened, which confers clinical resistance to the antagonist vismodegib in cancer treatment.

In light of recent literature, several considerations are important for future therapeutic development for SHH MB. The first consideration is the variable genetic backgrounds of SHH-MB in infants, children and adults. For example, patients with mutations upstream in the SHH pathway (*SHH* amplifications, *PTCH1* and *SMO* mutations) in general may respond more favourably to SMO inhibitors, while those with mutations downstream (*GLI2* mutations) may be more resistant to treatment (Kool et al. 2014). The second is the development of resistance. An understanding of the radiation and chemotherapy resistance mechanisms of MB is necessary for efficient targeting of medulloblastoma.

Assessing the influence of crosstalk from other signalling pathways will significantly contribute to novel therapeutics for MB with regard to combination therapeutics.

4.5 Perspectives

Currently, the selection of patients with MB that qualify for the clinical trial with the SMO inhibitor LDE225 is based on a five gene signature that indicates Hh pathway activation (Weller et al. 2013). However, this diagnostic test will not be sufficient to identify LDE225-responsive patients, since it cannot distinguish between different aberrations causing Hh activation, e. g. between *PTCH1* mutation and *GLI1/2* amplification. The innovation of our collaborative project resides in the development of more precise molecular diagnostic tests that not only detect global activation of the Hh pathway, but also allow for the precise definition of the underlying genetic alterations in each individual tumor. This will enable the robust pre-therapeutic stratification of patients for the most suitable Hh inhibitor. In the long-term perspective, these diagnostic assays will be exploited for patient selection in ongoing and future clinical trials with Hh inhibitors for precision oncology.

As just tumors with downstream mutations may be more resistant to treatment, these mutations should be further investigated in mouse studies. One further mouse model which should be developed for future studies carries a *GLI2* mutation or the combination of *GLI2* amplifications and *TP53* mutations, as this was found to occur in children (ages 4-17) (Kool et al. 2014). This model should be characterized in detail and used for treatment studies with ATO and/or GANT61.

In addition to the GEMMs, the antitumor activity of Hh inhibitors in relevant preclinical models including PDX (patient-derived xenograft; human SHH-MB) models could be analysed in parallel with molecular characterization of the corresponding human tumor samples, the results of the project will provide novel insights into which molecular aberrations causing Hh activation are amenable to which type of Hh pathway inhibitor. Depending on the drug responses using single drugs and the molecular alterations identified in these treated tumors, the experiments will be repeated and rational drug combinations will be used to see whether the induced drug resistance can be prevented. The studies in PDX models will be corroborated by our studies in GEMMs with defined aberrations of the Hh signalling pathway. Since more and more Hh inhibitors are being developed to block Hh signalling at distinct levels of the pathway and since more and more molecular lesions are being identified that cause aberrant Hh activation in human cancers, the challenge is to precisely tailor the most suitable Hh inhibitor to the individual patient's tumor aberrations. For example, patients harboring Smoothened (SMO) mutation will

likely respond to SMO inhibitors, while patients exhibiting *GLI2* amplification are expected to benefit from GLI inhibitors. The results of our preclinical studies will be translated into the ongoing and future clinical trials with Hh inhibitors in children. Since the development of rationally targeted cancer therapeutics requires a full understanding of the pharmacokinetic/pharmacodynamics (PK/PD) relationship of the investigational agents, we will also utilize the preclinical models of Hh pathway activation to correlate Hh inhibitor levels in the plasma with pathway inhibition and with antitumor effects. The results of these preclinical PK/PD studies will provide useful PK exposure targets as well as PD endpoints that can be used as gates for further clinical development.

By elucidating primary and acquired resistance mechanisms to SMO inhibitors, which are currently the leading Hh inhibitors under clinical evaluation, the results of the project will pave the way for novel therapeutic strategies to overcome resistance or, alternatively, to avoid resistance by dispatching tumors before they become refractory. For example, GLI1/2 inhibitors such as arsenic trioxide (ATO) may offer an alternative treatment option for cases that are refractory to SMO inhibitors, e.g. due to *GLI2* amplification. Another example is the design of combination therapies to concomitantly block compensatory pathways that become activated upon acquired resistance to SMO inhibitors, e.g. by using PI3K/AKT/mTOR inhibitors. Thus, the results of this project will contribute to the development of alternative treatment strategies for Hh inhibitor-resistant patients in many ways, i.e. 1) by discovering the different molecular lesions that cause Hh activation in primary tumor samples, 2) by identifying the mechanism of resistance to Hh inhibitors in PDX models and GEMMs and 3) by evaluating alternative treatment options in refractory mouse models to either circumvent resistance or to avoid the emergence of resistance by pre-emptively treating with a combination. The results of these studies will be translated into the ongoing and future clinical trials with Hh inhibitors in children to design alternative treatment options for patients with primary or acquired resistance to Hh inhibitors. Furthermore, the understanding of common escape mechanisms will help to develop new diagnostics to prescreen patients for the enrolment into clinical trials with Hh inhibitors.

All GEMMs and PDX models will be molecularly characterized by whole exome sequencing, low-coverage WGS (whole genome sequencing), and DNA methylation and gene expression profiling. Tumors that become resistant to Hh pathway inhibition will again be molecularly characterized by sequencing and profiling and data will be compared

to the untreated/vehicle-treated tumors to identify the molecular mechanism(s) of acquired resistance. Based on these molecular findings, rational combination treatments will be used including drugs targeting other pathways co-operating with Hh signalling.
All data generated with the mouse models will be compared with molecular data which are currently generated from clinical SHH-MB samples treated with LDE225, the SMO inhibitor that is being used in a phase III clinical trial in Germany embedded in the overall HIT-REZ concept which promotes early clinical trials and therapy optimization studies for children and young adults with recurrent MB and ependymoma. Our increased understanding of primary and secondary resistance mechanism in SHH-MB will form a basis not only for rational combination therapies for primary and relapsed SHH-MB tumors, but also for the development of second-generation Hh inhibitors and for the development of diagnostic tests that can be applied in a clinical setting to predict which patients will be responsive to which drugs.

5 References

Aberle, H., A. Bauer, J. Stappert, A. Kispert and R. Kemler (1997). "beta-catenin is a target for the ubiquitin-proteasome pathway." EMBO J 16(13): 3797-3804.

Adams, J. R., K. Xu, J. C. Liu, N. M. Agamez, A. J. Loch, R. G. Wong, W. Wang, K. L. Wright, T. F. Lane, E. Zacksenhaus and S. E. Egan (2011). "Cooperation between Pik3ca and p53 mutations in mouse mammary tumor formation." Cancer Res 71(7): 2706-2717.

Adamson, D. C., Q. Shi, M. Wortham, P. A. Northcott, C. Di, C. G. Duncan, J. Li, R. E. McLendon, D. D. Bigner, M. D. Taylor and H. Yan (2010). "OTX2 is critical for the maintenance and progression of Shh-independent medulloblastomas." Cancer Res 70(1): 181-191.

Akiyoshi, T., M. Nakamura, K. Koga, H. Nakashima, T. Yao, M. Tsuneyoshi, M. Tanaka and M. Katano (2006). "Gli1, downregulated in colorectal cancers, inhibits proliferation of colon cancer cells involving Wnt signalling activation." Gut 55(7): 991-999.

Alda, M. (2015). "Lithium in the treatment of bipolar disorder: pharmacology and pharmacogenetics." Mol Psychiatry 20(6): 661-670.

Alston, R. D., R. Newton, A. Kelsey, M. J. Newbould, J. M. Birch, B. Lawson and R. J. McNally (2003). "Childhood medulloblastoma in northwest England 1954 to 1997: incidence and survival." Dev Med Child Neurol 45(5): 308-314.

Altmann, J. B. S. (1997). "Development of the Cerebellar System in Relation to its Evolution, Structure, and Functions." New York: CRC Press: 783.

Alvarez-Medina, R., G. Le Dreau, M. Ros and E. Marti (2009). "Hedgehog activation is required upstream of Wnt signalling to control neural progenitor proliferation." Development 136(19): 3301-3309.

Amakye, D., Z. Jagani and M. Dorsch (2013). "Unraveling the therapeutic potential of the Hedgehog pathway in cancer." Nat Med 19(11): 1410-1422.

Amit, S., A. Hatzubai, Y. Birman, J. S. Andersen, E. Ben-Shushan, M. Mann, Y. Ben-Neriah and I. Alkalay (2002). "Axin-mediated CKI phosphorylation of beta-catenin at Ser 45: a molecular switch for the Wnt pathway." Genes Dev 16(9): 1066-1076.

Anne, S. L., E. E. Govek, O. Ayrault, J. H. Kim, X. Zhu, D. A. Murphy, L. Van Aelst, M. F. Roussel and M. E. Hatten (2013). "WNT3 inhibits cerebellar granule neuron progenitor proliferation and medulloblastoma formation via MAPK activation." PLoS One 8(11): e81769.

Arnold, K., A. Sarkar, M. A. Yram, J. M. Polo, R. Bronson, S. Sengupta, M. Seandel, N. Geijsen and K. Hochedlinger (2011). "Sox2(+) adult stem and progenitor cells are important for tissue regeneration and survival of mice." Cell Stem Cell 9(4): 317-329.

Athar, M., C. Li, A. L. Kim, V. S. Spiegelman and D. R. Bickers (2014). "Sonic hedgehog signaling in Basal cell nevus syndrome." Cancer Res 74(18): 4967-4975.

Ayrault, O., F. Zindy, J. Rehg, C. J. Sherr and M. F. Roussel (2009). "Two tumor suppressors, p27Kip1 and patched-1, collaborate to prevent medulloblastoma." Mol Cancer Res 7(1): 33-40.

Aza-Blanc, P., F. A. Ramirez-Weber, M. P. Laget, C. Schwartz and T. B. Kornberg (1997). "Proteolysis that is inhibited by hedgehog targets Cubitus interruptus protein to the nucleus and converts it to a repressor." Cell 89(7): 1043-1053.

Bai, C. B., W. Auerbach, J. S. Lee, D. Stephen and A. L. Joyner (2002). "Gli2, but not Gli1, is required for initial Shh signaling and ectopic activation of the Shh pathway." Development 129(20): 4753-4761.

Bale, S. J., R. T. Falk and G. R. Rogers (1998). "Patching together the genetics of Gorlin syndrome." J Cutan Med Surg 3(1): 31-34.

Beauchamp, E. M., L. Ringer, G. Bulut, K. P. Sajwan, M. D. Hall, Y. C. Lee, D. Peaceman, M. Ozdemirli, O. Rodriguez, T. J. Macdonald, C. Albanese, J. A. Toretsky and A. Uren (2011). "Arsenic trioxide inhibits human cancer cell growth and tumor development in mice by blocking Hedgehog/GLI pathway." J Clin Invest 121(1): 148-160.

Behrens, J., B. A. Jerchow, M. Wurtele, J. Grimm, C. Asbrand, R. Wirtz, M. Kuhl, D. Wedlich and W. Birchmeier (1998). "Functional interaction of an axin homolog, conductin, with beta-catenin, APC, and GSK3beta." Science 280(5363): 596-599.

Berman, D. M., S. S. Karhadkar, A. R. Hallahan, J. I. Pritchard, C. G. Eberhart, D. N. Watkins, J. K. Chen, M. K. Cooper, J. Taipale, J. M. Olson and P. A. Beachy (2002). "Medulloblastoma growth inhibition by hedgehog pathway blockade." Science 297(5586): 1559-1561.

Bhanot, P., M. Brink, C. H. Samos, J. C. Hsieh, Y. Wang, J. P. Macke, D. Andrew, J. Nathans and R. Nusse (1996). "A new member of the frizzled family from Drosophila functions as a Wingless receptor." Nature 382(6588): 225-230.

Binning, M. J., T. Niazi, C. A. Pedone, B. Lal, C. G. Eberhart, K. J. Kim, J. Laterra and D. W. Fults (2008). "Hepatocyte growth factor and sonic Hedgehog expression in cerebellar neural progenitor cells costimulate medulloblastoma initiation and growth." Cancer Res 68(19): 7838-7845.

Brechbiel, J., K. Miller-Moslin and A. A. Adjei (2014). "Crosstalk between hedgehog and other signaling pathways as a basis for combination therapies in cancer." Cancer Treat Rev 40(6): 750-759.

Broderick, D. K., C. Di, T. J. Parrett, Y. R. Samuels, J. M. Cummins, R. E. McLendon, D. W. Fults, V. E. Velculescu, D. D. Bigner and H. Yan (2004). "Mutations of PIK3CA in anaplastic oligodendrogliomas, high-grade astrocytomas, and medulloblastomas." Cancer Res 64(15): 5048-5050.

Browd, S. R., A. M. Kenney, O. N. Gottfried, J. W. Yoon, D. Walterhouse, C. A. Pedone and D. W. Fults (2006). "N-myc can substitute for insulin-like growth factor signaling in a mouse model of sonic hedgehog-induced medulloblastoma." Cancer Res 66(5): 2666-2672.

Brugieres, L., G. Pierron, A. Chompret, B. B. Paillerets, F. Di Rocco, P. Varlet, A. Pierre-Kahn, O. Caron, J. Grill and O. Delattre (2010). "Incomplete penetrance of the predisposition to medulloblastoma associated with germ-line SUFU mutations." J Med Genet 47(2): 142-144.

Buonamici, S., J. Williams, M. Morrissey, A. Wang, R. Guo, A. Vattay, K. Hsiao, J. Yuan, J. Green, B. Ospina, Q. Yu, L. Ostrom, P. Fordjour, D. L. Anderson, J. E. Monahan, J. F. Kelleher, S. Peukert, S. Pan, X. Wu, S. M. Maira, C. Garcia-Echeverria, K. J. Briggs, D. N. Watkins, Y. M. Yao, C. Lengauer, M. Warmuth, W. R. Sellers and M. Dorsch (2010). "Interfering with resistance to smoothened antagonists by inhibition of the PI3K pathway in medulloblastoma." Sci Transl Med 2(51): 51ra70.

Cage, T. A., Y. Chanthery, L. Chesler, M. Grimmer, Z. Knight, K. Shokat, W. A. Weiss and W. C. Gustafson (2015). "Downregulation of MYCN through PI3K Inhibition in Mouse Models of Pediatric Neural Cancer." Front Oncol 5: 111.

Chamorro, M. N., D. R. Schwartz, A. Vonica, A. H. Brivanlou, K. R. Cho and H. E. Varmus (2005). "FGF-20 and DKK1 are transcriptional targets of beta-catenin and FGF-20 is implicated in cancer and development." EMBO J 24(1): 73-84.

Clevers, H. (2006). "Wnt/beta-catenin signaling in development and disease." Cell 127(3): 469-480.

Clifford, S. C., M. E. Lusher, J. C. Lindsey, J. A. Langdon, R. J. Gilbertson, D. Straughton and D. W. Ellison (2006). "Wnt/Wingless pathway activation and chromosome 6 loss characterize a distinct molecular sub-group of medulloblastomas associated with a favorable prognosis." Cell Cycle 5(22): 2666-2670.

Coon, V., T. Laukert, C. A. Pedone, J. Laterra, K. J. Kim and D. W. Fults (2010). "Molecular therapy targeting Sonic hedgehog and hepatocyte growth factor signaling in a mouse model of medulloblastoma." Mol Cancer Ther 9(9): 2627-2636.

Corbit, K. C., P. Aanstad, V. Singla, A. R. Norman, D. Y. Stainier and J. F. Reiter (2005). "Vertebrate Smoothened functions at the primary cilium." Nature 437(7061): 1018-1021.

Dijkgraaf, G. J., B. Alicke, L. Weinmann, T. Januario, K. West, Z. Modrusan, D. Burdick, R. Goldsmith, K. Robarge, D. Sutherlin, S. J. Scales, S. E. Gould, R. L. Yauch and F. J. de Sauvage (2011). "Small molecule inhibition of GDC-0449 refractory smoothened mutants and downstream mechanisms of drug resistance." Cancer Res 71(2): 435-444.

Ding, V. W., R. H. Chen and F. McCormick (2000). "Differential regulation of glycogen synthase kinase 3beta by insulin and Wnt signaling." J Biol Chem 275(42): 32475-32481.

Dino, M. R., R. J. Schuerger, Y. Liu, N. T. Slater and E. Mugnaini (2000). "Unipolar brush cell: a potential feedforward excitatory interneuron of the cerebellum." Neuroscience 98(4): 625-636.

Duband, J. L. (2010). "Diversity in the molecular and cellular strategies of epithelium-to-mesenchyme transitions: Insights from the neural crest." Cell Adh Migr 4(3): 458-482.

Duffner, P. K., M. E. Horowitz, J. P. Krischer, H. S. Friedman, P. C. Burger, M. E. Cohen, R. A. Sanford, R. K. Mulhern, H. E. James, C. R. Freeman and et al. (1993). "Postoperative chemotherapy and delayed radiation in children less than three years of age with malignant brain tumors." N Engl J Med 328(24): 1725-1731.

Eberhart, C. G., J. L. Kepner, P. T. Goldthwaite, L. E. Kun, P. K. Duffner, H. S. Friedman, D. R. Strother and P. C. Burger (2002). "Histopathologic grading of medulloblastomas: a Pediatric Oncology Group study." Cancer 94(2): 552-560.

Echelard, Y., D. J. Epstein, B. St-Jacques, L. Shen, J. Mohler, J. A. McMahon and A. P. McMahon (1993). "Sonic hedgehog, a member of a family of putative signaling molecules, is implicated in the regulation of CNS polarity." Cell 75(7): 1417-1430.
Edlund, T. and T. M. Jessell (1999). "Progression from extrinsic to intrinsic signaling in cell fate specification: a view from the nervous system." Cell 96: 211-224.

Ellison, D. W., J. Dalton, M. Kocak, S. L. Nicholson, C. Fraga, G. Neale, A. M. Kenney, D. J. Brat, A. Perry, W. H. Yong, R. E. Taylor, S. Bailey, S. C. Clifford and R. J. Gilbertson (2011). "Medulloblastoma: clinicopathological correlates of SHH, WNT, and non-SHH/WNT molecular subgroups." Acta Neuropathol 121(3): 381-396.

Ellison, D. W., O. E. Onilude, J. C. Lindsey, M. E. Lusher, C. L. Weston, R. E. Taylor, A. D. Pearson and S. C. Clifford (2005). "beta-catenin status predicts a favorable outcome in childhood medulloblastoma: The United Kingdom Children's Cancer Study Group Brain Tumour Committee." J Clin Oncol 23(31): 7951-7957.

Engelman, J. A. and J. Settleman (2008). "Acquired resistance to tyrosine kinase inhibitors during cancer therapy." Curr Opin Genet Dev 18(1): 73-79.

Erdmann, G., G. Schutz and S. Berger (2007). "Inducible gene inactivation in neurons of the adult mouse forebrain." BMC Neurosci 8: 63.

Evans, A. E., R. D. Jenkin, R. Sposto, J. A. Ortega, C. B. Wilson, W. Wara, I. J. Ertel, S. Kramer, C. H. Chang, S. L. Leikin and et al. (1990). "The treatment of medulloblastoma. Results of a prospective randomized trial of radiation therapy with and without CCNU, vincristine, and prednisone." J Neurosurg 72(4): 572-582.

Fellner, C. (2012). "Vismodegib (Erivedge) For Advanced Basal Cell Carcinoma." Pharmacy and Therapeutics 37(12): 670-682.

Filbin, M. G., S. K. Dabral, M. F. Pazyra-Murphy, S. Ramkissoon, A. L. Kung, E. Pak, J. Chung, M. A. Theisen, Y. Sun, Y. Franchetti, Y. Sun, D. S. Shulman, N. Redjal, B. Tabak, R. Beroukhim, Q. Wang, J. Zhao, M. Dorsch, S. Buonamici, K. L. Ligon, J. F. Kelleher and R. A. Segal (2013).

"Coordinate activation of Shh and PI3K signaling in PTEN-deficient glioblastoma: new therapeutic opportunities." Nat Med 19(11): 1518-1523.

Finlay, G. J., W. R. Wilson and B. C. Baguley (1986). "Comparison of in vitro activity of cytotoxic drugs towards human carcinoma and leukaemia cell lines." Eur J Cancer Clin Oncol 22(6): 655-662.

Flora, A., T. J. Klisch, G. Schuster and H. Y. Zoghbi (2009). "Deletion of Atoh1 disrupts Sonic Hedgehog signaling in the developing cerebellum and prevents medulloblastoma." Science 326(5958): 1424-1427.

Geddes, J. R., S. Burgess, K. Hawton, K. Jamison and G. M. Goodwin (2004). "Long-term lithium therapy for bipolar disorder: systematic review and meta-analysis of randomized controlled trials." Am J Psychiatry 161(2): 217-222.

Geoerger, B., Isabelle Aerts, Michela Casanova, Julia C. Chisholm, Darren R Hargrave, Sarah Leary, David M Ashley, Eric Bouffet, Tobey MacDonald, Eunju Hurh, Jyotirmoy Dey, Stacey Kalambakas, D. D. Amakye and M. W. Kieran (2012). "A phase I/II study of LDE225, a smoothened (Smo) antagonist, in pediatric patients with recurrent medulloblastoma (MB) or other solid tumors." J Clin Oncol (Meeting Abstracts) 30: 9519.

Gibson, P., Y. Tong, G. Robinson, M. C. Thompson, D. S. Currle, C. Eden, T. A. Kranenburg, T. Hogg, H. Poppleton, J. Martin, D. Finkelstein, S. Pounds, A. Weiss, Z. Patay, M. Scoggins, R. Ogg, Y. Pei, Z. J. Yang, S. Brun, Y. Lee, F. Zindy, J. C. Lindsey, M. M. Taketo, F. A. Boop, R. A. Sanford, A. Gajjar, S. C. Clifford, M. F. Roussel, P. J. McKinnon, D. H. Gutmann, D. W. Ellison, R. Wechsler-Reya and R. J. Gilbertson (2010). "Subtypes of medulloblastoma have distinct developmental origins." Nature 468(7327): 1095-1099.

Goodrich, L. V., L. Milenkovic, K. M. Higgins and M. P. Scott (1997). "Altered neural cell fates and medulloblastoma in mouse patched mutants." Science 277(5329): 1109-1113.

Grammel, D., M. Warmuth-Metz, A. O. von Bueren, M. Kool, T. Pietsch, H. A. Kretzschmar, D. H. Rowitch, S. Rutkowski, S. M. Pfister and U. Schuller (2012). "Sonic hedgehog-associated medulloblastoma arising from the cochlear nuclei of the brainstem." Acta Neuropathol 123(4): 601-614.

Grosche, J., H. Kettenmann and A. Reichenbach (2002). "Bergmann glial cells form distinct morphological structures to interact with cerebellar neurons." J Neurosci Res 68(2): 138-149.

Hahn, H., L. Wojnowski, G. Miller and A. Zimmer (1999). "The patched signaling pathway in tumorigenesis and development: lessons from animal models." J Mol Med (Berl) 77(6): 459-468.

Hahn, H., L. Wojnowski, K. Specht, R. Kappler, J. Calzada-Wack, D. Potter, A. Zimmer, U. Muller, E. Samson, L. Quintanilla-Martinez and A. Zimmer (2000). "Patched target Igf2 is indispensable for the formation of medulloblastoma and rhabdomyosarcoma." J Biol Chem 275(37): 28341-28344.

Hallahan, A. R., J. I. Pritchard, S. Hansen, M. Benson, J. Stoeck, B. A. Hatton, T. L. Russell, R. G. Ellenbogen, I. D. Bernstein, P. A. Beachy and J. M. Olson (2004). "The SmoA1 mouse model reveals that notch signaling is critical for the growth and survival of sonic hedgehog-induced medulloblastomas." Cancer Res 64(21): 7794-7800.

Hallonet, M. E. and N. M. Le Douarin (1993). "Tracing neuroepithelial cells of the mesencephalic and metencephalic alar plates during cerebellar ontogeny in quail-chick chimaeras." Eur J Neurosci 5(9): 1145-1155.

Hamilton, S. R., B. Liu, R. E. Parsons, N. Papadopoulos, J. Jen, S. M. Powell, A. J. Krush, T. Berk, Z. Cohen, B. Tetu and et al. (1995). "The molecular basis of Turcot's syndrome." N Engl J Med 332(13): 839-847.

Hatten, M. E. (1999). "Central nervous system neuronal migration." Annu Rev Neurosci 22: 511-539.

Hatten, M. E., J. Alder, K. Zimmerman and N. Heintz (1997). "Genes involved in cerebellar cell specification and differentiation." Curr Opin Neurobiol 7(1): 40-47.

Hatten, M. E. and N. Heintz (1995). "Mechanisms of neural patterning and specification in the developing cerebellum." Annu Rev Neurosci 18: 385-408.

Hatten, M. E. and M. F. Roussel (2011). "Development and cancer of the cerebellum." Trends Neurosci 34(3): 134-142.

Hatton, B. A., P. S. Knoepfler, A. M. Kenney, D. H. Rowitch, I. M. de Alboran, J. M. Olson and R. N. Eisenman (2006). "N-myc is an essential downstream effector of Shh signaling during both normal and neoplastic cerebellar growth." Cancer Res 66(17): 8655-8661.

Hatton, B. A., E. H. Villavicencio, K. D. Tsuchiya, J. I. Pritchard, S. Ditzler, B. Pullar, S. Hansen, S. E. Knoblaugh, D. Lee, C. G. Eberhart, A. R. Hallahan and J. M. Olson (2008). "The Smo/Smo model: hedgehog-induced medulloblastoma with 90% incidence and leptomeningeal spread." Cancer Res 68(6): 1768-1776.

He, T. C., A. B. Sparks, C. Rago, H. Hermeking, L. Zawel, L. T. da Costa, P. J. Morin, B. Vogelstein and K. W. Kinzler (1998). "Identification of c-MYC as a target of the APC pathway." Science 281(5382): 1509-1512.

Hill, R. M., S. Kuijper, J. C. Lindsey, K. Petrie, E. C. Schwalbe, K. Barker, J. K. Boult, D. Williamson, Z. Ahmad, A. Hallsworth, S. L. Ryan, E. Poon, S. P. Robinson, R. Ruddle, F. I. Raynaud, L. Howell, C. Kwok, A. Joshi, S. L. Nicholson, S. Crosier, D. W. Ellison, S. B. Wharton, K. Robson, A. Michalski, D. Hargrave, T. S. Jacques, B. Pizer, S. Bailey, F. J. Swartling, W. A. Weiss, L. Chesler and S. C. Clifford (2015). "Combined MYC and P53 defects emerge at medulloblastoma relapse and define rapidly progressive, therapeutically targetable disease." Cancer Cell 27(1): 72-84.

Hoshino, M., S. Nakamura, K. Mori, T. Kawauchi, M. Terao, Y. V. Nishimura, A. Fukuda, T. Fuse, N. Matsuo, M. Sone, M. Watanabe, H. Bito, T. Terashima, C. V. Wright, Y. Kawaguchi,

K. Nakao and Y. Nabeshima (2005). "Ptf1a, a bHLH transcriptional gene, defines GABAergic neuronal fates in cerebellum." Neuron 47(2): 201-213.

Hovestadt, V., D. T. Jones, S. Picelli, W. Wang, M. Kool, P. A. Northcott, M. Sultan, K. Stachurski, M. Ryzhova, H. J. Warnatz, M. Ralser, S. Brun, J. Bunt, N. Jager, K. Kleinheinz, S. Erkek, U. D. Weber, C. C. Bartholomae, C. von Kalle, C. Lawerenz, J. Eils, J. Koster, R. Versteeg, T. Milde, O. Witt, S. Schmidt, S. Wolf, T. Pietsch, S. Rutkowski, W. Scheurlen, M. D. Taylor, B. Brors, J. Felsberg, G. Reifenberger, A. Borkhardt, H. Lehrach, R. J. Wechsler-Reya, R. Eils, M. L. Yaspo, P. Landgraf, A. Korshunov, M. Zapatka, B. Radlwimmer, S. M. Pfister and P. Lichter (2014). "Decoding the regulatory landscape of medulloblastoma using DNA methylation sequencing." Nature 510(7506): 537-541.

Huangfu, D. and K. V. Anderson (2006). "Signaling from Smo to Ci/Gli: conservation and divergence of Hedgehog pathways from Drosophila to vertebrates." Development 133(1): 3-14.

Huse, J. T. and E. C. Holland (2010). "Targeting brain cancer: advances in the molecular pathology of malignant glioma and medulloblastoma." Nat Rev Cancer 10(5): 319-331.

Hyman, J. M., A. J. Firestone, V. M. Heine, Y. Zhao, C. A. Ocasio, K. Han, M. Sun, P. G. Rack, S. Sinha, J. J. Wu, D. E. Solow-Cordero, J. Jiang, D. H. Rowitch and J. K. Chen (2009). "Small-molecule inhibitors reveal multiple strategies for Hedgehog pathway blockade." Proc Natl Acad Sci U S A 106(33): 14132-14137.

Itoh, K., V. E. Krupnik and S. Y. Sokol (1998). "Axis determination in Xenopus involves biochemical interactions of axin, glycogen synthase kinase 3 and beta-catenin." Curr Biol 8(10): 591-594.

Jaworski, T., I. Dewachter, B. Lechat, M. Gees, A. Kremer, D. Demedts, P. Borghgraef, H. Devijver, S. Kugler, S. Patel, J. R. Woodgett and F. Van Leuven (2011). "GSK-3alpha/beta kinases and amyloid production in vivo." Nature 480(7376): E4-5; discussion E6.

Jho, E. H., T. Zhang, C. Domon, C. K. Joo, J. N. Freund and F. Costantini (2002). "Wnt/beta-catenin/Tcf signaling induces the transcription of Axin2, a negative regulator of the signaling pathway." Mol Cell Biol 22(4): 1172-1183.

Johnson, R. L., A. L. Rothman, J. Xie, L. V. Goodrich, J. W. Bare, J. M. Bonifas, A. G. Quinn, R. M. Myers, D. R. Cox, E. H. Epstein, Jr. and M. P. Scott (1996). "Human homolog of patched, a candidate gene for the basal cell nevus syndrome." Science 272(5268): 1668-1671.

Jones, D. T., N. Jager, M. Kool, T. Zichner, B. Hutter, M. Sultan, Y. J. Cho, T. J. Pugh, V. Hovestadt, A. M. Stutz, T. Rausch, H. J. Warnatz, M. Ryzhova, S. Bender, D. Sturm, S. Pleier, H. Cin, E. Pfaff, L. Sieber, A. Wittmann, M. Remke, H. Witt, S. Hutter, T. Tzaridis, J. Weischenfeldt, B. Raeder, M. Avci, V. Amstislavskiy, M. Zapatka, U. D. Weber, Q. Wang, B. Lasitschka, C. C. Bartholomae, M. Schmidt, C. von Kalle, V. Ast, C. Lawerenz, J. Eils, R. Kabbe, V. Benes, P. van Sluis, J. Koster, R. Volckmann, D. Shih, M. J. Betts, R. B. Russell, S. Coco, G. P. Tonini, U. Schuller, V. Hans, N. Graf, Y. J. Kim, C. Monoranu, W. Roggendorf, A. Unterberg, C. Herold-Mende, T. Milde, A. E. Kulozik, A. von Deimling, O. Witt, E. Maass, J. Rossler, M. Ebinger, M. U. Schuhmann, M. C. Fruhwald, M. Hasselblatt, N. Jabado, S. Rutkowski, A. O.

von Bueren, D. Williamson, S. C. Clifford, M. G. McCabe, V. P. Collins, S. Wolf, S. Wiemann, H. Lehrach, B. Brors, W. Scheurlen, J. Felsberg, G. Reifenberger, P. A. Northcott, M. D. Taylor, M. Meyerson, S. L. Pomeroy, M. L. Yaspo, J. O. Korbel, A. Korshunov, R. Eils, S. M. Pfister and P. Lichter (2012). "Dissecting the genomic complexity underlying medulloblastoma." Nature 488(7409): 100-105.

Jones, D. T., N. Jäger, M. Kool, T. Zichner, B. Hutter, M. Sultan, Y. J. Cho, T. J. Pugh, V. Hovestadt, A. M. Stutz, T. Rausch, H. J. Warnatz, M. Ryzhova, S. Bender, D. Sturm, S. Pleier, H. Cin, E. Pfaff, L. Sieber, A. Wittmann, M. Remke, H. Witt, S. Hutter, T. Tzaridis, J. Weischenfeldt, B. Raeder, M. Avci, V. Amstislavskiy, M. Zapatka, U. D. Weber, Q. Wang, B. Lasitschka, C. C. Bartholomae, M. Schmidt, C. von Kalle, V. Ast, C. Lawerenz, J. Eils, R. Kabbe, V. Benes, P. van Sluis, J. Koster, R. Volckmann, D. Shih, M. J. Betts, R. B. Russell, S. Coco, G. P. Tonini, U. Schüller, V. Hans, N. Graf, Y. J. Kim, C. Monoranu, W. Roggendorf, A. Unterberg, C. Herold-Mende, T. Milde, A. E. Kulozik, A. von Deimling, O. Witt, E. Maass, J. Rossler, M. Ebinger, M. U. Schuhmann, M. C. Fruhwald, M. Hasselblatt, N. Jabado, S. Rutkowski, A. O. von Bueren, D. Williamson, S. C. Clifford, M. G. McCabe, V. P. Collins, S. Wolf, S. Wiemann, H. Lehrach, B. Brors, W. Scheurlen, J. Felsberg, G. Reifenberger, P. A. Northcott, M. D. Taylor, M. Meyerson, S. L. Pomeroy, M. L. Yaspo, J. O. Korbel, A. Korshunov, R. Eils, S. M. Pfister and P. Lichter (2012). "Dissecting the genomic complexity underlying medulloblastoma." Nature 488(7409): 100-105.

Joyner, A. L. (1996). "Engrailed, Wnt and Pax genes regulate midbrain--hindbrain development." Trends Genet 12(1): 15-20.

Joyner, A. L., A. Liu and S. Millet (2000). "Otx2, Gbx2 and Fgf8 interact to position and maintain a mid-hindbrain organizer." Curr Opin Cell Biol 12(6): 736-741.

Kawauchi, D., G. Robinson, T. Uziel, P. Gibson, J. Rehg, C. Gao, D. Finkelstein, C. Qu, S. Pounds, D. W. Ellison, R. J. Gilbertson and M. F. Roussel (2012). "A mouse model of the most aggressive subgroup of human medulloblastoma." Cancer Cell 21(2): 168-180.

Kenney, A. M., M. D. Cole and D. H. Rowitch (2003). "Nmyc upregulation by sonic hedgehog signaling promotes proliferation in developing cerebellar granule neuron precursors." Development 130(1): 15-28.

Kessler, J. D., H. Hasegawa, S. N. Brun, B. A. Emmenegger, Z. J. Yang, J. W. Dutton, F. Wang and R. J. Wechsler-Reya (2009). "N-myc alters the fate of preneoplastic cells in a mouse model of medulloblastoma." Genes Dev 23(2): 157-170.

Kim, J., B. T. Aftab, J. Y. Tang, D. Kim, A. H. Lee, M. Rezaee, J. Kim, B. Chen, E. M. King, A. Borodovsky, G. J. Riggins, E. H. Epstein, Jr., P. A. Beachy and C. M. Rudin (2013). "Itraconazole and arsenic trioxide inhibit Hedgehog pathway activation and tumor growth associated with acquired resistance to smoothened antagonists." Cancer Cell 23(1): 23-34.

Kim, J., J. J. Lee, J. Kim, D. Gardner and P. A. Beachy (2010). "Arsenic antagonizes the Hedgehog pathway by preventing ciliary accumulation and reducing stability of the Gli2 transcriptional effector." Proc Natl Acad Sci U S A 107(30): 13432-13437.

Klaus, A. and W. Birchmeier (2008). "Wnt signalling and its impact on development and cancer." Nat Rev Cancer 8(5): 387-398.

Klein, P. S. and D. A. Melton (1996). "A molecular mechanism for the effect of lithium on development." Proc Natl Acad Sci U S A 93(16): 8455-8459.

Klisch, T. J., Y. Xi, A. Flora, L. Wang, W. Li and H. Y. Zoghbi (2011). "In vivo Atoh1 targetome reveals how a proneural transcription factor regulates cerebellar development." Proc Natl Acad Sci U S A 108(8): 3288-3293.

Knoepfler, P. S., P. F. Cheng and R. N. Eisenman (2002). "N-myc is essential during neurogenesis for the rapid expansion of progenitor cell populations and the inhibition of neuronal differentiation." Genes Dev 16(20): 2699-2712.

Kool, M., D. T. Jones, N. Jager, P. A. Northcott, T. J. Pugh, V. Hovestadt, R. M. Piro, L. A. Esparza, S. L. Markant, M. Remke, T. Milde, F. Bourdeaut, M. Ryzhova, D. Sturm, E. Pfaff, S. Stark, S. Hutter, H. Seker-Cin, P. Johann, S. Bender, C. Schmidt, T. Rausch, D. Shih, J. Reimand, L. Sieber, A. Wittmann, L. Linke, H. Witt, U. D. Weber, M. Zapatka, R. Konig, R. Beroukhim, G. Bergthold, P. van Sluis, R. Volckmann, J. Koster, R. Versteeg, S. Schmidt, S. Wolf, C. Lawerenz, C. C. Bartholomae, C. von Kalle, A. Unterberg, C. Herold-Mende, S. Hofer, A. E. Kulozik, A. von Deimling, W. Scheurlen, J. Felsberg, G. Reifenberger, M. Hasselblatt, J. R. Crawford, G. A. Grant, N. Jabado, A. Perry, C. Cowdrey, S. Croul, G. Zadeh, J. O. Korbel, F. Doz, O. Delattre, G. D. Bader, M. G. McCabe, V. P. Collins, M. W. Kieran, Y. J. Cho, S. L. Pomeroy, O. Witt, B. Brors, M. D. Taylor, U. Schuller, A. Korshunov, R. Eils, R. J. Wechsler-Reya, P. Lichter and S. M. Pfister (2014). "Genome sequencing of SHH medulloblastoma predicts genotype-related response to smoothened inhibition." Cancer Cell 25(3): 393-405.

Kool, M., A. Korshunov and S. M. Pfister (2012). "Update on molecular and genetic alterations in adult medulloblastoma." Memo 5(3): 228-232.

Kool, M., A. Korshunov, M. Remke, D. T. Jones, M. Schlanstein, P. A. Northcott, Y. J. Cho, J. Koster, A. Schouten-van Meeteren, D. van Vuurden, S. C. Clifford, T. Pietsch, A. O. von Bueren, S. Rutkowski, M. McCabe, V. P. Collins, M. L. Backlund, C. Haberler, F. Bourdeaut, O. Delattre, F. Doz, D. W. Ellison, R. J. Gilbertson, S. L. Pomeroy, M. D. Taylor, P. Lichter and S. M. Pfister (2012). "Molecular subgroups of medulloblastoma: an international meta-analysis of transcriptome, genetic aberrations, and clinical data of WNT, SHH, Group 3, and Group 4 medulloblastomas." Acta Neuropathol 123(4): 473-484.

Kool, M., J. Koster, J. Bunt, N. E. Hasselt, A. Lakeman, P. van Sluis, D. Troost, N. S. Meeteren, H. N. Caron, J. Cloos, A. Mrsic, B. Ylstra, W. Grajkowska, W. Hartmann, T. Pietsch, D. Ellison, S. C. Clifford and R. Versteeg (2008). "Integrated genomics identifies five medulloblastoma subtypes with distinct genetic profiles, pathway signatures and clinicopathological features." PLoS One 3(8): e3088.

Korshunov, A., M. Remke, M. Kool, T. Hielscher, P. A. Northcott, D. Williamson, E. Pfaff, H. Witt, D. T. Jones, M. Ryzhova, Y. J. Cho, A. Wittmann, A. Benner, W. A. Weiss, A. von Deimling, W. Scheurlen, A. E. Kulozik, S. C. Clifford, V. Peter Collins, F. Westermann, M. D.

Taylor, P. Lichter and S. M. Pfister (2012). "Biological and clinical heterogeneity of MYCN-amplified medulloblastoma." Acta Neuropathol 123(4): 515-527.

Kortmann, R. D., J. Kuhl, B. Timmermann, U. Mittler, C. Urban, V. Budach, E. Richter, N. Willich, M. Flentje, F. Berthold, I. Slavc, J. Wolff, C. Meisner, O. Wiestler, N. Sorensen, M. Warmuth-Metz and M. Bamberg (2000). "Postoperative neoadjuvant chemotherapy before radiotherapy as compared to immediate radiotherapy followed by maintenance chemotherapy in the treatment of medulloblastoma in childhood: results of the German prospective randomized trial HIT '91." Int J Radiat Oncol Biol Phys 46(2): 269-279.

Lacroix, C., I. Fish, H. Torosyan, P. Parathaman, J. J. Irwin, B. K. Shoichet and S. Angers (2016). "Identification of Novel Smoothened Ligands Using Structure-Based Docking." PLoS One 11(8): e0160365.

Lancaster, M. A., D. J. Gopal, J. Kim, S. N. Saleem, J. L. Silhavy, C. M. Louie, B. E. Thacker, Y. Williams, M. S. Zaki and J. G. Gleeson (2011). "Defective Wnt-dependent cerebellar midline fusion in a mouse model of Joubert syndrome." Nat Med 17(6): 726-731.

Landsberg, R. L., R. B. Awatramani, N. L. Hunter, A. F. Farago, H. J. DiPietrantonio, C. I. Rodriguez and S. M. Dymecki (2005). "Hindbrain rhombic lip is comprised of discrete progenitor cell populations allocated by Pax6." Neuron 48(6): 933-947.

Lauth, M., A. Bergstrom, T. Shimokawa and R. Toftgard (2007). "Inhibition of GLI-mediated transcription and tumor cell growth by small-molecule antagonists." Proc Natl Acad Sci U S A 104(20): 8455-8460.

Lauth, M. and R. Toftgard (2011). "Hedgehog signaling and pancreatic tumor development." Adv Cancer Res 110: 1-17.

Lee, M. J., B. A. Hatton, E. H. Villavicencio, P. C. Khanna, S. D. Friedman, S. Ditzler, B. Pullar, K. Robison, K. F. White, C. Tunkey, M. LeBlanc, J. Randolph-Habecker, S. E. Knoblaugh, S. Hansen, A. Richards, B. J. Wainwright, K. McGovern and J. M. Olson (2012). "Hedgehog pathway inhibitor saridegib (IPI-926) increases lifespan in a mouse medulloblastoma model." Proc Natl Acad Sci U S A 109(20): 7859-7864.

Lee, Y., R. Kawagoe, K. Sasai, Y. Li, H. R. Russell, T. Curran and P. J. McKinnon (2007). "Loss of suppressor-of-fused function promotes tumorigenesis." Oncogene 26(44): 6442-6447.

Lee, Y., H. L. Miller, H. R. Russell, K. Boyd, T. Curran and P. J. McKinnon (2006). "Patched2 modulates tumorigenesis in patched1 heterozygous mice." Cancer Res 66(14): 6964-6971.

Leone, D. P., S. Genoud, S. Atanasoski, R. Grausenburger, P. Berger, D. Metzger, W. B. Macklin, P. Chambon and U. Suter (2003). "Tamoxifen-inducible glia-specific Cre mice for somatic mutagenesis in oligodendrocytes and Schwann cells." Mol Cell Neurosci 22(4): 430-440.

Lin, T. L. and W. Matsui (2012). "Hedgehog pathway as a drug target: Smoothened inhibitors in development." Onco Targets Ther 5: 47-58.

Lipinski, R. J., P. R. Hutson, P. W. Hannam, R. J. Nydza, I. M. Washington, R. W. Moore, G. G. Girdaukas, R. E. Peterson and W. Bushman (2008). "Dose- and route-dependent teratogenicity, toxicity, and pharmacokinetic profiles of the hedgehog signaling antagonist cyclopamine in the mouse." Toxicol Sci 104(1): 189-197.

Lorenz, A., M. Deutschmann, J. Ahlfeld, C. Prix, A. Koch, R. Smits, R. Fodde, H. A. Kretzschmar and U. Schüller (2011). "Severe alterations of cerebellar cortical development after constitutive activation of Wnt signaling in granule neuron precursors." Mol Cell Biol 31(16): 3326-3338.

Louis, D. N., H. Ohgaki, O. D. Wiestler, W. K. Cavenee, P. C. Burger, A. Jouvet, B. W. Scheithauer and P. Kleihues (2007). "The 2007 WHO classification of tumours of the central nervous system." Acta Neuropathol 114(2): 97-109.

Louis, D. N., A. Perry, G. Reifenberger, A. von Deimling, D. Figarella-Branger, W. K. Cavenee, H. Ohgaki, O. D. Wiestler, P. Kleihues and D. W. Ellison (2016). "The 2016 World Health Organization Classification of Tumors of the Central Nervous System: a summary." Acta Neuropathol 131(6): 803-820.

Low, J. A. and F. J. de Sauvage (2010). "Clinical experience with Hedgehog pathway inhibitors." J Clin Oncol 28(36): 5321-5326.

Machold, R. and G. Fishell (2005). "Math1 is expressed in temporally discrete pools of cerebellar rhombic-lip neural progenitors." Neuron 48(1): 17-24.

Madisen, L., T. A. Zwingman, S. M. Sunkin, S. W. Oh, H. A. Zariwala, H. Gu, L. L. Ng, R. D. Palmiter, M. J. Hawrylycz, A. R. Jones, E. S. Lein and H. Zeng (2010). "A robust and high-throughput Cre reporting and characterization system for the whole mouse brain." Nat Neurosci 13(1): 133-140.

Manto, M., D. L. Gruol, J. Schmahmann, N. Koibuchi and F. E. Rossi (2013). Handbook of the Cerebellum and Cerebellar Disorders.

Mao, J., K. L. Ligon, E. Y. Rakhlin, S. P. Thayer, R. T. Bronson, D. Rowitch and A. P. McMahon (2006). "A novel somatic mouse model to survey tumorigenic potential applied to the Hedgehog pathway." Cancer Res. 66: 10171-10178.

Mao, J., K. L. Ligon, E. Y. Rakhlin, S. P. Thayer, R. T. Bronson, D. Rowitch and A. P. McMahon (2006). "A novel somatic mouse model to survey tumorigenic potential applied to the Hedgehog pathway." Cancer Res 66(20): 10171-10178.

Marino, S. (2005). "Medulloblastoma: developmental mechanisms out of control." Trends Mol Med 11(1): 17-22.

Mazumdar, T., J. Devecchio, A. Agyeman, T. Shi and J. A. Houghton (2011). "Blocking Hedgehog survival signaling at the level of the GLI genes induces DNA damage and extensive cell death in human colon carcinoma cells." Cancer Res 71(17): 5904-5914.

McCall, T. D., C. A. Pedone and D. W. Fults (2007). "Apoptosis suppression by somatic cell transfer of Bcl-2 promotes Sonic hedgehog-dependent medulloblastoma formation in mice." Cancer Res 67(11): 5179-5185.

McManamy, C. S., J. Pears, C. L. Weston, Z. Hanzely, J. W. Ironside, R. E. Taylor, R. G. Grundy, S. C. Clifford and D. W. Ellison (2007). "Nodule formation and desmoplasia in medulloblastomas-defining the nodular/desmoplastic variant and its biological behavior." Brain Pathol 17(2): 151-164.

Metcalfe, C., B. Alicke, A. Crow, M. Lamoureux, G. J. Dijkgraaf, F. Peale, S. E. Gould and F. J. de Sauvage (2013). "PTEN loss mitigates the response of medulloblastoma to Hedgehog pathway inhibition." Cancer Res 73(23): 7034-7042.

Milenkovic, L. and M. P. Scott (2010). "Not lost in space: trafficking in the hedgehog signaling pathway." Sci Signal 3(117): pe14.

Mulhern, R. K., S. L. Palmer, T. E. Merchant, D. Wallace, M. Kocak, P. Brouwers, K. Krull, M. Chintagumpala, R. Stargatt, D. M. Ashley, V. L. Tyc, L. Kun, J. Boyett and A. Gajjar (2005). "Neurocognitive consequences of risk-adapted therapy for childhood medulloblastoma." J Clin Oncol 23(24): 5511-5519.

Northcott, P. A., A. M. Dubuc, S. Pfister and M. D. Taylor (2012). "Molecular subgroups of medulloblastoma." Expert Rev Neurother 12(7): 871-884.

Northcott, P. A., T. Hielscher, A. Dubuc, S. Mack, D. Shih, M. Remke, H. Al-Halabi, S. Albrecht, N. Jabado, C. G. Eberhart, W. Grajkowska, W. A. Weiss, S. C. Clifford, E. Bouffet, J. T. Rutka, A. Korshunov, S. Pfister and M. D. Taylor (2011). "Pediatric and adult sonic hedgehog medulloblastomas are clinically and molecularly distinct." Acta Neuropathol 122(2): 231-240.

Northcott, P. A., D. T. W. Jones, M. Kool, G. W. Robinson, R. J. Gilbertson, Y. J. Cho, S. L. Pomeroy, A. Korshunov, P. Lichter, M. D. Taylor and S. M. Pfister (2012). "Medulloblastomics: The End of the Beginning." Nat Rev Cancer 12(12): 818-834.

Northcott, P. A., A. Korshunov, H. Witt, T. Hielscher, C. G. Eberhart, S. Mack, E. Bouffet, S. C. Clifford, C. E. Hawkins, P. French, J. T. Rutka, S. Pfister and M. D. Taylor (2011). "Medulloblastoma comprises four distinct molecular variants." J Clin Oncol 29(11): 1408-1414.

Northcott, P. A., Y. Nakahara, X. Wu, L. Feuk, D. W. Ellison, S. Croul, S. Mack, P. N. Kongkham, J. Peacock, A. Dubuc, Y. S. Ra, K. Zilberberg, J. McLeod, S. W. Scherer, J. Sunil Rao, C. G. Eberhart, W. Grajkowska, Y. Gillespie, B. Lach, R. Grundy, I. F. Pollack, R. L. Hamilton, T. Van Meter, C. G. Carlotti, F. Boop, D. Bigner, R. J. Gilbertson, J. T. Rutka and M. D. Taylor (2009). "Multiple recurrent genetic events converge on control of histone lysine methylation in medulloblastoma." Nat Genet 41(4): 465-472.

Northcott, P. A., D. J. Shih, J. Peacock, L. Garzia, A. S. Morrissy, T. Zichner, A. M. Stutz, A. Korshunov, J. Reimand, S. E. Schumacher, R. Beroukhim, D. W. Ellison, C. R. Marshall, A. C. Lionel, S. Mack, A. Dubuc, Y. Yao, V. Ramaswamy, B. Luu, A. Rolider, F. M. Cavalli, X. Wang,

M. Remke, X. Wu, R. Y. Chiu, A. Chu, E. Chuah, R. D. Corbett, G. R. Hoad, S. D. Jackman, Y. Li, A. Lo, K. L. Mungall, K. M. Nip, J. Q. Qian, A. G. Raymond, N. T. Thiessen, R. J. Varhol, I. Birol, R. A. Moore, A. J. Mungall, R. Holt, D. Kawauchi, M. F. Roussel, M. Kool, D. T. Jones, H. Witt, L. A. Fernandez, A. M. Kenney, R. J. Wechsler-Reya, P. Dirks, T. Aviv, W. A. Grajkowska, M. Perek-Polnik, C. C. Haberler, O. Delattre, S. S. Reynaud, F. F. Doz, S. S. Pernet-Fattet, B. K. Cho, S. K. Kim, K. C. Wang, W. Scheurlen, C. G. Eberhart, M. Fevre-Montange, A. Jouvet, I. F. Pollack, X. Fan, K. M. Muraszko, G. Y. Gillespie, C. Di Rocco, L. Massimi, E. M. Michiels, N. K. Kloosterhof, P. J. French, J. M. Kros, J. M. Olson, R. G. Ellenbogen, K. Zitterbart, L. Kren, R. C. Thompson, M. K. Cooper, B. Lach, R. E. McLendon, D. D. Bigner, A. Fontebasso, S. Albrecht, N. Jabado, J. C. Lindsey, S. Bailey, N. Gupta, W. A. Weiss, L. Bognar, A. Klekner, T. E. Van Meter, T. Kumabe, T. Tominaga, S. K. Elbabaa, J. R. Leonard, J. B. Rubin, L. M. Liau, E. G. Van Meir, M. Fouladi, H. Nakamura, G. Cinalli, M. Garami, P. Hauser, A. G. Saad, A. Iolascon, S. Jung, C. G. Carlotti, R. Vibhakar, Y. S. Ra, S. Robinson, M. Zollo, C. C. Faria, J. A. Chan, M. L. Levy, P. H. Sorensen, M. Meyerson, S. L. Pomeroy, Y. J. Cho, G. D. Bader, U. Tabori, C. E. Hawkins, E. Bouffet, S. W. Scherer, J. T. Rutka, D. Malkin, S. C. Clifford, S. J. Jones, J. O. Korbel, S. M. Pfister, M. A. Marra and M. D. Taylor (2012). "Subgroup-specific structural variation across 1,000 medulloblastoma genomes." Nature 488(7409): 49-56.

Nusse, R. and H. E. Varmus (1982). "Many tumors induced by the mouse mammary tumor virus contain a provirus integrated in the same region of the host genome." Cell 31(1): 99-109.

O'Brien, W. T. and P. S. Klein (2009). "Validating GSK3 as an in vivo target of lithium action." Biochem Soc Trans 37(Pt 5): 1133-1138.

Ohli, J., J. E. Neumann, D. Grammel and U. Schuller (2015). "Localization of SHH medulloblastoma in mice depends on the age at its initiation." Acta Neuropathol 130(2): 307-309.

Oliver, T. G., L. L. Grasfeder, A. L. Carroll, C. Kaiser, C. L. Gillingham, S. M. Lin, R. Wickramasinghe, M. P. Scott and R. J. Wechsler-Reya (2003). "Transcriptional profiling of the Sonic hedgehog response: a critical role for N-myc in proliferation of neuronal precursors." Proc Natl Acad Sci U S A 100(12): 7331-7336.

Oliver, T. G., T. A. Read, J. D. Kessler, A. Mehmeti, J. F. Wells, T. T. Huynh, S. M. Lin and R. J. Wechsler-Reya (2005). "Loss of patched and disruption of granule cell development in a pre-neoplastic stage of medulloblastoma." Development 132(10): 2425-2439.

Palay, S. L. and V. Chan-Palay (1974). Cerebellar cortex: cytology and organization.

Pan, S., X. Wu, J. Jiang, W. Gao, Y. Wan, D. Cheng, D. Han, J. Liu, N. P. Englund, Y. Wang, S. Peukert, K. Miller-Moslin, J. Yuan, R. Guo, M. Matsumoto, A. Vattay, Y. Jiang, J. Tsao, F. Sun, A. C. Pferdekamper, S. Dodd, T. Tuntland, W. Maniara, J. F. Kelleher, 3rd, Y. M. Yao, M. Warmuth, J. Williams and M. Dorsch (2010). "Discovery of NVP-LDE225, a Potent and Selective Smoothened Antagonist." ACS Med Chem Lett 1(3): 130-134.

Parsons, D. W., M. Li, X. Zhang, S. Jones, R. J. Leary, J. C. Lin, S. M. Boca, H. Carter, J. Samayoa, C. Bettegowda, G. L. Gallia, G. I. Jallo, Z. A. Binder, Y. Nikolsky, J. Hartigan, D. R. Smith, D. S. Gerhard, D. W. Fults, S. VandenBerg, M. S. Berger, S. K. Marie, S. M. Shinjo, C. Clara, P. C.

Phillips, J. E. Minturn, J. A. Biegel, A. R. Judkins, A. C. Resnick, P. B. Storm, T. Curran, Y. He, B. A. Rasheed, H. S. Friedman, S. T. Keir, R. McLendon, P. A. Northcott, M. D. Taylor, P. C. Burger, G. J. Riggins, R. Karchin, G. Parmigiani, D. D. Bigner, H. Yan, N. Papadopoulos, B. Vogelstein, K. W. Kinzler and V. E. Velculescu (2011). "The genetic landscape of the childhood cancer medulloblastoma." Science 331(6016): 435-439.

Pastorino, L., P. Ghiorzo, S. Nasti, L. Battistuzzi, R. Cusano, C. Marzocchi, M. L. Garre, M. Clementi and G. B. Scarra (2009). "Identification of a SUFU germline mutation in a family with Gorlin syndrome." Am J Med Genet A 149A(7): 1539-1543.

Paul, P., N. Volny, S. Lee, J. Qiao and D. H. Chung (2013). "Gli1 transcriptional activity is negatively regulated by AKT2 in neuroblastoma." Oncotarget 4(8): 1149-1157.

Pei, Y., C. E. Moore, J. Wang, A. K. Tewari, A. Eroshkin, Y. J. Cho, H. Witt, A. Korshunov, T. A. Read, J. L. Sun, E. M. Schmitt, C. R. Miller, A. F. Buckley, R. E. McLendon, T. F. Westbrook, P. A. Northcott, M. D. Taylor, S. M. Pfister, P. G. Febbo and R. J. Wechsler-Reya (2012). "An animal model of MYC-driven medulloblastoma." Cancer Cell 21(2): 155-167.

Peifer, M., L. M. Pai and M. Casey (1994). "Phosphorylation of the Drosophila adherens junction protein Armadillo: roles for wingless signal and zeste-white 3 kinase." Dev Biol 166(2): 543-556.

Peng, Z., Z. Ji, F. Mei, M. Lu, Y. Ou and X. Cheng (2013). "Lithium inhibits tumorigenic potential of PDA cells through targeting hedgehog-GLI signaling pathway." PLoS One 8(4): e61457.

Pfister, S., M. Remke, A. Benner, F. Mendrzyk, G. Toedt, J. Felsberg, A. Wittmann, F. Devens, N. U. Gerber, S. Joos, A. Kulozik, G. Reifenberger, S. Rutkowski, O. D. Wiestler, B. Radlwimmer, W. Scheurlen, P. Lichter and A. Korshunov (2009). "Outcome prediction in pediatric medulloblastoma based on DNA copy-number aberrations of chromosomes 6q and 17q and the MYC and MYCN loci." J Clin Oncol 27(10): 1627-1636.

Pfister, S. M., A. Korshunov, M. Kool, M. Hasselblatt, C. Eberhart and M. D. Taylor (2010). "Molecular diagnostics of CNS embryonal tumors." Acta Neuropathol 120(5): 553-566.

Pöschl, J., M. Bartels, J. Ohli, E. Bianchi, K. Kuteykin-Teplyakov, D. Grammel, J. Ahlfeld and U. Schüller (2014). "Wnt/beta-catenin signaling inhibits the Shh pathway and impairs tumor growth in Shh-dependent medulloblastoma." Acta Neuropathol 127(4): 605-607.

Pöschl, J., S. Stark, P. Neumann, S. Grobner, D. Kawauchi, D. T. Jones, P. A. Northcott, P. Lichter, S. M. Pfister, M. Kool and U. Schüller (2014). "Genomic and transcriptomic analyses match medulloblastoma mouse models to their human counterparts." Acta Neuropathol 128(1): 123-136.

Pugh, T. J., S. D. Weeraratne, T. C. Archer, D. A. Pomeranz Krummel, D. Auclair, J. Bochicchio, M. O. Carneiro, S. L. Carter, K. Cibulskis, R. L. Erlich, H. Greulich, M. S. Lawrence, N. J. Lennon, A. McKenna, J. Meldrim, A. H. Ramos, M. G. Ross, C. Russ, E. Shefler, A. Sivachenko, B. Sogoloff, P. Stojanov, P. Tamayo, J. P. Mesirov, V. Amani, N. Teider, S. Sengupta, J. P. Francois, P. A. Northcott, M. D. Taylor, F. Yu, G. R. Crabtree, A. G. Kautzman,

S. B. Gabriel, G. Getz, N. Jager, D. T. Jones, P. Lichter, S. M. Pfister, T. M. Roberts, M. Meyerson, S. L. Pomeroy and Y. J. Cho (2012). "Medulloblastoma exome sequencing uncovers subtype-specific somatic mutations." Nature 488(7409): 106-110.

Purves, D. (2004). Neuroscience 3rd edn Sunderland, Massachusetts, Sinauer Associates.

Rakic, P. and R. L. Sidman (1973). "Weaver mutant mouse cerebellum: defective neuronal migration secondary to abnormality of Bergmann glia." Proc Natl Acad Sci U S A 70(1): 240-244.

Rao, G., C. A. Pedone, C. M. Coffin, E. C. Holland and D. W. Fults (2003). "c-Myc enhances sonic hedgehog-induced medulloblastoma formation from nestin-expressing neural progenitors in mice." Neoplasia 5(3): 198-204.

Rausch, T., D. T. Jones, M. Zapatka, A. M. Stutz, T. Zichner, J. Weischenfeldt, N. Jager, M. Remke, D. Shih, P. A. Northcott, E. Pfaff, J. Tica, Q. Wang, L. Massimi, H. Witt, S. Bender, S. Pleier, H. Cin, C. Hawkins, C. Beck, A. von Deimling, V. Hans, B. Brors, R. Eils, W. Scheurlen, J. Blake, V. Benes, A. E. Kulozik, O. Witt, D. Martin, C. Zhang, R. Porat, D. M. Merino, J. Wasserman, N. Jabado, A. Fontebasso, L. Bullinger, F. G. Rucker, K. Dohner, H. Dohner, J. Koster, J. J. Molenaar, R. Versteeg, M. Kool, U. Tabori, D. Malkin, A. Korshunov, M. D. Taylor, P. Lichter, S. M. Pfister and J. O. Korbel (2012). "Genome sequencing of pediatric medulloblastoma links catastrophic DNA rearrangements with TP53 mutations." Cell 148(1-2): 59-71.

Riobo, N. A., K. Lu, X. Ai, G. M. Haines and C. P. Emerson, Jr. (2006). "Phosphoinositide 3-kinase and Akt are essential for Sonic Hedgehog signaling." Proc Natl Acad Sci U S A 103(12): 4505-4510.

Robinson, G., M. Parker, T. A. Kranenburg, C. Lu, X. Chen, L. Ding, T. N. Phoenix, E. Hedlund, L. Wei, X. Zhu, N. Chalhoub, S. J. Baker, R. Huether, R. Kriwacki, N. Curley, R. Thiruvenkatam, J. Wang, G. Wu, M. Rusch, X. Hong, J. Becksfort, P. Gupta, J. Ma, J. Easton, B. Vadodaria, A. Onar-Thomas, T. Lin, S. Li, S. Pounds, S. Paugh, D. Zhao, D. Kawauchi, M. F. Roussel, D. Finkelstein, D. W. Ellison, C. C. Lau, E. Bouffet, T. Hassall, S. Gururangan, R. Cohn, R. S. Fulton, L. L. Fulton, D. J. Dooling, K. Ochoa, A. Gajjar, E. R. Mardis, R. K. Wilson, J. R. Downing, J. Zhang and R. J. Gilbertson (2012). "Novel mutations target distinct subgroups of medulloblastoma." Nature 488(7409): 43-48.

Rodon, J., H. A. Tawbi, A. L. Thomas, R. G. Stoller, C. P. Turtschi, J. Baselga, J. Sarantopoulos, D. Mahalingam, Y. Shou, M. A. Moles, L. Yang, C. Granvil, E. Hurh, K. L. Rose, D. D. Amakye, R. Dummer and A. C. Mita (2014). "A phase I, multicenter, open-label, first-in-human, dose-escalation study of the oral smoothened inhibitor Sonidegib (LDE225) in patients with advanced solid tumors." Clin Cancer Res 20(7): 1900-1909.

Rogers, H. A., S. Miller, J. Lowe, M. A. Brundler, B. Coyle and R. G. Grundy (2009). "An investigation of WNT pathway activation and association with survival in central nervous system primitive neuroectodermal tumours (CNS PNET)." Br J Cancer 100(8): 1292-1302.

Romer, J. and T. Curran (2005). "Targeting medulloblastoma: small-molecule inhibitors of the Sonic Hedgehog pathway as potential cancer therapeutics." Cancer Res 65(12): 4975-4978.

Romer, J. T., H. Kimura, S. Magdaleno, K. Sasai, C. Fuller, H. Baines, M. Connelly, C. F. Stewart, S. Gould, L. L. Rubin and T. Curran (2004). "Suppression of the Shh pathway using a small molecule inhibitor eliminates medulloblastoma in Ptc1(+/-)p53(-/-) mice." Cancer Cell 6(3): 229-240.

Roussel, M. F. and M. E. Hatten (2011). "Cerebellum development and medulloblastoma." Curr Top Dev Biol 94: 235-282.

Rubinfeld, B., I. Albert, E. Porfiri, C. Fiol, S. Munemitsu and P. Polakis (1996). "Binding of GSK3beta to the APC-beta-catenin complex and regulation of complex assembly." Science 272(5264): 1023-1026.

Rudin, C. M., C. L. Hann, J. Laterra, R. L. Yauch, C. A. Callahan, L. Fu, T. Holcomb, J. Stinson, S. E. Gould, B. Coleman, P. M. LoRusso, D. D. Von Hoff, F. J. de Sauvage and J. A. Low (2009). "Treatment of medulloblastoma with hedgehog pathway inhibitor GDC-0449." N Engl J Med 361(12): 1173-1178.

Saal, L. H., K. Holm, M. Maurer, L. Memeo, T. Su, X. Wang, J. S. Yu, P. O. Malmstrom, M. Mansukhani, J. Enoksson, H. Hibshoosh, A. Borg and R. Parsons (2005). "PIK3CA mutations correlate with hormone receptors, node metastasis, and ERBB2, and are mutually exclusive with PTEN loss in human breast carcinoma." Cancer Res 65(7): 2554-2559.

Salic, A., E. Lee, L. Mayer and M. W. Kirschner (2000). "Control of beta-catenin stability: reconstitution of the cytoplasmic steps of the wnt pathway in Xenopus egg extracts." Mol Cell 5(3): 523-532.

Samuels, Y., Z. Wang, A. Bardelli, N. Silliman, J. Ptak, S. Szabo, H. Yan, A. Gazdar, S. M. Powell, G. J. Riggins, J. K. Willson, S. Markowitz, K. W. Kinzler, B. Vogelstein and V. E. Velculescu (2004). "High frequency of mutations of the PIK3CA gene in human cancers." Science 304(5670): 554.

Sanchez, P. and A. Ruiz i Altaba (2005). "In vivo inhibition of endogenous brain tumors through systemic interference of Hedgehog signaling in mice." Mech Dev 122(2): 223-230.

Schüller, U., V. M. Heine, J. Mao, A. T. Kho, A. K. Dillon, Y. G. Han, E. Huillard, T. Sun, A. H. Ligon, Y. Qian, Q. Ma, A. Alvarez-Buylla, A. P. McMahon, D. H. Rowitch and K. L. Ligon (2008). "Acquisition of granule neuron precursor identity is a critical determinant of progenitor cell competence to form Shh-induced medulloblastoma." Cancer Cell 14(2): 123-134.

Schwalbe, E. C., J. C. Lindsey, D. Straughton, T. L. Hogg, M. Cole, H. Megahed, S. L. Ryan, M. E. Lusher, M. D. Taylor, R. J. Gilbertson, D. W. Ellison, S. Bailey and S. C. Clifford (2011). "Rapid diagnosis of medulloblastoma molecular subgroups." Clin Cancer Res 17(7): 1883-1894.

Scotting, P. J., D. A. Walker and G. Perilongo (2005). "Childhood solid tumours: a developmental disorder." Nat Rev Cancer 5(6): 481-488.

Sekulic, A., M. R. Migden, A. E. Oro, L. Dirix, K. D. Lewis, J. D. Hainsworth, J. A. Solomon, S. Yoo, S. T. Arron, P. A. Friedlander, E. Marmur, C. M. Rudin, A. L. Chang, J. A. Low, H. M. Mackey, R. L. Yauch, R. A. Graham, J. C. Reddy and A. Hauschild (2012). "Efficacy and safety of vismodegib in advanced basal-cell carcinoma." N Engl J Med 366(23): 2171-2179.

Shakhova, O., C. Leung, E. van Montfort, A. Berns and S. Marino (2006). "Lack of Rb and p53 delays cerebellar development and predisposes to large cell anaplastic medulloblastoma through amplification of N-Myc and Ptch2." Cancer Res 66(10): 5190-5200.

Stambolic, V., L. Ruel and J. R. Woodgett (1996). "Lithium inhibits glycogen synthase kinase-3 activity and mimics wingless signalling in intact cells." Curr Biol 6(12): 1664-1668.

Stecca, B., C. Mas, V. Clement, M. Zbinden, R. Correa, V. Piguet, F. Beermann and I. A. A. Ruiz (2007). "Melanomas require HEDGEHOG-GLI signaling regulated by interactions between GLI1 and the RAS-MEK/AKT pathways." Proc Natl Acad Sci U S A 104(14): 5895-5900.

Storosum, J. G., T. Wohlfarth, A. Schene, A. Elferink, B. J. van Zwieten and W. van den Brink (2007). "Magnitude of effect of lithium in short-term efficacy studies of moderate to severe manic episode." Bipolar Disord 9(8): 793-798.

Tait, D. M., H. Thornton-Jones, H. J. Bloom, J. Lemerle and P. Morris-Jones (1990). "Adjuvant chemotherapy for medulloblastoma: the first multi-centre control trial of the International Society of Paediatric Oncology (SIOP I)." Eur J Cancer 26(4): 464-469.

Tang, J. Y., J. M. Mackay-Wiggan, M. Aszterbaum, R. L. Yauch, J. Lindgren, K. Chang, C. Coppola, A. M. Chanana, J. Marji, D. R. Bickers and E. H. Epstein, Jr. (2012). "Inhibiting the hedgehog pathway in patients with the basal-cell nevus syndrome." N Engl J Med 366(23): 2180-2188.

Taylor, M. D., N. Gokgoz, I. L. Andrulis, T. G. Mainprize, J. M. Drake and J. T. Rutka (2000). "Familial posterior fossa brain tumors of infancy secondary to germline mutation of the hSNF5 gene." Am J Hum Genet 66(4): 1403-1406.

Taylor, M. D., L. Liu, C. Raffel, C. C. Hui, T. G. Mainprize, X. Zhang, R. Agatep, S. Chiappa, L. Gao, A. Lowrance, A. Hao, A. M. Goldstein, T. Stavrou, S. W. Scherer, W. T. Dura, B. Wainwright, J. A. Squire, J. T. Rutka and D. Hogg (2002). "Mutations in SUFU predispose to medulloblastoma." Nat Genet 31(3): 306-310.

Taylor, M. D., P. A. Northcott, A. Korshunov, M. Remke, Y. J. Cho, S. C. Clifford, C. G. Eberhart, D. W. Parsons, S. Rutkowski, A. Gajjar, D. W. Ellison, P. Lichter, R. J. Gilbertson, S. L. Pomeroy, M. Kool and S. M. Pfister (2012). "Molecular subgroups of medulloblastoma: the current consensus." Acta Neuropathol 123(4): 465-472.

Taylor, R. E., C. C. Bailey, K. Robinson, C. L. Weston, D. Ellison, J. Ironside, H. Lucraft, R. Gilbertson, D. M. Tait, D. A. Walker, B. L. Pizer, J. Imeson and L. S. Lashford (2003). "Results of a randomized study of preradiation chemotherapy versus radiotherapy alone for nonmetastatic medulloblastoma: The International Society of Paediatric Oncology/United Kingdom Children's Cancer Study Group PNET-3 Study." J Clin Oncol 21(8): 1581-1591.

ten Donkelaar, H. J., M. Lammens and A. Hori (2006). Clinical Neuroembryology, Springer.

Thomas, W. D., J. Chen, Y. R. Gao, B. Cheung, J. Koach, E. Sekyere, M. D. Norris, M. Haber, T. Ellis, B. Wainwright and G. M. Marshall (2009). "Patched1 deletion increases N-Myc protein stability as a mechanism of medulloblastoma initiation and progression." Oncogene 28(13): 1605-1615.

Thompson, M. C., C. Fuller, T. L. Hogg, J. Dalton, D. Finkelstein, C. C. Lau, M. Chintagumpala, A. Adesina, D. M. Ashley, S. J. Kellie, M. D. Taylor, T. Curran, A. Gajjar and R. J. Gilbertson (2006). "Genomics identifies medulloblastoma subgroups that are enriched for specific genetic alterations." J Clin Oncol 24(12): 1924-1931.

Tremblay, M. R., M. Nesler, R. Weatherhead and A. C. Castro (2009). "Recent patents for Hedgehog pathway inhibitors for the treatment of malignancy." Expert Opin Ther Pat 19(8): 1039-1056.

Uziel, T., F. Zindy, C. J. Sherr and M. F. Roussel (2006). "The CDK inhibitor p18Ink4c is a tumor suppressor in medulloblastoma." Cell Cycle 5(4): 363-365.

Uziel, T., F. Zindy, S. Xie, Y. Lee, A. Forget, S. Magdaleno, J. E. Rehg, C. Calabrese, D. Solecki, C. G. Eberhart, S. E. Sherr, S. Plimmer, S. C. Clifford, M. E. Hatten, P. J. McKinnon, R. J. Gilbertson, T. Curran, C. J. Sherr and M. F. Roussel (2005). "The tumor suppressors Ink4c and p53 collaborate independently with Patched to suppress medulloblastoma formation." Genes Dev 19(22): 2656-2667.

Vistica, D. T., P. Skehan, D. Scudiero, A. Monks, A. Pittman and M. R. Boyd (1991). "Tetrazolium-based assays for cellular viability: a critical examination of selected parameters affecting formazan production." Cancer Res 51(10): 2515-2520.

Wang, V. Y., M. F. Rose and H. Y. Zoghbi (2005). "Math1 expression redefines the rhombic lip derivatives and reveals novel lineages within the brainstem and cerebellum." Neuron 48(1): 31-43.

Wang, Y., Q. Ding, C. J. Yen, W. Xia, J. G. Izzo, J. Y. Lang, C. W. Li, J. L. Hsu, S. A. Miller, X. Wang, D. F. Lee, J. M. Hsu, L. Huo, A. M. Labaff, D. Liu, T. H. Huang, C. C. Lai, F. J. Tsai, W. C. Chang, C. H. Chen, T. T. Wu, N. S. Buttar, K. K. Wang, Y. Wu, H. Wang, J. Ajani and M. C. Hung (2012). "The crosstalk of mTOR/S6K1 and Hedgehog pathways." Cancer Cell 21(3): 374-387.

Wang, Y., Z. Zhou, C. T. Walsh and A. P. McMahon (2009). "Selective translocation of intracellular Smoothened to the primary cilium in response to Hedgehog pathway modulation." Proc Natl Acad Sci U S A 106(8): 2623-2628.

Watanabe, Y., D. Duprez, A. H. Monsoro-Burq, C. Vincent and N. M. Le Douarin (1998). "Two domains in vertebral development: antagonistic regulation by SHH and BMP4 proteins." Development 125(14): 2631-2639.

Wechsler-Reya, R. J. and M. P. Scott (1999). "Control of neuronal precursor proliferation in the cerebellum by Sonic Hedgehog." Neuron 22(1): 103-114.

Wefers, A. K., M. Warmuth-Metz, J. Poschl, A. O. von Bueren, C. M. Monoranu, K. Seelos, A. Peraud, J. C. Tonn, A. Koch, T. Pietsch, C. Herold-Mende, C. Mawrin, A. Schouten-van Meeteren, D. van Vuurden, K. von Hoff, S. Rutkowski, S. M. Pfister, M. Kool and U. Schuller (2014). "Subgroup-specific localization of human medulloblastoma based on pre-operative MRI." Acta Neuropathol 127(6): 931-933.

Weller, M., S. M. Pfister, W. Wick, M. E. Hegi, G. Reifenberger and R. Stupp (2013). "Molecular neuro-oncology in clinical practice: a new horizon." Lancet Oncol 14(9): e370-379.

Welsch, U. (2006). "Sobotta Lehrbuch Histologie: Zytologie, Histologie, Mikroskopische Anatomie; mit 21 Tabellen." Elsevier, Urban & Fischer.

Wetmore, C., D. E. Eberhart and T. Curran (2001). "Loss of p53 but not ARF accelerates medulloblastoma in mice heterozygous for patched." Cancer Res 61(2): 513-516.

Weyer, A. and K. Schilling (2003). "Developmental and cell type-specific expression of the neuronal marker NeuN in the murine cerebellum." J Neurosci Res 73(3): 400-409.

Wielenga, V. J., R. Smits, V. Korinek, L. Smit, M. Kielman, R. Fodde, H. Clevers and S. T. Pals (1999). "Expression of CD44 in Apc and Tcf mutant mice implies regulation by the WNT pathway." Am J Pathol 154(2): 515-523.

Willert, K., C. Y. Logan, A. Arora, M. Fish and R. Nusse (1999). "A Drosophila Axin homolog, Daxin, inhibits Wnt signaling." Development 126(18): 4165-4173.

Wingate, R. J. (2001). "The rhombic lip and early cerebellar development." Curr Opin Neurobiol 11(1): 82-88.

Wingate, R. J. and M. E. Hatten (1999). "The role of the rhombic lip in avian cerebellum development." Development 126(20): 4395-4404.

Yang, Z. J., T. Ellis, S. L. Markant, T. A. Read, J. D. Kessler, M. Bourboulas, U. Schuller, R. Machold, G. Fishell, D. H. Rowitch, B. J. Wainwright and R. J. Wechsler-Reya (2008). "Medulloblastoma can be initiated by deletion of Patched in lineage-restricted progenitors or stem cells." Cancer Cell 14(2): 135-145.

Yang, Z. J., T. Ellis, S. L. Markant, T. A. Read, J. D. Kessler, M. Bourboulas, U. Schüller, R. Machold, G. Fishell, D. H. Rowitch, B. J. Wainwright and R. J. Wechsler-Reya (2008). "Medulloblastoma can be initiated by deletion of Patched in lineage-restricted progenitors or stem cells." Cancer Cell 14(2): 135-145.

Yauch, R. L., G. J. Dijkgraaf, B. Alicke, T. Januario, C. P. Ahn, T. Holcomb, K. Pujara, J. Stinson, C. A. Callahan, T. Tang, J. F. Bazan, Z. Kan, S. Seshagiri, C. L. Hann, S. E. Gould, J. A. Low, C. M. Rudin and F. J. de Sauvage (2009). "Smoothened mutation confers resistance to a Hedgehog pathway inhibitor in medulloblastoma." Science 326(5952): 572-574.

Yost, C., M. Torres, J. R. Miller, E. Huang, D. Kimelman and R. T. Moon (1996). "The axis-inducing activity, stability, and subcellular distribution of beta-catenin is regulated in Xenopus embryos by glycogen synthase kinase 3." Genes Dev 10(12): 1443-1454.

Yuan, H., J. Mao, L. Li and D. Wu (1999). "Suppression of glycogen synthase kinase activity is not sufficient for leukemia enhancer factor-1 activation." J Biol Chem 274(43): 30419-30423.

Zhukova, N., V. Ramaswamy, M. Remke, E. Pfaff, D. J. Shih, D. C. Martin, P. Castelo-Branco, B. Baskin, P. N. Ray, E. Bouffet, A. O. von Bueren, D. T. Jones, P. A. Northcott, M. Kool, D. Sturm, T. J. Pugh, S. L. Pomeroy, Y. J. Cho, T. Pietsch, M. Gessi, S. Rutkowski, L. Bognar, A. Klekner, B. K. Cho, S. K. Kim, K. C. Wang, C. G. Eberhart, M. Fevre-Montange, M. Fouladi, P. J. French, M. Kros, W. A. Grajkowska, N. Gupta, W. A. Weiss, P. Hauser, N. Jabado, A. Jouvet, S. Jung, T. Kumabe, B. Lach, J. R. Leonard, J. B. Rubin, L. M. Liau, L. Massimi, I. F. Pollack, Y. Shin Ra, E. G. Van Meir, K. Zitterbart, U. Schuller, R. M. Hill, J. C. Lindsey, E. C. Schwalbe, S. Bailey, D. W. Ellison, C. Hawkins, D. Malkin, S. C. Clifford, A. Korshunov, S. Pfister, M. D. Taylor and U. Tabori (2013). "Subgroup-specific prognostic implications of TP53 mutation in medulloblastoma." J Clin Oncol 31(23): 2927-2935.

Zibat, A., E. Missiaglia, A. Rosenberger, K. Pritchard-Jones, J. Shipley, H. Hahn and S. Fulda (2010). "Activation of the hedgehog pathway confers a poor prognosis in embryonal and fusion gene-negative alveolar rhabdomyosarcoma." Oncogene 29(48): 6323-6330.

Zinke, J., F. T. Schneider, P. N. Harter, S. Thom, N. Ziegler, R. Toftgard, K. H. Plate and S. Liebner (2015). "beta-Catenin-Gli1 interaction regulates proliferation and tumor growth in medulloblastoma." Mol Cancer 14: 17.

Zurawel, R. H., S. A. Chiappa, C. Allen and C. Raffel (1998). "Sporadic medulloblastomas contain oncogenic beta-catenin mutations." Cancer Res 58(5): 896-899.

6 Appendix

6.1 Supplementary Figures

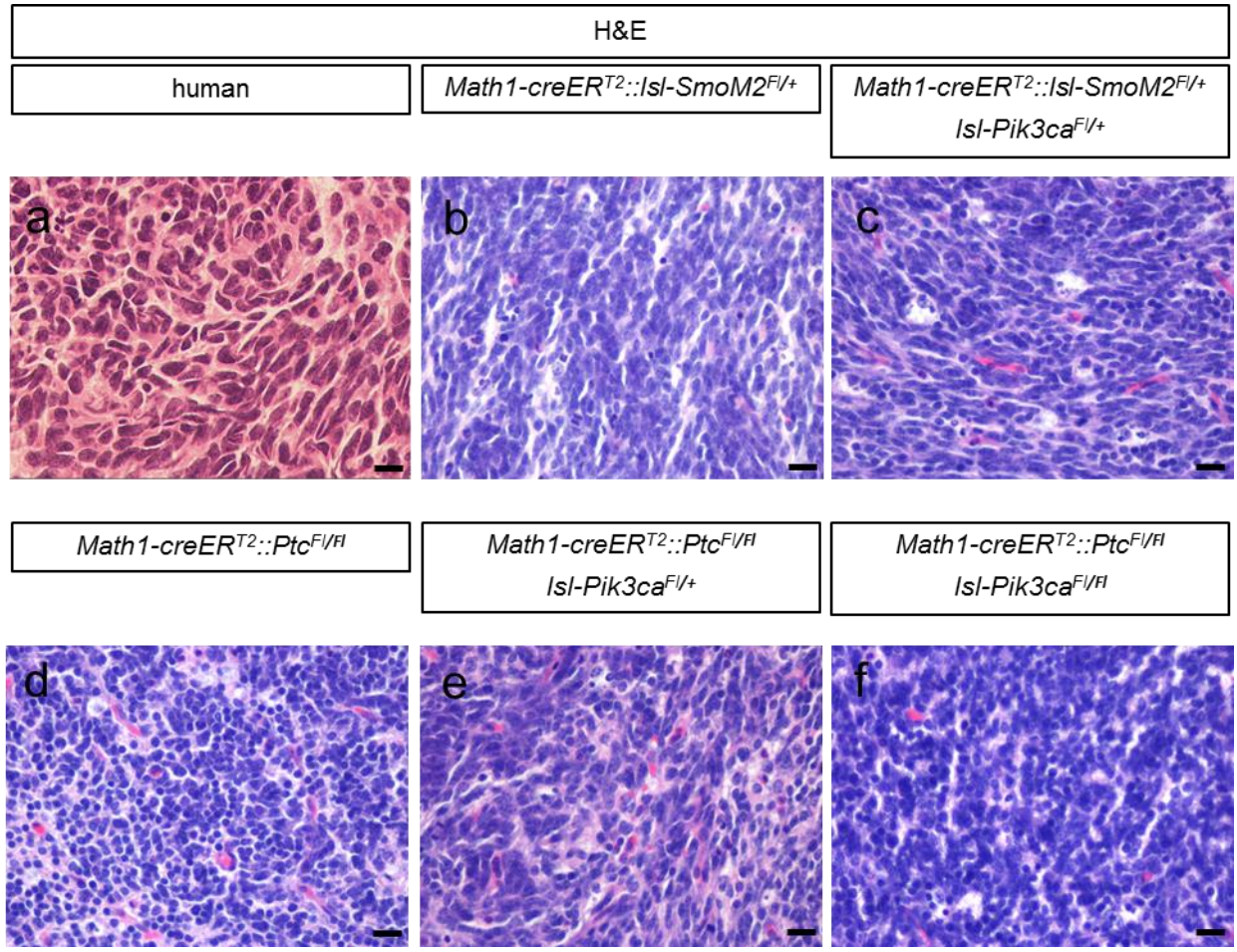

Figure 25 H&E staining of human (a) and mice (b-f) tumors. Comparison of the morphology of murine tumors with different genotypes to each other and to human SHH-MB. All tumors display classic morphology (small, blue, round cells). *Scale bars* 20 µm.

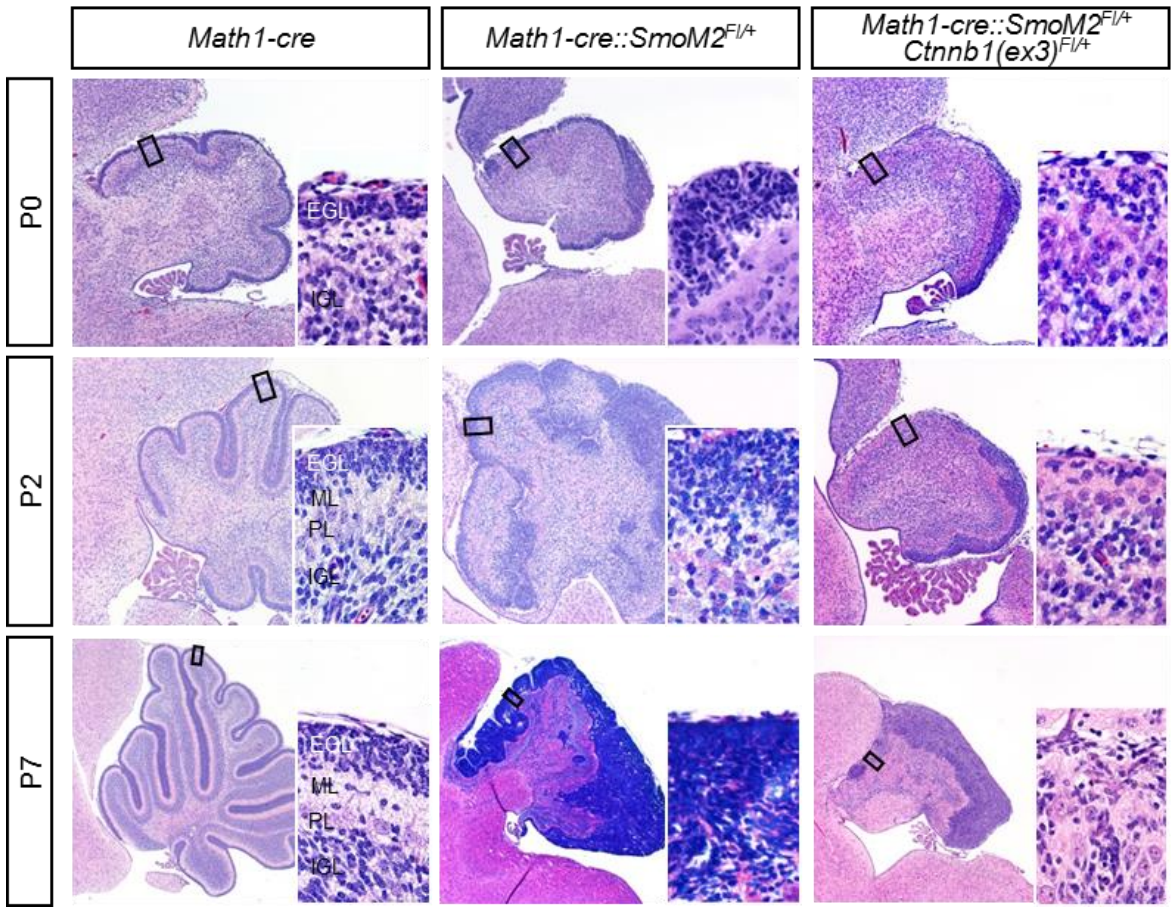

Figure 26 Reduced growth of Shh-medulloblastoma after activation of the Wnt-pathway. H&E stains of sagittal cerebellar sections. Activation of the Shh-pathway in *Math1*-positive cerebellar GNPs resulted in a thickened EGL at P0 and the formation of medulloblastoma that were readily detectable at P2 (*Math1-cre::SmoM2*$^{Fl/+}$ genotype). Co-activation of the Wnt/β-catenin-signalling-pathway (*Math1-cre::SmoM2*$^{Fl/+}$*Ctnnb1(ex3)*$^{Fl/+}$ mice) notably reduced growth of medulloblastoma and led to a decreased cerebellar size when compared to *Math1-cre* controls. Adequate cerebellar layering was not seen (see inset with higher magnification). EGL: external granule cell layer, ML: molecular layer, PL: Purkinje cell layer, IGL: internal granule cell layer

6.2 List of Figures

6.3 List of Tables

6.4 List of Abbreviations

(C)GNP	(cerebellar) granule neuron precursor
µg	microgram
µl	microliter
µM	micro-molar
BrdU	bromodesoxyuridine
C57/Bl6	C57 black 6; common inbred strain of laboratory mouse.
cDNA	complementary DNA
CNS	central nervous system
cre	cyclization recombinase or causes recombination
CSF	cerebrospinal fluid
DNA	deoxyribonucleic acid
E	embryonic day
EGF	epidermal growth factor
EGL	external granular layer
ETMRs	embryonal tumors with multi-layered rosettes
FACS	fluorescnence-actiated cell sorting
FAP	Familiary Adenomatous Polyposis
FGF	fibroblast growth factor
Fl/+	heterozygous for a „floxed“ allele
Fl/Fl	homozygous for a „floxed“ allele
FVB	friend virus B
Fw	forward
Fz	frizzled receptor
gDNA	genomic DNA
GEMM	genetically engineered mouse model
GL261	glioma cell line
h	hour
H&E	hematoxylin and eosin
Hek	*Human embryonal kidney*
HEK 293T	human embryonic kidney cells

i.p.	intraperitoneal
IGL	inner granular layer
IRES	internal ribosome entry site
IVC	individually ventilated cages
LCA	large cell/anaplastic
LiCl	lithium chloride
loxP	locus of X-over P1
lsl	lox stop lox
MB	medulloblastoma
min	minute
ML	molecular layer
ml	milliliter
mM	milli-molar
MRI	magnetic resonance imaging
MTT	3-(4,5-dimethylthiazol-2-yl)-2,5-diphenyltetrazolium bromide
NeuN	neuronal nuclei
OD	optical density
P	postnatal day
PCL	purkinje cell layer
PCR	polymerase chain reaction
Pen/Strep	Penicillin/Streptomycin
PLO	poly-L-ornithine
PNETs	primitive neuroectodermal tumors
qRT-PCR	quantitative real-time PCR
RCAS	replication competent ASLV long terminal repeat with Splice acceptor
RL	rhombic lip
RNA	ribonucleic acid
rpm	revolutions per minute
RT	Room temperature
RU49	zinc finger transcription factor
Rv	reverse

sec	second
Shh/SHH	sonic hedgehog
S-phase	synthesis phase
Tam	Tamoxifen
TVA	avian retrovirus receptor
U	unit
UW473	medulloblastoma cell line
WGS	whole genome sequencing
WHO	World Health Organization
Wnt/WNT	The name Wnt is a portmanteau of int (=proto-oncogene „integration1“) and Wg (Drosophila gene „wingless“) and stands for "Wingless-related integration site"

6.5 Gene names and definition of gene symbols

Gene symbols written in capital letters indicate human or mouse protein (e.g. MYC)

Gene symbols written in italic capital letters indicate human or mouse gene (e.g. *MYC*)

Gene symbol	Gene name in full
AKT	protein kinase B
APC	adenomatous polyposis coli
ATOH1/MATH1	Protein atonal homolog 1
BMP-4	Bone morphogenetic protein 4
CBP/CREBBP	CREB-binding protein
CD44	CD44 molecule (Indian blood group)
CDK6	cyclin-dependent kinase 6
CK1	casein kinase 1
CTNNB1	ß-catenin
DKK1	dickkopf-related protein 1
Dvl	dishevelled
EZH2	enhancer of zeste homolog 2
GFP	green fluorescent protein
GLI1	GLI family zinc finger 1
GLI2	GLI family zinc finger 2
GLI3	GLI family zinc finger 3
GSK3ß	Glycogen synthase kinase 3 ß
hGFAP	human glial fibrillary acidic protein
HOXA2	homeobox A2
KDM6A	lysine (K)-specific demethylase 6A
Lac Z	beta-D-galactosidase
LRP	low-density lipoprotein receptor-related protein
MLL2/3	myeloid/lymphoid or mixed-lineage leukemia protein 2/3
MYC (C-MYC)	myelocytomatosis viral oncogene homolog (avian)

MYCN	myelocytomatosis viral related oncogene, neuroblastoma derived (avian)
OTX2	orthodenticle homeobox 2
p18-Ink4c	cyclin-dependent kinase 4 inhibitor C
p27-Kip	cyclin-dependent kinase inhibitor 1B
p53 (TP53)	tumor protein p53
PIK3CA	phosphatidylinositol-4,5-bisphosphate3-kinase catalytic subunit alpha
PTCH1	patched 1
SFRP1	secreted frizzled-related protein 1
SMO	smoothened, frizzled family receptor
SNCAIP	synuclein alpha interacting protein
ß2M	beta-2-microglobulin
SUFU	suppressor-of-fused
TCF/LEF	transcription factor/lymphoid enhancer-binding factor
YFP	yellow fluorescent protein
ZMYM3	zinc finger MYM-type containing 3

6.6 Curriculum Vitae

6.7 List of publications

Pöschl, J., M. Bartels, **J. Ohli**, E. Bianchi, K. Kuteykin-Teplyakov, D. Grammel, J. Ahlfeld and U. Schüller (2014). "Wnt/beta-catenin signaling inhibits the Shh pathway and impairs tumor growth in Shh-dependent medulloblastoma." Acta Neuropathol 127(4): 605-607.

Ohli, J., J. E. Neumann, D. Grammel and U. Schüller (2015). "Localization of SHH medulloblastoma in mice depends on the age at its initiation." Acta Neuropathol 130(2): 307-309.

Zou, C., Y. Shi, **J. Ohli**, U. Schüller, M. M. Dorostkar and J. Herms (2016). "Neuroinflammation impairs adaptive structural plasticity of dendritic spines in a preclinical model of Alzheimer's disease." Acta Neuropathol 131(2): 235-246.

Li, L., K. B. Grausam, J. Wang, M. P. Lun, **J. Ohli**, H. G. Lidov, M. L. Calicchio, E. Zeng, J. L. Salisbury, R. J. Wechsler-Reya, M. K. Lehtinen, U. Schüller and H. Zhao (2016). "Sonic Hedgehog promotes proliferation of Notch-dependent monociliated choroid plexus tumour cells." Nat Cell Biol 18(4): 418-430.

Fielitz, K., Althoff, K., De Preter, K., Nonnekens, J.**, Ohli, J.**, Elges, S., Hartmann, W., Klöppel, G., Knösel, T., Schulte, M., Klein-Hitpass, L., Beisser, D., Reis, H., Eyking, A., Cario, E., Schulte, J., Schüller, U (2016). „Characterization of pancreatic glucagon-producing tumors and pituitary gland tumors in transgenic mice overexpressing MYCN in hGFAP-positive cells.“ Oncotarget, doi: 10.18632/oncotarget.12766.

Merk D, **Ohli J**, Merk N, Ahlfeld J, Schmid S, Filser S, Harrison L, Weißhaar M, Erkek S, Shakarami M, Neumann J, Marra M, Li Y, Mungall A, Moore R, Ma Y, Jones S, Plenker D, Morrissy S, Lutz B, Ertl-Wagner B, Rossi A, Sendtner M, Pfister S, Taylor M, Kool M, Schüller U, “CBP has opposing functions during cerebellar development and is a targetable tumor suppressor at late stages of medulloblastoma initiation.” Cancer Cell in revision

Engel, N; Neumann, J; Ahlfeld, J; Wefers, A; Merk, D**; Ohli, J**; Schüller, U. „Canonical Wnt signaling drives tumor-like lesions from Sox2-positive precursors of the murine olfactory epithelium“. PloS One, accepted

6.8 Acknowledgement

Mein Dank gilt:

Prof. Dr. med. Ulrich Schüller. Danke, dass du mir während meiner gesamten Doktorarbeit mit Rat und Tat zur Seite gestanden hast, mir bei vielen Diskussionen den Spaß an der wissenschaftlichen Arbeit näher gebracht hast und mir geholfen hast, die großen und kleinen Probleme des wissenschaftlichen Alltags zu meistern.

Prof. Dr. Wolfgang Enard. Herzlichen Dank für die Übernahme des Erstgutachtens an der biologischen Fakultät.

Prof. Dr. Angelika Böttger. Vielen Dank an meine Zweitgutachterin, stellvertretend für alle Gutachter dieser Arbeit.

Danke an die gesamte Arbeitsgruppe Schüller für die schöne und angenehme Arbeitsatmosphäre. Vor allem Silvia Occhionero, Pia Schindler und Chrissi Burmester – vielen Dank für eure ständige Unterstützung im Labor.

Ein großes Dankeschön geht auch an den Tierstall im ZNP, vor allem an Pitt Liebmann.

Vielen Dank auch an Michael Schmidt.

Den „Gieses“. Vielen Dank, dass ihr mich die letzten Monate hier am ZNP, als „letzten Schüller“ noch bei euch aufgenommen habt.

Meiner Familie, die mich stets daran erinnern, dass das Leben nicht nur aus Arbeit und Wissenschaft besteht.

Der letzte Dank gebührt natürlich Matthias, der mich während der Zeit immer unterstützt hat.

Eidesstattliche Erklärung

Ich versichere hiermit an Eides statt, dass die vorgelegte Dissertation von mir selbständig und ohne unerlaubte Hilfe angefertigt ist.

München, den ....

(Unterschrift)

Erklärung

Hiermit erkläre ich, *

☐ dass die Dissertation nicht ganz oder in wesentlichen Teilen einer anderen Prüfungskommission vorgelegt worden ist.

☐ dass ich mich anderweitig einer Doktorprüfung ohne Erfolg **nicht** unterzogen habe.

☐ dass ich mich mit Erfolg der Doktorprüfung im Hauptfach ..... und in den Nebenfächern ..... bei der Fakultät für ..... der .....

(Hochschule/Universität) unterzogen habe.

☐ dass ich ohne Erfolg versucht habe, eine Dissertation einzureichen oder mich der Doktorprüfung zu unterziehen.

München, den..... .....

(Unterschrift)

*) Nichtzutreffendes streichen